RODNEY A. BUSQUIM E SILVA

Implications of advanced computational methods for reactivity initiated accidents in nuclear reactors

São Paulo

2015

RODNEY A. BUSQUIM E SILVA

Implications of advanced computational methods for reactivity initiated accidents in nuclear reactors

Submitted to the Escola Politécnica da Universidade de São Paulo in partial fulfillment of the requirements for the degree of Doctor of Sciences.

Advisor: Prof. Dr. Mujid S. Kazimi

Co-Advisor: Prof Dr. José Jaime da Cruz

São Paulo

2015

RODNEY A. BUSQUIM E SILVA

Implications of advanced computational methods for reactivity initiated accidents in nuclear reactors

Submitted to the Escola Politécnica da Universidade de São Paulo in partial fulfillment of the requirements for the degree of Doctor of Sciences.

Area: Systems Engineering

Advisor: Prof. Dr. Mujid S. Kazimi

Co-Advisor: Prof Dr. José Jaime da Cruz

São Paulo

2015

Este exemplar foi revisado e corrigido em relação à versão original, sob responsabilidade única do autor e com a anuência de seu orientador.

São Paulo, _____ de _____ de _____

Assinatura do autor: _____

Assinatura do orientador: _____

Catalogação-na-publicação

Busquim e Silva, Rodney Aparecido
Application of advanced computational tools under reactivity initiated accident / R. A. Busquim e Silva -- versão corr. -- São Paulo, 2015.
169 p.

Tese (Doutorado) - Escola Politécnica da Universidade de São Paulo. Departamento de Engenharia de Telecomunicações e Controle.

1.Engenharia Nuclear 2.Reatores Nucleares 3.Engenharia Elétrica 4.Filtro de Kalman Estendido I.Universidade de São Paulo. Escola Politécnica. Departamento de Engenharia de Telecomunicações e Controle II.t.

BUSQUIM E SILVA, R.A. **Implications of advanced computational methods for reactivity initiated accidents in nuclear reactors.** São Paulo. 2015. Doutorado. Escola Politécnica, Universidade de São Paulo, São Paulo, 2015.

ACKNOWLEDGEMENTS

I would like to express special thanks to my wife, Sandra, and my daughter, Giovanna, for always believing and supporting me during the moments when “having a job and pursuing a PhD” was a challenge by itself. I never would have made it here without you both.

My deepest gratitude to my advisor, Dr. Mujid Kazimi, who took me as his student during my graduate studies at MIT and who agreed to remain as my advisor on this endeavor. His immense knowledge and expertise in the nuclear field were a key motivation.

I am deeply grateful to my friend and co-advisor, Dr. José Jaime da Cruz, for the long discussions and comments on the revisions of this thesis. His leadership, support and hard work have set an example since I was an undergraduate student at USP.

I wish to thank Dr. Koroush Shirvan for his insightful and detailed discussions on the codes used in this work, and for sharing his knowledge and views on a number of issues related to the thesis´ topic.

A special mention of Admiral Andre Luis Ferreira Marques for the comments at different stages of my research. His help, insights and advices were invaluable during the thesis development.

Many thanks to my parents who have ensured that I have received the best education and opportunities possible.

I would like to gratefully acknowledge the financial support of the Sao Paulo Research Foundation (FAPESP).

The support of the *Escola Politécnica da Universidade de São Paulo*, and also of the *Massachusetts Institute of Technology*, was great appreciated. As an alumnus of both engineering schools, I recognize their use of knowledge as a beacon to the future.

The greatest enemy of knowledge is not ignorance, it is the illusion of knowledge.
Stephen Hawking

ABSTRACT

Advanced computational tools are applied to simulate a nuclear power plant (NPP) control rod assembly ejection (CRE) accident. The impact of these reactivity-initiated accidents (RIAs) on core reactivity behavior, 3D power distribution and stochastic reactivity estimation are evaluated. The three tools used are: the thermal-hydraulic (TH) RELAP5 (R5) code, the neutronic (NK) PARCS (P3D) code, and the coupled version P3D/R5, with specially developed linkage using the environment code MATLAB. This study considers three different-size cores: NPP1 (2772 MWt); NPP2 (530 MWt); and NPP3 (1061 MWt). The three cores have the same general design and control rod assembly (CRA) positions, and the ejected CRA has similar worth and at the same rod ejection pace. The CRE is assessed under both hot zero power (HZP) and hot full power (HFP) conditions.

The analyses indicate that RIA modeling and simulation should be carried out through a systematic coding and configuration approaches, otherwise the results will not capture the true transient behavior of the core under analysis. The simulation of one code depends on the appropriate configuration of parameters generated by the other code and on the correct determination of the TH/NK mapping weight factors for the various mesh regions in each of the models. From the design point of view, the standalone codes predict milder magnitude of power and reactivity increase compared to the coupled P3D/R5 simulation. The magnitudes of reduced peak power and reactivity become larger as the core size shrinks. The HFP simulation shows that the three NPPs have the same transient peak value, but the post-transient steady power is lower for a smaller core. The HZP analysis indicates that the transient peak is lower for the smaller core, but the post-transient power occurs at the same level.

The three-dimensional (3D) power distributions are different among the HFP and HZP cases, but do not depend on the size of the core. The results indicate: i) HFP: core power increases in the area surrounding the ejected rod/bank assembly, and this increase becomes lower as the NPPs shrinks – however, the power is well-distributed after the transient; and ii) HZP: the area surrounding the CRA stays hotter, but the 3D peak assembly factor becomes lower, during and after the transients, as the NPPs shrinks. These features confirm that the smaller cores yield a safer response to a given inserted reactivity compared to larger cores.

A stochastic extended Kalman filter (EKF) algorithm is implemented to estimate the reactivity based on the reactor power profile, after the addition of random noise. The inverse point kinetics (IPK) deterministic method is also implemented and the results of the application of EKF and IPK are compared to the P3D/R5 simulation. The following sophisticated strategies made the EKF algorithm robust and accurate: the system is modeled by a set of continuous time nonlinear stochastic differential equations; the code uses a time step directly based on the power measured and applies that to the model for online discretization and linearization; filter tuning goes automatically up from the first time step; and the state noise covariance matrix is updated online at each time step.

It was found that the IPK reactivity has higher noise content compared to the EKF reactivity for all cases. Thus, the EKF presents superior and more accurate results. Furthermore, under a small reactivity insertion, the IPK reactivity varies widely from positive to negative values: this variation is not observed within the EKF. A sensitivity analysis for three distinct standard deviation (SD) noise measurements suggests that EKF is superior to IPK method, independent of the noise load magnitude. As the noise content increases, the error between the IPK and P3D/R5 reactivity also increases. A sensitivity analysis for five distinct carry-over effects of different random noise loads indicates that the random addition

of different noise loads to the reactor power does not change the overall performance of both algorithms.

Keywords: Nuclear power plant. Nuclear core analysis. Thermal hydraulic and neutronics coupling. RELAP5. PARCS 3D. Reactivity. Extended Kalman filter. Inverse point kinetics.

RESUMO

Este trabalho aplica métodos computacionais avançados para simular a ejeção de barras de controle (CRE) em uma planta térmica nuclear (NPP). São avaliados o impacto da ocorrência de acidentes iniciados por reatividade (RIAs) na reatividade total, na distribuição da potência em três dimensões (3D) e na determinação da reatividade. As ferramentas utilizadas são: o código termo-hidráulico (TH) RELAP5 (R5), o código neutrônico (NK) PARCS (P3D), a versão acoplada P3D/R5, e o ambiente computacional MATLAB. Este estudo considera três reatores nucleares de diferentes tamanhos: NPP1 (2772 MWT); NPP2 (530 MWt); e NPP3 (1061 MWt). Os três núcleos possuem projeto similar e idêntica posição dos grupos das barras de controle (CRA), além do mesmo valor de reatividade diferencial das CRA ejetadas e idêntica velocidade de ejeção. A ocorrência da CRE é avaliada sob condições de *hot zero power* (HZP) e de *hot full power* (HFP).

As análises indicam que a modelagem e a simulação de RIAs devem ser realizadas sistematicamente, caso contrário os resultados não irão refletir o comportamento em regime transitório do núcleo. A simulação de um modelo em um código depende da apropriada configuração de parâmetros gerados pelo outro código e da determinação adequada do mapeamento TH/NK para as várias malhas dos modelos. Do ponto de vista de projeto, a utilização de códigos independentes resulta em cálculos de potência e reatividade conservadores em comparação com os resultados utilizando-se P3D/R5. Os picos de potência e de reatividade são menores à medida que o núcleo encolhe. A simulação em condições de HFP resulta em valores de pico de potência similares durante transitório para as três NPPs, mas a potência de pós-transitórios é menor para o menor núcleo. A análise em condições de HZP também indica que o valor máximo durante o transitório é menor para o menor núcleo, mas o pós-transitórios ocorre aos mesmos níveis de potência das demais NPPS.

A distribuição de potência em 3D também apresenta resultados distintos para condições de HFP e HZP, mas tais resultados são independentes do tamanho do núcleo: i) HFP: há um aumento da potência do núcleo em torno da CRE, mas tal comportamento diminui para núcleos menores - no entanto, a potência é bem distribuída após o transitório; e ii) HZP: há aumento de potência na área do CRE, mas o pico de potência em 3D é menor durante e depois dos transitórios para núcleos menores. Tais características indicam que os núcleos menores respondem de forma mais segura quando da inserção de reatividade em comparação a reatores de maiores dimensões.

O método estocástico de filtragem de Kalman estendido (EKF) foi codificado para estimar a reatividade com base no perfil de potência da NPP, após a adição de ruído aleatório. O método determinístico da cinética pontual inversa (IPK) também foi implementado e os resultados da aplicação dos algoritmos do EKF e IPK foram comparados com os resultados da simulação do P3D/R5. As seguintes estratégias, implementadas neste trabalho, possibilitaram a aplicação robusta e precisa do EKF: o sistema foi modelado por um conjunto de equações diferenciais não-lineares estocásticas de tempo contínuo; o algoritmo obtém o passo de tempo diretamente da potência medida e aplica-o ao modelo para a discretização e linearização online; o ajuste do filtro ocorre automaticamente a partir do primeiro passo de tempo; e a matriz de covariância do ruído no estado é atualizada *online*.

Verificou-se que a reatividade calculada pelo método IPK possui maior nível de ruído quando comparada ao EKF para todos os casos estudados. Portanto, o EKF apresenta resultados superiores e mais precisos. Além disso, sob uma pequena inserção de reatividade, a reatividade calculada pelo método IPK varia consideravelmente de valores positivos para negativos: esta variação não é observada com o EKF. Uma análise de sensibilidade para três

desvios padrão (SD) sugere que o algoritmo EKF é superior ao método IPK, independente da magnitude do ruído. Com o aumento da magnitude do ruído, o erro entre as reatividades calculadas pelo IPK e pelo P3D/R5 aumenta. A análise de sensibilidade para cinco ruídos aleatórios indica que a adição de ruído na potência do reator não altera o desempenho global de ambos os algoritmos.

Palavras-Chave: Reatores nucleares. Análise do núcleo. RELAP5. PARCS 3D. Reatividade. Acoplamento termo hidráulico e neutrônico. Filtro de Kalman estendido. Cinética pontual inversa.

TABLE OF CONTENTS

LIST OF FIGURES

LIST OF TABLES

LIST OF ACRONYMS

0D	Zero-Dimensional Space
1D	One-Dimensional Space
2D	Two-Dimensional Space
3D	Three-Dimensional Space
API	Application Programming Interface
ARI	All Rods In
ARO	All Rods Out
ATWS	Anticipated Transient Without Scan
B&W	Babcock & Wilcox
BWR	Boiling Water Reactor
CHF	Critical Heat Flux
CMFD	Coarse Mesh Finite Difference
CRA	Control Rod Assembly
CRA#8	Control Rod Assembly Ejected
CRB	Control Rod Bank
CRB#8	Control Rod Bank Ejected
CRDM	Control Rod Drive Mechanism
CRE	Control Rod Assembly Ejection
DOE	USA Department of Energy
EFPD	Effective Full Power Days
EKF	Extended Kalman Filter
EOC	End of Cycle
EU	European Union
FA	Fuel Assembly
FPGA	Field-Programmable Gate Array
Gd	Gadolinium
GI	General Interface
HDL	Hardware Description Language
HFP	Hot Zero Power
HZP	Hot Full Power
INL	Idaho National Laboratory
IPK	Inverse Point Kinetics
IRIS	International Rector Innovative and Secure
KF	Kalman Filter
LHGR	Linear Heat Generation Rate
LOCA	Loss of Coolant Accidents
LOFW	Loss of Feed Water Flow
LWR	Light Water Reactor
MATLAB	Matrix Laboratory
MOX	Mixed Oxide Fuel

MSLB	Main Steam Line Break
MWt	Thermal Mega Watt
NEA	Nuclear Energy Agency
NK	Neutronic
NPP	Nuclear Power Plant
NPP1	Nuclear Power Plant #1
NPP1	Nuclear Power Plant #2
NPP1	Nuclear Power Plant #3
NPP2a	Nuclear Power Plant #2a
NRC	USA Nuclear Regulatory Commission
OECD	Organization for Economic Co-operation and Development
OTSG	Once-through Two Loops Steam Generators
P3D	PARCS 3D 2.71d
PARCS	Purdue Advanced Reactor Core Simulator
PK	Point Kinetics
PKRE	Point Kinetics Reactor Equations
PLC	Programmable Logic Controller
PVM	Parallel Virtual Machine
PWR	Pressurized Water Reactor
R5	RELAP5 Mod3.2
RELAP	Reactor Excursion and Leak Analysis Program
RIA	Reactivity-Initiated Accident
SD	Standart Deviation
SMR	Small Modular Reactor
TH	Thermal-Hydraulic
TMI	Three Mile Island
USA	United States of America

LIST OF SYMBOLS

λ	Prompt neutron lifetime
$w_{i,j,k}$	Weight factor, where *i* is the inlet TH axial volume; *j* is outlet TH channel; *k* is the inlet or outlet NK region
d	Axial distance from the TH inlet/outlet junction to the NK neutronic node
h	Inlet/outlet TH cell height
$F(x(t))$	State model
x(t)	State vector
$H(x(t_k), t_k)$	Observation model
t	Continuous time
t_k	*k*-th discrete-time point
W(t)	State noise
Q'(t)	Spectral density matrix of the state noise
$y(t_k)$	Measurement vector
$V(t_k)$	Measurement noise
$R(t_k)$	Noise covariance matrix
T	Discretization/sampling period
δ_{km}	Kronecker delta
$\hat{x}(t_k/t_k)$	Estimated state
$P(t_k/t_k)$	Error covariance matrix of the estimated state
$\bar{x}(t_k)$	Reference state
$\delta x(t)$	Residual state
$\Phi(t_{k+1}, t_k)$	State transition matrix
I	Identity matrix
K	EKF gain matrix
$\rho(t)$	Reactivity
n(t)	Neutron density

$C_i(t)$	Effective concentration of delayed neutron of group *i*
β	Total effective delayed neutron fraction
β_i	Effective delayed neutron fraction of group *i;*
λ_i	Effective decay constant of group *i;*
Λ	Mean neutron generation time
ℓ	Mean lifetime of a neutron in the a reactor
$k(t)$	Multiplication factor
$P(t)$	Power level
$D(\tau)$	Delayed Neutron Kernel
α	Stochastic reactivity jump
w	Stochastic reactivity slope
S	Neutron source
A	Jacobian matrix
k_{eff}	Effective multiplication factor
\$	Reactivity unity
$\dot{T}_F$	Rate of change in the fuel temperature
$\dot{T}_M$	Rate of change in the moderator temperature
$\dot{\alpha}_M$	Rate of change for the steam volume fraction
n_{AR}	Number of axial regions
n_{FA}	Number of FAs

1. INTRODUCTION

Nuclear energy has been recognized to be among the best options to meet the growing energy demand by supplying carbon-free clean energy to minimize global warming. Nuclear power is competitive with other power sources, and advanced nuclear power plants (NPPs) have been proven to be reliable, supplying more than 30 countries with part of their needs of electricity. Furthermore, the growing electricity demand and the large amount of uranium available, among other factors, have increased the interest in advanced NPP designs and the demand for higher performance of the existent reactors. Therefore, the number of NPPs under construction has been increasing, and more countries are planning to support the deployment of nuclear technology for peaceful applications. Although only few countries are able to design and supply NPPs, and despite the Fukushima accident [1] that has slowed down the construction of new NPPs, there are 437 nuclear power reactors in operation and 60 NPPs under construction [2].

Advanced modeling and simulation play a significant role in the modern nuclear industry, and in the development of advanced NPPs. The design, licensing and operation of reactors rely on a myriad of computer codes, which have been developed and used in the last 30 years. Furthermore, the operation of NPPs demands that a large number of postulated accidents, during normal operation or operational transients, must be well characterized and with design features that mitigate their consequences. However, the NPP's demanding capital cost and the radioactive nature of their fuel demand make it unlikely that severe accidents be evaluated by means of integral experimental programs. Therefore, computer reactor models have been developed to simulate the NPP behavior during transients and normal operation. This approach provides insights that improve the reactor design and performance, leading to cost reduction and increased safety.

This work develops and applies advanced computational tools to simulate the control rod ejection (CRE) accident to assess reactivity behavior, three-dimensional (3D) core power distribution and stochastic reactivity estimation during the accidents. A CRE is defined as partial or total control rods withdrawals from its reactor core position, due to a failure of the control rod drive mechanism (CRDM) or its housing, which may drive the core to a reactivity-initiated accident (RIA) conditions. The CRE is usually simulated using coupled thermal hydraulic (TH) and neutronic (NK) codes due to nuclear core processes that are not

independent of each other. Thus, the interaction among the TH/NK processes during steady-state and transients, i.e. the feedback effects, must be well evaluated during a CRE. These interactions are very similar to classic control theory [3]. The impact of a RIA is evaluated using the TH RELAP5 (R5) code, the NK PARCS (P3D), and the coupled version P3D/R5. The computational framework MATLAB code is used for data analysis and for algorithm implementation. This study considers three reactors with different-size cores: NPP1, with an output of 2,772 MWt; NPP2, with an output of 530 MWt; and NPP3, with an output of 1,061 MWt. The RIA is investigated under both hot zero power (HZP) and hot full power (HFP) core conditions.

In addition, the stochastic extended Kalman filter (EKF) algorithm estimates the reactivity based on the noisy reactor power profile, and a MATLAB script adds the noise. A deterministic inverse point kinetics (IPK) method is also implemented and the results of both EKF and IPK algorithms are compared to the P3D/R5 reactivity. The following coding strategies are implemented to have a robust and accurate EKF algorithm: the system is modeled by continuous-time nonlinear stochastic differential equations; the code uses the time step directly from the calculated power and applies it to the model for online discretization and linearization; the filter tuning goes automatically up to the first time step; and the state noise covariance matrix is updated online at each time step.

1.1. Motivation

The nuclear core analysis depends strongly on the reactor design. Nonetheless, the study of the nuclear core can be divided into different areas such as TH, NK, materials, structural, safety, security and economics. Two fundamentals quantities in the reactor analysis are the nuclear reaction rate and the thermal hydraulic behavior. The core neutron population drives both. Therefore, determination of the criticality conditions and power distribution, i.e. the core neutronic multiplication factor and neutron flux, are among the most significant parameters in nuclear reactor design and safety analysis.

Besides the steady-state behavior under normal operation, the light water reactor (LWR) transient analysis has significant interest because of accidents that may damage the fuel and release radioactivity materials. As a result, the transient analysis must be performed using nuclear codes capable of modeling and simulating the significant physical process and their

interactions, such as the core neutron generation and transport, the fluid dynamic, the heat generation, the moderator density, and the core materials.

The standalone use of 3D NK and TH codes has achieved high degree of acceptance for traditional and advanced NPP. The TH codes simulate not only the core, but also other components in the plant, like pumps, pressurizers, control systems and steam generators. Usually, for these codes, a simple neutronic point kinetics model (which assumes fixed core power distribution) or a 1D neutronic model simplify the transient core power distribution. On the other hand, a standalone 3D NK code solves the neutron diffusion equations, and includes the feedback effects using large mesh or nodal methods. The coupling of 3D codes from both the TH and NK domains needs additional assumptions and skills to take into account the strong interactions, particularly at transient conditions. The accuracy of the simulation results is important for reactor design, safety and licensing.

Simple core models may be useful for limited situations. However, the complete reactor core analysis demands complex models that anticipate the consequences of transients and postulated accidents that must be mitigated by design solutions [4]. The simulation and modeling processes usually include the gathering and organization of all model/system information, the system model nodalization within the codes, the input preparation, the input quality assurance, the code running, and data acquisition and analysis. Within the RIA scope and by using coupled codes, the TH code models the process of fission energy transport (time and space dependent) and associated temperatures and coolant flow rates while the NK code models the process of neutron production and transport (temperature and materials dependent), thus providing the energy generation distribution within the core.

RIA's conditions may lead to an undesirable increase in the fission rate and, therefore, in the reactor power [5]. The consequences of the rapidly insertions of reactivity are: the fast increasing in the fuel temperature; in the core power; and in the power distribution. As a consequence, the undesired increase in nuclear power may damage the nuclear fuel, and in severe cases, the whole core. The LWRs under commercial operation have engineered safety systems, in addition to the inherent reactor feedback mechanisms, to dismiss the occurrence of RIAs.

The occurrence of a RIA in a pressurized water reactor (PWR) may change the core neutron population significantly and almost instantaneously. Nevertheless, PWRs represent the dominant part of the World's NPP fleet today, and small modular reactors (SMR) could be

deployed within the next decade. The occurrence of a CRE in a SMR is among the most severe accidents that could occur in a modular reactor [6]. The deployment of SMR suggests that a study of its behavior compared to traditional NPPs is important. Therefore, the impact of a RIA on reactivity behavior and 3D core power distribution, for three different power reactor core sizes has been performed. The results show an inherently safer performance of smaller cores relative to larger sizes. This suggests that new large reactor designs should perform a more comprehensive sensitivity analysis of RIA accidents.

Lastly, the determination of neutronic reactivity is important for solving practical NPP issues related to accident analysis, reactor control and safety. The estimation of the reactivity, by means of the EKF stochastic estimation tool, aids the assessment of an accurate reactivity calculation during a CRE, increasing the safety by minimizing uncertainties during a RIA. The use of control theory estimation tools, such as EKF, is not common in the nuclear field and only few studies present results based on simulations or offline data analysis [7] [8].

1.2. Scope of this Work

This work focuses on the study of the reactivity behavior and 3D power distribution under a CRE RIA using advanced computational nuclear codes and methods to simulate steady and transient states. Moreover, the impact of use of standalone TH and NK codes and a coupled one is assessed. Equally important, the total reactivity and nuclear power distribution for three different core sizes and power levels, but similar designs, are analyzed. Furthermore, a 3D power distribution analysis is also evaluated among the three codes. Last, a stochastic reactivity estimation tool is implemented and its results are benchmarked against the IPK deterministic method.

Within these schemes, the R5 code models the TH behavior, the P3D models the NK trends, and the total power, reactivity and 3D power distribution is assessed using the coupled P3D/R5 code. In addition, the use of the MATLAB simulation environment, a third party code, brings advantages for data acquisition and analysis, and for the implementation of the reactivity calculation algorithms. Therefore, a non-linear stochastic EKF and the deterministic IPK are implemented using MATLAB.

The first part of this work (from Chapter 1 to Chapter 5) presents the main information needed to follow this study: Chapter 1 presents the motivation and scope; a review of previous

works, which have guided the development of this thesis, is presented in Chapter 2; the work's methodology for the deployment of the three NPP models, which are examined using the P3D/R5 coupled package, is presented in Chapter 3. Chapter 4 presents the NPP1 Three Mile Island (TMI) Babcock & Wilcox (B&W) NPP main technical specifications and also the NPP2 and NPP3 main modeling parameters and assumptions. Finally, Chapter 5 presents the EKF modeling assumptions, simulation strategy and equations.

The second part of the study (from Chapter 6 to Chapter 9) presents the simulations results and discussions. Therefore, Chapter 6 presents the reactivity worth identification; Chapter 7 describes the total reactivity and nuclear power distribution assessment; Chapter 8 presents the 3D power distribution analysis; and Chapter 9 presents the EKF and IPK simulation results. Chapter 10, the last part of this work, presents the conclusions and recommendations for further studies.

2. REVIEW OF PREVIOUS WORK

Since the 1990´s, several studies were undertaken to analyze the performance of TH and NK nuclear codes. For example, the NEACRP PWR rod ejection benchmark exercise [9], issued by the reactor physics committee of the Nuclear Energy Agency (NEA), an agency within the Organization for Economic Co-operation and Development (OECD), aimed to assess the discrepancies between 3D codes for transients in LWRs by simulation of the ejection of a control rod assembly (CRA) from the core. Furthermore, the work in reference [10] presents the solution for cold water injection events, related to the boiling water reactor (BWR), that was part of the NEACRP benchmark exercise. In addition, reference [11] presents the analysis of the NEACRP PWR rod ejection using the DIF3D-K nodal kinetics code, which was benchmarked against other codes used for solving the same exercise.

Following the effort to better understand the role of TH and NK nuclear codes regarding transients analysis, the TMI PWR main steam line break (MSLB) benchmark specifications [12] were released in 1999 with three exercises. The purposes of this benchmark were: i) to verify the capability of TH codes for analyzing complex transients with core-plant interactions; ii) to test fully NK/TH codes; and iii) to evaluate discrepancies among the prediction of the codes. The study of reference [13] presents a solution for the MSLB exercise using the coupled codes RELAP5 and PANBOX – in this case, the emphasis was on the development of a multidimensional core model.

Moreover, the work of reference [14] presents results of three MSLB exercises and summarizes the findings with regards to the current computational issues and coupled calculations. Another exercise, discussed in reference [15], presented a benchmark designed to provide the framework to assess the ability of NK codes to predict the transient response of a core loaded with mixed oxide fuel (MOX) and UO_2 fuel. The work presented in reference [16] shows the final results of the assessment of heterogeneous transport and nodal transient methods for MOX RIA. Reference [17] presents the internal integration scheme in which the solution of the system code is automatically obtained by TRAC-M [18], and only the spatial kinetics solution is obtained by the PARCS code.

Furthermore, efforts have also been made to develop flexible tools of coupled TH/NK in order to simulate the behavior of a NPP under steady-state and transient conditions. The United States of America (USA) and the European Union (EU) have been leading the

development of such codes, in addition to coupling tools, to perform more realistic simulations and to establish a common LWR simulation platform [19]. For instance, the work on reference [20] describes the implementation of the Parallel Virtual Machine (PVM) Application Programming Interface (API) in the RELAP5-3D, used for coupling different computer codes to simulate transient behavior. Reference [21] presents the changes in the RELAP5-3D needed to make the explicit coupling capabilities in the code fully functional.

The determination of the power level during a CRE accident has been studied in the last two decades, as presented in references [22], [23], [24], [25] and [26]. Furthermore, the work on reference [27] presents the changes introduced in RELAP5 MOD3.3/PARCSv2.7 codes to make the control rods behavior and Boron injection more dynamic and realistic. The reference [28] presents the development and validation of a numerical model for transient and dynamic simulation of a research reactor using experimental data. The work of reference [29] presents the analysis of a regulating control rod group withdrawal from 1% power level, as an anticipated transient without scram (ATWS) event. The state of the art method to analyze CRE accidents relies on homogenization, in which the average assembly power is used to estimate the fuel rod power [30]. The nuclear behavior under RIA conditions is of great interest to nuclear safety not only for traditional reactors, but also for advanced NPP.

The 2010 state of the art report of reference [5] presents the current understanding of RIA fuel safety issues applicable to high burn-up fuel, to new nuclear materials and to advanced fuel design. Moreover, it includes general information about the major RIA scenarios; state of the art of the fuel-cladding interaction; the main RIA phenomena that need to be addressed by modeling, simulations and tests; and the RIA test methodologies using experiments and code calculations. The control rod systems failures have been also taken into consideration for traditional LWRs, including the CRE accident. The work of reference [31] investigates the core behavior during a RIA due to a CRE. The occurrence of RIA was also the object of reference [32] after the discovery of two broken control rods at two Swedish boiling water reactor (BWR), the occurrence of a RIA was investigated assuming that any control rod could fall at any time.

Reference [33] discusses the transients that may be of interest in RIA in the LWR technology, which includes the interactions between neutronic and thermal-hydraulics that affect neutron moderation and accident conditions. That work presents fundamentals of NK and TH coupling starting with the stand-alone system modeling (i.e. TH), the 3D NK and fuel

simulation. A relatively recent report by OECD [34] reviewed the conservative safety criteria established during the 1960s and 1970s, within operational and design criteria, including CRE and critical heat flux (CHF), among others. This 2012 report was a result of several OECD task forces/groups that started in 1996.

Considerable work has been made by international organizations to develop coupled TH/NK codes. The work of reference [35] presents three benchmark studies supported by the OECD. Furthermore, references [36], [37], [38], [39], [40], [41] and [42] present efforts on the development of effective algorithms and schemes for TH/NK coupling. References [43] and [44] cover the work on the requirements for TH/NK coupling and feedback effects and on the use of the Monte Carlo particle transport code coupled with a computational fluid dynamic code. More recently, reference [45] presents a list of the main coupled codes used for transient calculations, such as RIA, MSLB, CRE, loss of feed water flow (LOFW) and ATWS. Table 2-1 summarizes the list of codes presented in that work.

Table 2-1 – Coupled TH/NK Packages

Coupled Codes (TH/NK)	NPPs
TRAC-BF1/SKETCH-N	PWR / BWR
RELAP5-MOD3.2/COBRA IIIC	PWR
QUABOX/CUBBOX	PWR
RELAP5-MOD3.2/NESTLE	LWR / AP-1000
RELAP5-MOD3.2.2/PARCS	LWR
RELAP5-MOD3.2/QUABBOX	PWR B&W
RELAP5-MOD3.2.2/3D-NESTLE	PWR B&W
TRAC-PF1/NEM	PWR B&W
ATLHLET/KIKO3D	VVER 440
ATLHLET/DYN3D	VVER 1000
RELAP5/PANTHER	PWR
ATHLET/QUABOX/CUBBOS	BWR
DeCart MOC/PARCS	LWR

The use of the Kalman filter (KF) predictive tool and derived filters, such as the Extended Kalman Filter (EKF), in the nuclear field is not common. The work of reference

[46] discusses the application of KF in a one-dimensional core model for estimation of the neutron flux and allocation of in-core detectors. Reference [47] suggests the use of a set of KF to implement on-line failure detection in the nuclear power plant instrumentation. The study presented in reference [7] shows that the use of a robust KF (a suboptimal state estimator that guarantees a limit on the error variance) to estimate a set of state variables: the neutron density, the precursor density, the average reactor fuel temperature, the coolant temperature inside the reactor and the coolant temperature entering the reactor core.

In addition, reference [8] presents a comparison between two estimation methods for predicting the shutdown reactivity in power reactor: the IPK and EKF, using offline data. That work indicates that the EKF better estimates the sub-criticality under noisy measurement conditions. The work of reference [48] presents qualitative results of the application of both methods under a noise covariance and measurement by applying a first order delay filter in the IPK method. The results indicate that KF is superior in all cases considered, although the tuning task is more difficult.

More recently, reference [49] presented the application of KF based on system identification, which is used for fault detection in a nuclear reactor. The suggested approach allows the parameters of the nonlinear system to be estimated and a fault tolerant control system is designed for the nuclear reactor during power level change operations. The proposed controller is an adaptive critic-based neuro-fuzzy controller. The reactivity model used in that work was first presented in reference [50].

3. METHODOLOGY

Severe NPP accidents represent events that could cause significant damage to the reactor core and that have a very small probability of occurrence. The core damage frequency has been estimated to be between $2x10^{-5}$ per reactor-year [51] (at once in 50,000 reactor-years) and $5x10^{-5}$ per reactor-year [52]. The severity of a nuclear RIA depends on the reactor core design, on the control rod grouping and location, and on the rod reactivity worth [5]. Nevertheless, given the large potential consequences of a severe accident, more and more attention is being paid to modeling of potential initiating events, such as RIAs and station blackout events. To make realistic simulation of such accidents, the NPPs' severe accidents modeling and simulation should cover:

a) Code definition, including its requirements;
b) Scope of the application/work;
c) Plant model development;
d) Definition of the scenarios/boundary conditions;
e) Code implementation;
f) Simulation of particular events;
g) Data acquisition; and
h) Data (i.e. results) analysis.

This work considers three reactors with different-size cores, but with similar designs, to assess the 3D core power distribution and reactivity behavior under CRE RIA conditions. In addition, a reactivity forecasting tool is implemented using a stochastic approach. This chapter presents the code definition, the scope of the problem, the simulation strategy and scenarios, and it provides an overview of the codes used for simulation. Furthermore, it presents the coupling mapping strategy, highlighting the interconnections among the computer codes.

3.1. Simulation Strategy

The modeling strategy includes the TH and NK modeling of each NPP with the standalone P3D & R5 codes, and with the P3D/R5 coupled package. Then, the explorations of

reactivity and power distribution have been carried out through a six step approach, which is shown in Table 3-1.

Table 3-1 – Simulation Strategy

Step	Task	Goals	Code
1	Steady-state standalone neutronic simulation.	Control rod worth calculation for all CRA positions and groups.	P3D
		Identification of the CRA position to be ejected (CRA#8).	
		Identification of the control rod bank/group (CRB) that inserts more than 1$ of reactivity during its ejection (CRB#8).	
2	Steady-state standalone thermal-hydraulic simulation.	Configuration of model's parameters without CRA/CRB#8 ejections.	R5
3	Transient standalone simulations.	Configuration of model's parameters based on the CRA/CRB#8 ejections.	P3D & R5
4	Steady-state coupled simulations.	Simulation and data analysis without CRA/CRB #8 ejection.	P3D/R5
5	Transient coupled simulations.	Simulation and data analysis of the reactivity and power distribution during RIA.	P3D/R5
6	State variable estimation.	Simulation and benchmark of the reactivity during a RIA using EKF.	MATLAB

Table 3-2 shows the NPPs under investigation and Table 3-3 presents the simulation scenarios. The HFP core condition takes the core running at 100% of its nominal power, and the HZP assumes the core running only at 0.01% of it. Besides the simulation of the ejection of one CRA under HZP and HFP core conditions, a CRB ejection is also simulated assuming HZP. The HZP is the most severe core condition for a reactivity initiated accident [5].

Table 3-2 – NPPs under Investigation

NPP	Size	Nominal Power
1	Traditional	2,772 MWt
2	Small	530 MWt
3	Medium	1,061 MWt

The NPP1 CRA/CRB #8 ejection time is assumed to be 0.1 sec based on references [5], [9], [30] and [12]. According to reference [5], the worst possible scenario for a rod ejection accident and its related addition of reactivity occurs within 0.1 sec in LWRs. However, it must be noted that the CRA ejection time depends on the extension of the core mechanical failure and on the reactor coolant pressure during failure. Though the cores have different sizes, to keep the same rod ejection pace, the RIA is set to occur at 0.067 sec (NPP2) and 0.075 sec (NPP3).

Table 3-3 – Simulation Scenarios of Control Rod Ejections

Case	Core Conditions	CRA#1 to 7 at t=0	CRA/CRB#8 at t=0	Transient
a	HFP	Fully/Partially withdraw (see item 6.1 for details)	Fully inserted	CRA#8 fully withdraw in $t \leq 0.1$ sec
b	HZP	Fully/Partially inserted (see item 6.1 for details)	Fully inserted	CRA#8 fully withdraw in $t \leq 0.1$ sec
c	HZP	Fully/Partially inserted (see item 6.1 for details)	Fully inserted	CRB#8 fully withdraw in $t \leq 0.1$ sec

In a first view, the core simulation at HFP reflects the occurrence of a CRE accident during normal operation of the plant, when usually only one control rod group is inserted in the core for safety reasons. Nevertheless, changes in the reactivity are due to the fuel depletion, and the Xenon transients are compensated by the changes in the soluble Boron concentration.

On the other hand, the core simulation at HZP seems very conservative. The core at the NPP startup is critical at very low power and the understanding of a CRE under this condition sounds better and reasonable for safety purposes because inserted rods introduce large

negative reactivity, which allows a higher power increasing from the core initial conditions after the CRA ejection.

3.2. Simulation Codes

The safety analysis of a NPP usually starts with a TH system code that may include point kinetics (PK) or a more complex model to estimate the thermal power generation within the core. The PK solution corresponds to the "zero-dimensional space" (0D) neutronic calculation without radial or axial power profile changes during transients. The NK simulations can be improved by using 3D models. The TH is usually done considering 1D by modeling several parallel channels, which improves the simulation results.

Accidents such as the MSLB; ATWS; LOFW; CRE and CHF have strong TH and NK coupling effects. Therefore, the use of TH models (system models) and 3D NK models (core models) in a coupled way has been increasingly applied to assure the accuracy and reliability of the predictions in the transient analysis. The TH system code usually solves for the mass, energy and momentum balance equations, besides describing control actions; feed water temperature; steam pressure; valves or others systems (it gives the system solution). The NK codes are mostly based on nodal expansion methods within the neutron diffusion theory – the macroscopic cross sections depend on feedback parameters like fuel temperature, moderator density and moderator temperature.

This work uses the P3D and R5 nuclear codes (standalone and coupled), which are advanced computer tools for simulation of normal operation (steady-state) and accidents (transient) scenarios (further information can be found in references [53] and [54]). In addition, the analysis and the EKF and IPK algorithms are implemented using the computing environmental software MATLAB.

3.2.1. PARCS Neutronic Code (P3D)

The Purdue Advanced Reactor Core Simulator (PARCS) is a 3D reactor core simulator spatial kinetics code that solves the steady-state and time-dependent, multi-group neutron diffusion and low order transport equations in three-dimensional Cartesian geometry [18] [55]. Furthermore, it has an embedded simplified TH solution, which accounts for the

feedback effect when running at standalone mode (PARCS uses an internal temperature calculation scheme based on input power). However, P3D is either a computer code that perform standalone calculations for LWR, or that can be coupled directly to the TH system code TRACE-M, or that can be coupled to R5 by means of the PVM interface [56].

P3D is used for NK calculations for both PWR and BWR for rectangular or hexagonal fuel assemblies (FAs). The P3D modeling features include: the capability of 3D physical reactor modeling and simulation or a faster one-dimensional space (1D) (for a dominant flux in the axial direction, for example in BWR) modeling; 3D geometric representation, which can be reduced down to zero-dimensional space (0D) by the choice of adequate boundary conditions; cross section representation, which can have a linear or quadratic dependence on the TH state variables; and TH feedback effect. However, the primarily internal TH solution in P3D is designed for code testing, even with an external solver (i.e. by coupling P3D with a TH code like R5).

Moreover, the main code's features are the following:

i) Eigenvalue calculations, which establish the initial steady-state to perform eigenvalue calculations to have the initial core reactor critical before the transient. There are two eigenvalue calculations: the k_{eff} and the critical boron concentration searches;
ii) Kinetics calculations, which solves the time dependent neutron diffusion equation for prompt and delayed neutrons during transients;
iii) Xenon, which updates the Xenon and Samarium number densities for slow core transients based on the balance equations and on the flux resulting from the eigenvalue calculations;
iv) Decay heat, which is a simplified model of the six groups of decay heat precursors. The precursor equations are solved similar to the delayed neutron equations. Although default values of the precursor fraction and decay constants of the six group are provided for UO_2 fueled cores, the user can specify his own value;
v) Pin power, which is the reconstruction of the pin power to obtain the local pin power; and
vi) Adjoint flux calculations, which are important in determining the reactivity.

Since the first version of P3D (1998), manifold sophisticate spatial kinetics calculation methods have been incorporated into the code, like the coarse mesh finite difference (CMFD) to solve homogenized nodes, allowing a fast transient calculation, skipping expensive nodal calculations when there is no strong flux variation during the transients. P3D code's language is FORTRAN90 and it has been tested in distinct operating systems, including UNIX, LINUX and Windows OS. P3D has been used for NK calculations by the United States Nuclear Regulatory Commission (NRC) [18]. This work uses the 2.71d PARCS version.

3.2.2. RELAP5 System Thermal-Hydraulic Code (R5)

The Reactor Excursion and Leak Analysis Program (RELAP) is a tool for analyzing loss of coolant accidents (LOCA) and systems transients in LWR [18]. RELAP nuclear code has been developed at Idaho National Laboratory (INL) in the last 30 years. The USA Department of Energy (DOE) and the NRC, among others institutions, have been supporting its development.

R5 (i.e. version 5 of RELAP) has been used for licensing and regulation, evaluation of operator guidelines and plant accident analysis. The code was developed to provide the first order effect needed for accurate prediction of system transients and to be cost effective enough to allow sensitivity and parametric studies. Although it was initially designed for nuclear applications, the last version can be used for nuclear and nonnuclear applications involving vapor, liquid, no condensable gases and nonvolatile solutions [54].

R5 calculates the expected evolution of TH properties during steady-state or transients, including the interaction among system components (R5 uses an internal temperature calculation scheme based on input power). It implements a two fluid and six-equations model to simulate the two phase coolant behavior, and consequently the system's TH behavior. The R5 numerical solution is based on semi-implicit finite-difference. Although it was originally designed to model TH phenomena in 1D volume, it can also be used to simulate more complex systems using multiple channels geometry – for example, the NPP core can be simulated by up to a few hundred parallel nodes connected at several axial positions. However, the PK model inherent to R5 cannot consider multidimensional effects caused by spatial variations of feedback parameters [5].

R5 is capable of modeling LWRs system components like valves, pumps, pipes, electric heaters, turbines, compressors, separators and pressurizes, among others. The code is specified for analyzing components' interactions without offering detailed simulation of fluid flow within components [57] and the mathematical models work together with an efficient code structure. The material properties are embedded into the code, but the user can supply them.

To summarize, R5 models the interaction of the reactor coolant system and the core for LOCA accidents and operational accidents (e.g. ATWS, loss offsite power, LOFW, station blackout and turbine trip) [54]. Moreover, R5 can be used to model the primary and secondary systems of a nuclear power plant, together with the system operation logic. This work uses the RELAP5/Mod3.2 version.

3.2.3. P3D/R5 Coupled Package

The correct use of coupled computer tools, e.g. R5 and P3D, to address the interaction among TH and NK phenomenon implies an appropriate NK and TH spatial meshing. The core nodalization in the radial and axial directions - and their correlation - has a significant effect on determining the local core TH parameters and the power distribution during transients. The TH conditions provided by the external systems code R5 at every time step to the NK spatial kinetics code P3D are: the moderator temperature; the vapor and liquid densities; the void fraction; and the averaged, centerline and surface nuclear fuel temperature. These parameters are required at each NK node for the feedback calculation. The nodal/space dependent power distribution is then calculated by P3D and sent to R5, which calculates the heat conduction in the core heat structures.

The TH/NK coupling strategy allows a more complete NPP systems analysis than the one done using standalone codes, which includes the feedback effect, the core NK behavior and the TH dynamics. The coupling could be internal or external:

i) the internal scheme implies that the set of TH and NK integral-differential equation systems will be solved together in one code – this is complicated, computer and time consuming; and

ii) the external coupling scheme is based on standalone codes exchanging external data. This scheme allows the user to master each code and to include additional calculations within third party software.

The P3D/R5 external TH/NK coupling strategy is presented in reference [36]. The TH code R5 addresses all the TH issues and the NK code P3D spatial kinetics solves the NK challenges. To be able to exchange parameters between both codes, according to a mapping predefined strategy, a General Interface (GI) is set. In the P3D current version, the GI is nested into the NK code. Figure 3-1, derived from the coupling scheme presented in reference [36], shows the TH/NK proposed coupling scheme.

Figure 3-1 - TH/NK Coupling Scheme

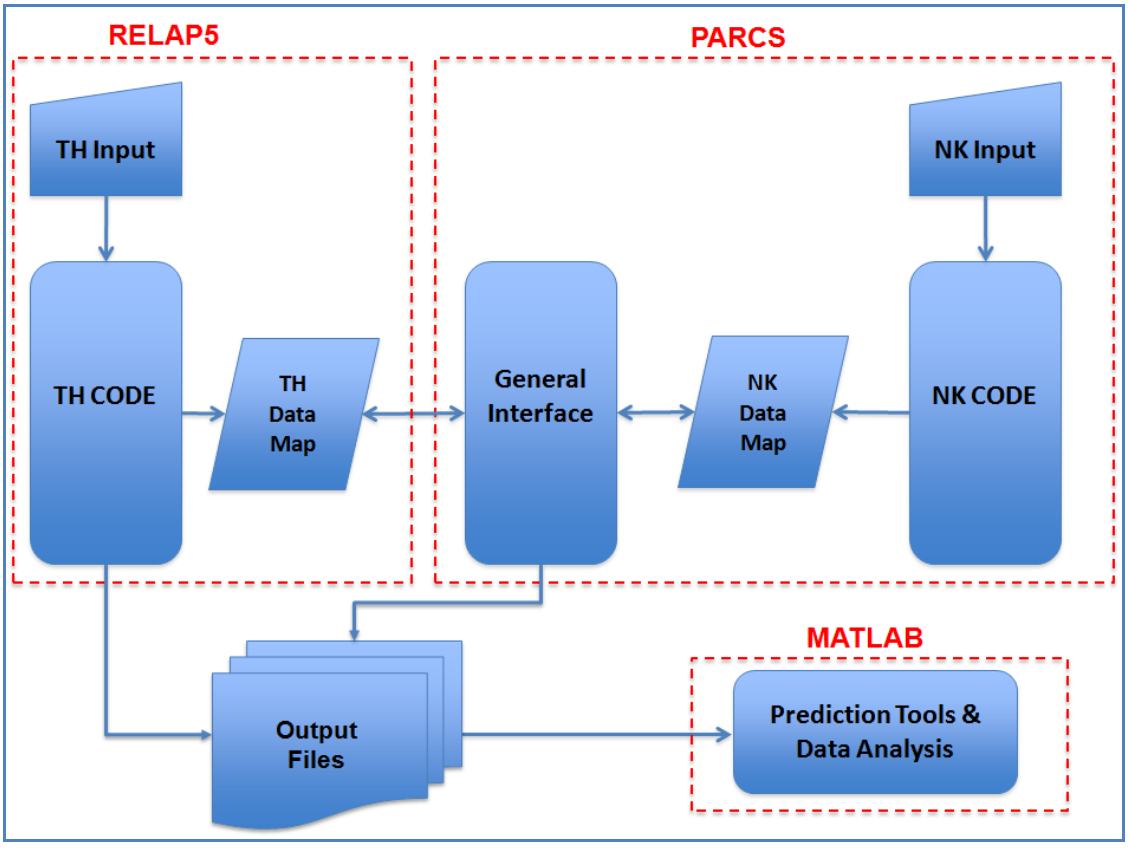

3.2.3.1. P3D/R5 Mapping Strategy

The P3D and the R5 codes work together (i.e. coupled) exchanging information through a GI, which manages the data flow between both codes using the PVM software package. The PVM allows the use of both codes as one single software. To be able to correctly exchange

the information between the codes, the NK nodes structure and the TH channel structure must match each other. This is done by the generation of an input file named MAPTAB. The adequate generation of the MAPTAB file and the correct determination of the mapping weight factors are among the most important tasks to obtain accurate coupled code solutions [53].

When coupled, a TH channel may have a one-to-one relation to a NK node, or a TH channel may consists of several NK nodes, or NK node can be divided in two or more TH channels. Nevertheless, the mapping determines where to set NK node power in the TH channel (for both direct moderator heating and heat structure fuel source) and where to assign TH properties in the NK node. Therefore, the coupling of the TH channels to the NK nodes (in radial and axial directions) depends on the adequate assignment of mapping weights between the two meshes [53].

The mapping is a correlation between grouped TH channels (or volumes/pipes) and grouped NK nodes (or regions/cells) in the radial and axial direction [15]. The mapping, and therefore the grouping, could consider the geometry, the TH properties, the fuel burn up, the peaking factors (power distribution), the neutron flux or the control rod patterns – it could also consider a mix of them. In this work, mapping is done by using the core model geometry. The mapping weight is based on the volumetric geometric fraction that correlates the TH and NK mesh in the radial and axial direction. Therefore, there are two main cards in the MAPTAB file responsible for the mapping:

a) "Card 1" correlates the TH channels card numbers (R5) and the NK nodes card numbers (P3D) by a weighting factor; and
b) "Card 2" correlates the heat structures components card numbers (R5) and the NK node card numbers (P3D) also by a weighting factor.

The mapping process adopted here uses an explicit generation method: the user is responsible for the assignments of the weighting factors. Then, a MATLAB script generates the MAPTAB file with both Card 1 and Card 2 described above. The mapping process follows the steps suggested by reference [53]:

i) Determination of the radial weights required for mapping the TH channels to the NK nodes. The radial weights will repeat axially throughout the model. The sum of the radial weights for each NK node must be 1; and

ii) Determination of the axial weights required for aligning the TH cells/volumes or heat structures to the NK axial regions. The sum of the axial plus radial weight must also be 1 for each node.

Therefore, “Card 1” is generated by first correlating the TH channels to the NK nodes in the horizontal direction. Figure 3-2 presents a mapping example for the NPP1 core configuration. The radial weights repeat axially at the same horizontal node position, however, with the radial node numbering increasing for each region axially. The radial weight is one unit if a NK node is contained within only one TH channel and it is less than one if it is contained in more than one TH channel (the weight is based on the volumetric geometry of both TH and NK nodes).

Next, by using the axial mesh and nodalization geometry of the core, the axial weights are found by aligning the centers of the TH volumes and the centers of NK nodes (both P3D and R5 calculate the properties in the regions/volume center), assuming that each TH cell receives NK contribution from the inlet and outlet adjacent regions, i.e. the TH volume *N* receives NK heat from the *n*-1 (inlet), *n* and *n*+1 (outlet) regions, and that the fluid flows in *x* direction, as presented in Figure 3-3. The axial weight is proportional to the geometric volume fractions between TH channels and NK nodes.

Figure 3-2 – Radial NK Nodes to TH Channels Mapping (1/4 core)

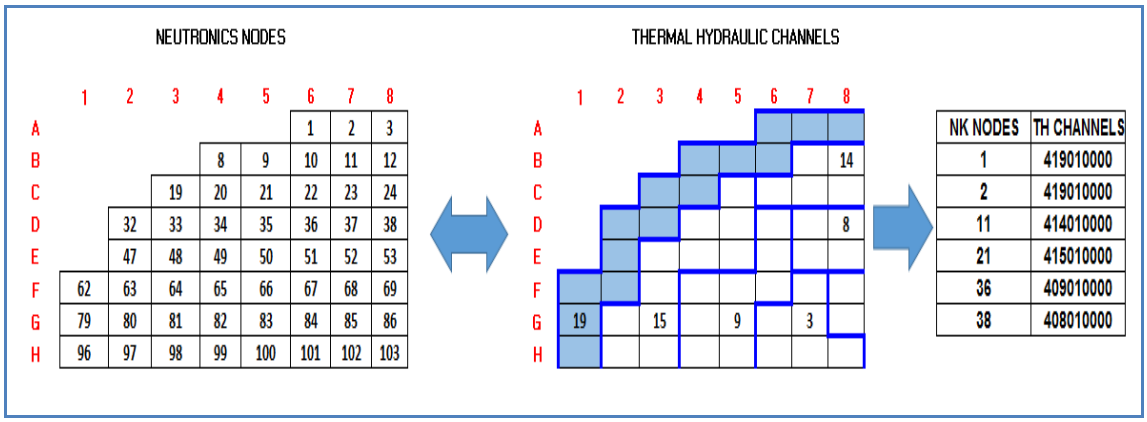

The final “Card 1” mapping’s weights are found by multiplying the radial and axial weights. The sum of the weights (axial and radial) must be equal to unity.

Figure 3-3 – Axial Mapping TH Channels (volumes) to NK Regions (heat structures)

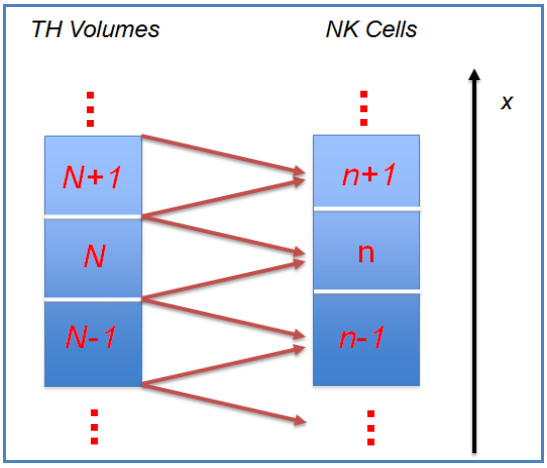

A similar procedure generates the "Card 2" weights. The radial weight generation considers the numbers of channels belonging to each node, and the sum of the weights per node must be one. The axial weights are found by first aligning the heat structures' cells, which represents the fuel node, and neutronic regions' centers, and then assign weights that consider the vertical geometry of the channels. For example, if one node is fully contained within the vertical top and bottom heat structures *x* coordinates, its weight will be unity. "Card 2" weight factors are also calculated by the multiplication of axial and radial weights.

3.2.4. MATLAB Computing Environmental Code

The Matrix Laboratory (MATLAB) is a high-level numerical computing environmental software developed by The MathWorks Inc [58] for technical computing and programming such as data acquisition, data analysis, mathematical modeling, algorithm development, parallel computing, and web development. MATLAB can be used for applications that include signal processing and communications, image and video processing, control systems, test and measurement, computational finance, computational biology, code generation and verification, application deployment, database connectivity and reporting [58].

The MATLAB's development started in the late 70s at University of New Mexico, and it reached other universities and laboratories. In 1984, MathWorks was founded and MATLAB started being used worldwide, not only for control engineering, but also for other science domains like image processing. MATLAB uses specific languages and codes that are input in by its command window (functions and scripts, among others). In addition,

MATLAB has been used widely in the last 25 years, in areas of engineering, science and economics, in academic and research areas and in the industry.

MATLAB also allows the interfacing with codes written in other languages, including C, C++, Java and FORTRAN, and it allows the connection of hardware, like field-programmable gate array (FPGA) or programmable logic controller (PLC) for hardware description language (HDL) coder and verification (hardware-software co-design and prototyping). MATLAB includes numerous tool box and packages, like Simulink, which adds graphical multi-domain simulation and model-based designs for dynamic systems, and MuPAD that allows symbolic computing capabilities. This work uses the R2012b MATLAB version.

3.3. P3D & R5 Configuration

The use of nuclear codes implies not only knowledge of the problem and of the model being simulated, but also the adequate selection of the code's parameters. To have the simulation results consistent among the three codes, the standalone simulation of one code depends on the use of parameters generated by the other code. For example, the reactivity coefficient generated in the P3D code must be plugged in the R5 transient calculations. Therefore, prior to a new set of simulations, the following configurations are performed:

i. The control rod assemblies' initial condition is found using the P3D simulation results: the initial position is the one that allows the initial k_{eff} critical;
ii. The configuration process depends on a set of iterations among the standalone and coupled versions of R5 and P3D. Furthermore, to be able to achieve the steady-state and generate the R5 restart file, which is used for the transient calculation, the mass flow rate, as well as the fluid temperature and density, must be consistent;
iii. The moderator and Doppler reactivity coefficients used in the R5 code come from the P3D steady-state simulation. The R5 standalone needs both coefficients to correctly simulate the control rod ejection transient;
iv. The averaged fuel temperature and moderator density during steady-state must be calculated using the P3D/R5 coupled code. The P3D standalone must use the same value for its TH calculation;

v. The P3D/R5 coupled code automatically uses the neutronic calculation from the P3D and the TH from the R5. Therefore, the R5 heat structure source information presented in the coupled code is ignored during simulation. However, for the R5 standalone runs, the heat structure source must be configured based on the P3D simulations results; and

vi. The initial mass flow rate, the pump velocity and the steam generator mass flow rate condition are changed proportionally to the reactor power for both NPP2 and NPP3 at the R5 model.

These tasks are not sequential and that they are performed more than once for each set of runs.

3.4. Chapter Summary

This chapter presented the NPPs under investigation, the simulation strategy and simulation scenarios. Furthermore, it briefly described the R5, P3D and MATLAB codes used for modeling and simulation. The coupling and mapping strategy was also presented. The simulation and strategy scenarios include first the identification of the control rod to be ejected, CRA/CRB#8, and then the procedure to carry on the P3D/R5 simulation of three base cases: HZP and HFP CRA#8 ejections and a CRB#8 ejection, also under HZP core conditions. The exploration of reactivity and power distribution has been carried out through a six-step approach. To have the results consistent among the three codes, the parameters resulting from the standalone simulations set both P3D and R5 configurations prior to new runs.

4. MAIN REFERENCE NPPs DATA

The NPP1 power plant design is based on the 2,772 MWt PWR B&W, which is well known by several studies published after the TMI Unit 1 accident [59]. The main TMI NPP's technical specifications can be found in the 1999 benchmark study released by the NEA/OECD for a MSLB [12]. Furthermore, the TH model is based on the MSLB R5 model developed by University of Michigan [60]. Therefore, only the main reactor parameters model will be presented here – further information about the design can be found at reference [12]. Although the PWRs represent the largest part of the World's NPP fleet, SMRs could be deployed within the next decade and their development motivates the assessment of inherently safe performance of smaller cores relative to RIAs. Therefore, the smaller core dimensions are based on the mPower SMR [61] [62] [63], and the medium size core dimensions are based on the International Rector Innovative and Secure (IRIS) NPP [64].

The severity of the transients is strongly dependent on individual core designs and control rod groupings. Therefore, the effect of shrinking the core is compensated for by ejecting a CRA/CRB that presents similar reactivity worth. For simplicity and due to the small changes in the reactor coolant TH conditions, during the fast transient behavior, the secondary mass flow rates of NPP2 and NPP3 have been taken proportional to the reactor power.

4.1. NPP1 Main Modeling Data

4.1.1. General Data

The NPP1 core has a 17 by 17 assembly's configuration common nowadays. There are 177 FA and 64 reflector assemblies (total of 241 assemblies: each one is 21.81 cm width). There are 60 CRAs grouped into 7 banks (full length control rods), as presented in Table 4-1. The core active height is 357.12 cm and there is a 21.81 cm height reflector on the top and another one at the bottom of the core, adding to a total height of 400.74 cm.

The position of the CRA insertion is given from the bottom of the lower reflector: a height of 378.93 cm means a completely withdrawn CRA and a height of 36.23 cm means a completely inserted CRA. The insertion is measured in steps, each one of 0.35 cm (0 steps equals a completely inserted CRA and 971 steps equals a completely withdraw CRA).

Table 4-1 – CRA Banks

CRA Bank	Number of CRA per Core	Purpose
1	8	Safety
2	8	Safety
3	8	Safety
4	8	Safety
5	12	Power Tuning
6	8	Power Tuning
7	9	Power Tuning

The main FA geometry data are presented in Table 4-2. In addition, Figure 4-1 and Figure 4-2 present the reactor vessel and coolant system top and side views.

Table 4-2 - Fuel Assembly Geometry

Item	Value
Pellet Diameter [mm]	9.39
Outside clad diameter [mm]	10.93
Clad thickness [mm]	0.67
Fuel Rod Pitch [mm]	14.43
Number of fuel pins	208
Number of guide tubes	16
Number of instrument positions	1

Figure 4-1 – Reactor Vessel and Coolant System Top View

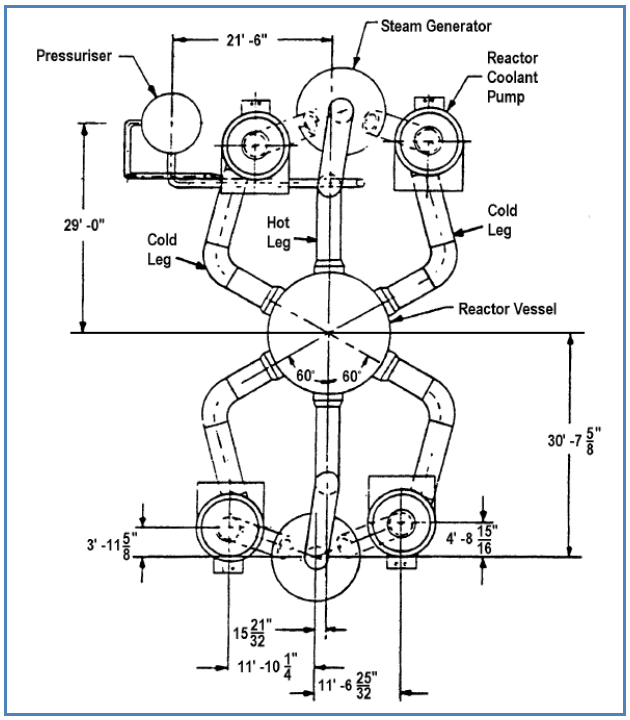

Source: Reference [12]

Figure 4-2 - Reactor Vessel and Coolant System Side View

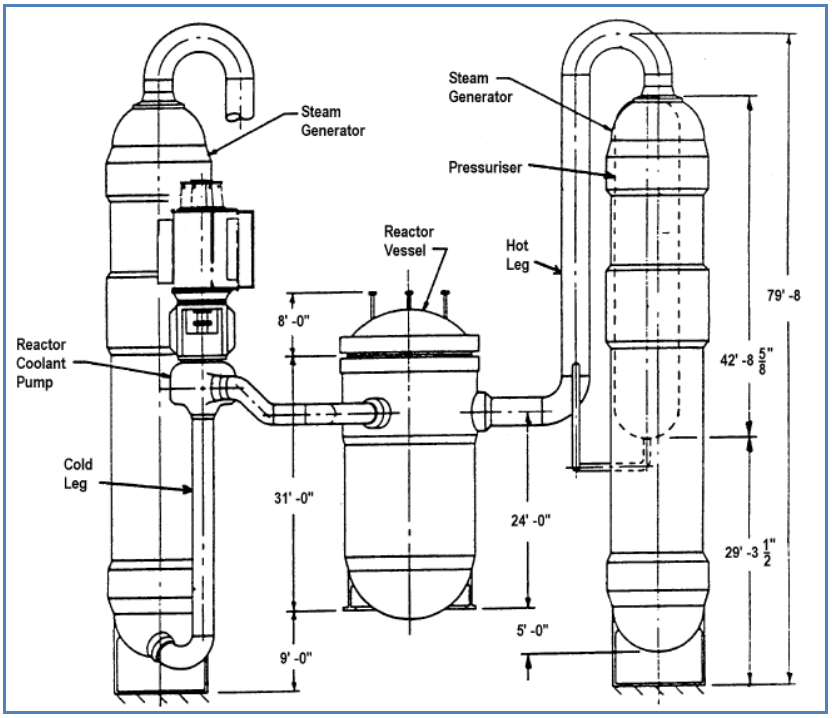

Source: Reference [12]

4.1.2. Main NK Data

For NK modeling purposes, each radial node has the same FA width of 21.81 cm and each assembly is considered as neutronically homogeneous. The core radial FA and control rod configurations are presented in Figure 4-3, where the number within an assembly indicates the CRA assembly bank identification. Figure 4-4 presents the NK nodes numbering automatically generated by the P3D code.

Figure 4-3–FA and Control Rod Radial Configuration

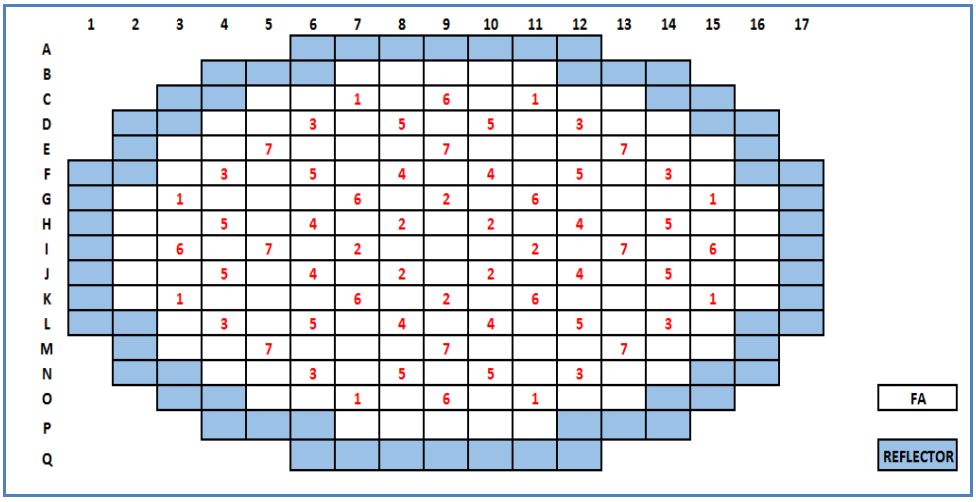

Figure 4-4 - NK P3D Core Nodalization

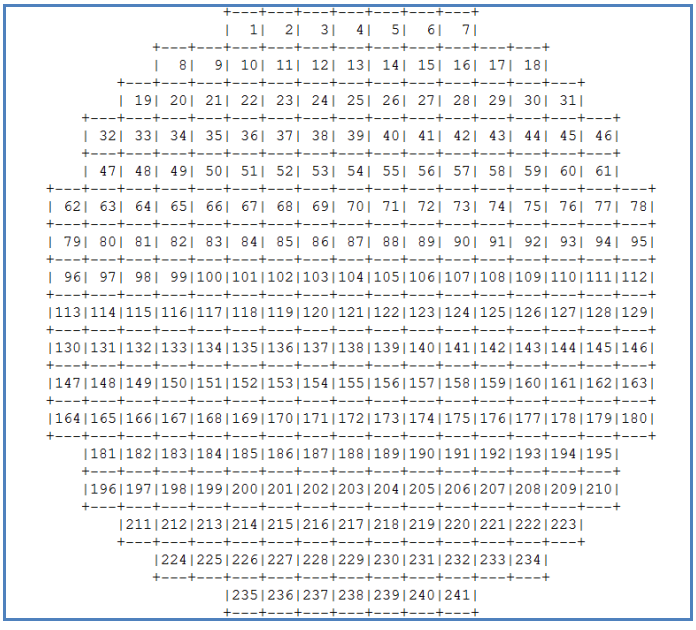

The FA has different U^{235} enrichments and burn up (the 2D quarter core map is presented in Figure 4-5), and different number of burnable absorbers. The Boron concentration, according to reference [12], is 5 ppm. The reactor is assumed to be in end of cycle (EOC) – 650 effective full power days (EFPD) – 24.58 GWd/MT, and with equilibrium of Xe and Sm concentration. There are 30 assemblies' types within the core (29 FA plus the reflector) defined by material composition and burn-up, as can be seen in Table 4-3. The set of cross sections was provided by University of Michigan [53], according to the NEA/OECD benchmark exercise – there is no Boron dependence on the NK cross section provided for the MSLB exercise. Axially, there are different compositions for each assembly – each composition has a complete set of diffusion coefficients and macroscopic cross sections for scattering, absorption, and fission as a function of the moderator density and fuel temperature. The cross section library information, together with the axial core composition, which is defined by the material design and burn-up, can be found in reference [12]. The core is also divided axially in 28 NK regions, according to Figure 4-7 (a).

Figure 4-5 - NK P3D Core Nodalization

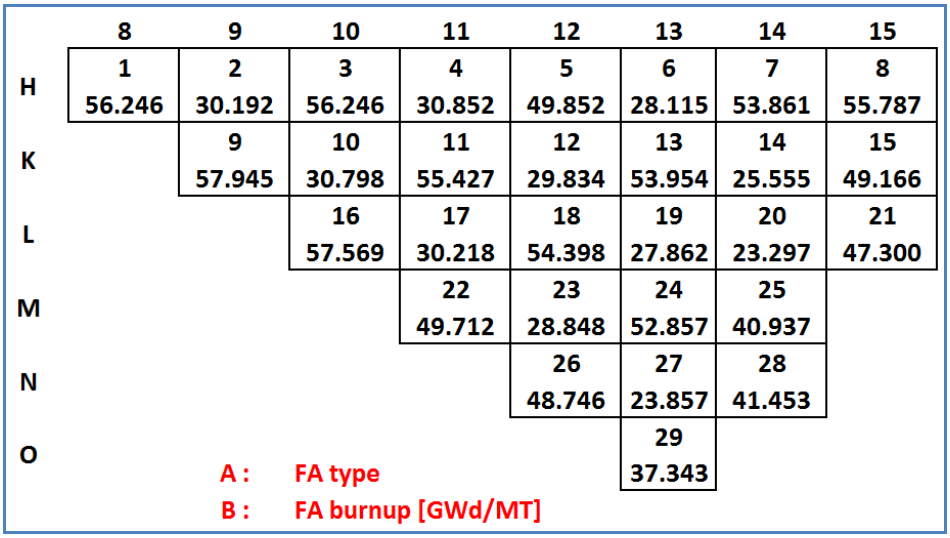

Table 4-3 – Assembly Types Main Data

FA type	Enrichment [w/o]	Burnable Poisson [%]	Gd Pin
1	4.00	No	No
2	4.95	3.5	4

FA type	Enrichment [w/o]	Burnable Poisson [%]	Gd Pin
16	4.95	3.5	4
17	4.95	3.5	4

FA type	Enrichment [w/o]	Burnable Poisson [%]	Gd Pin
3	5.00	3.5	4
4	4.95	3.5	4
5	4.40	No	No
6	5.00	No	4
7	4.85	3.5	4
8	4.85	3.5	4
9	4.95	3.5	4
10	4.95	3.5	4
11	4.85	3.5	4
12	4.95	3.5	4
13	5.00	3.5 pulled	4
14	5.00	No	8
15	4.95	No	8

FA type	Enrichment [w/o]	Burnable Poisson [%]	Gd Pin
18	4.95	3.5	4
19	5.00	3.5	4
20	4.40	No	No
21	4.85	3.5	4
22	4.40	No	No
23	4.95	3.5	No
24	4.95	3.5	4
25	5.00	No	8
26	5.00	No	4
27	5.00	No	No
28	4.95	3.5	4
29	5.00	No	4
30	Reflector		

The NK model considers two prompt and six delayed neutron groups. The delayed neutrons data (time constants and fraction of delayed neutrons) are shown in Table 4-4. The energy release per fission for the two prompt neutron groups is 0.3213e-10 and 0.3206e-10 W-s/fission. The effective decay heat energy fraction of the total thermal power at steady-state is 0.07143. The prompt neutron lifetime λ is 0.18445e-04 seconds.

Table 4-4 – Delayed Neutron Group Decay and Fraction Data

Group	Decay Constant [s^{-1}]	Fraction of Delayed Neutrons [%]
1	0.012818	0.0153
2	0.031430	0.1086
3	0.125062	0.0965
4	0.329776	0.2019
5	1.414748	0.0791
6	3.822362	0.0197
Total Fraction of Delayed Neutron:		0.5211

4.1.3. Main TH Data

For TH purposes, the active core is divided axially into six fuel volumes and two reflectors (see Figure 4-7 (b) for the axial height). Radially, there are 18 TH channels and one channel that represents the reflectors (channel 19), as shown in Table 4-5 and Figure 4-6.

Table 4-5 – TH Volumes

Channels	Location	Flow Area Equivalent
1 to 6	Inner Ring	7.5 FAs
7 to 12	Middle Ring	10 FAs
13 to 18	Outer Ring	12 FAs
19	By pass	12 FAs

Figure 4-6 – TH Core Radial Configuration

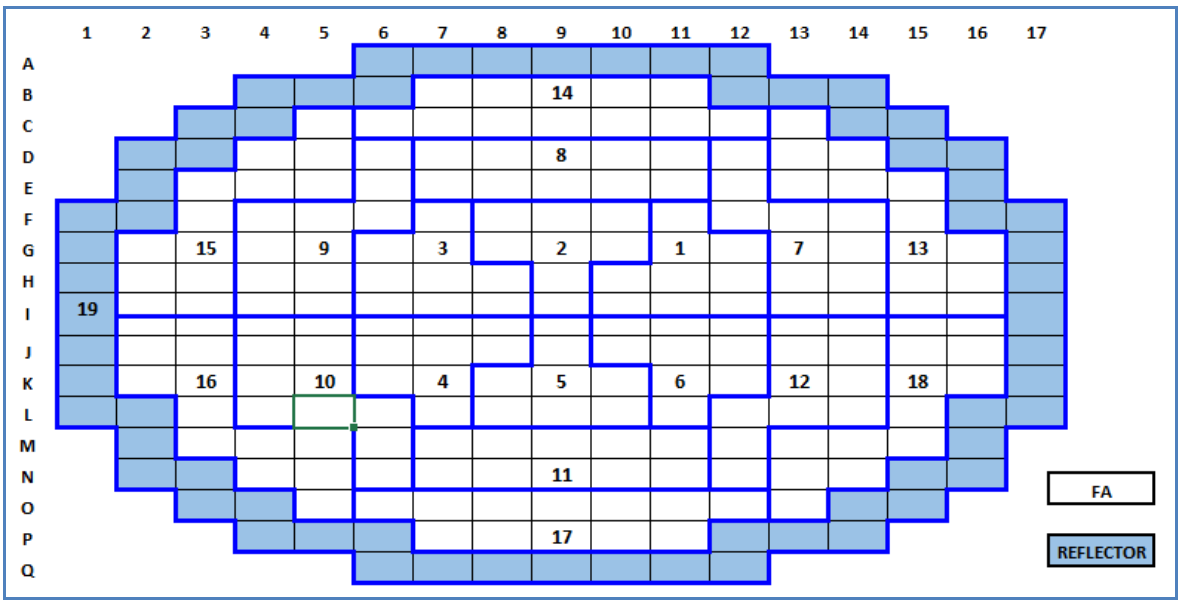

Figure 4-7 – (a) Axial NK Nodes and (b) Axial TH Regions

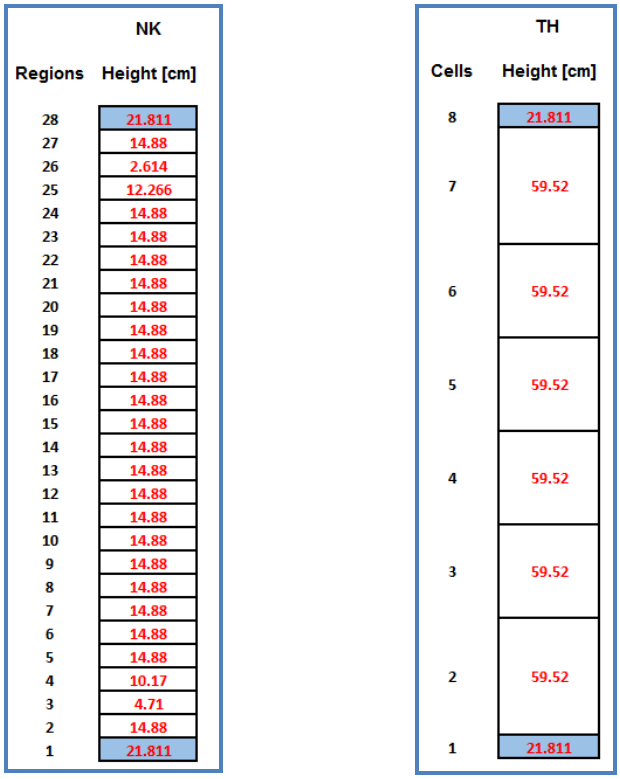

NK

Regions	Height [cm]
28	21.811
27	14.88
26	2.614
25	12.266
24	14.88
23	14.88
22	14.88
21	14.88
20	14.88
19	14.88
18	14.88
17	14.88
16	14.88
15	14.88
14	14.88
13	14.88
12	14.88
11	14.88
10	14.88
9	14.88
8	14.88
7	14.88
6	14.88
5	14.88
4	10.17
3	4.71
2	14.88
1	21.811

(a) **(b)**

The model of NPP1 has two loops with once-through steam generators (OTSG), each one with one hot leg and two cold legs. There are four reactor coolant pumps. All reactor vessel design and volume data, needed for the R5 modeling, can be found in reference [12]. Nevertheless, the main NPP1 data is presented in Table 4-6.

Table 4-6 –Thermal-Hydraulic Main Data

Parameter	Value
Total Core Power	2,772 MWt
Operating Temperature	318 ºC
Water Volume	113.6 m^3
Inlet Coolant Operating Temperature	291 ºC
Outlet Coolant Operating Temperature	318 ºC
Core Pressure Drop	200 kPa
Average Core Coolant Velocity	5.03 m/s

Parameter	Value
Cold Leg Coolant Velocity	14.69 m/s
Hot Leg Coolant Velocity	19.45 m/s
Lower plenum pressure	15.36 MPa
Outlet plenum pressure	15.17 MPa
Reactor Coolant Flow Rate (4 pumps)	5,668 kg/s/pump
Coolant System Pressure	14.96 MPa
Total Coolant System Flow Rate	17,602.2 kg/s
Core Flow Rate	16,052.4 kg/s
Bypass Flow Rate	1,549.8 kg/s
Feed Water/steam flow per Steam Generator	761.59 kg/s
Steam Generator Outlet Pressure	6.41 MPa
Steam Generator Outlet Temperature	299.48 ºC
Steam Temperature	299 (20 ºC superheated)
Initial Steam Generator Inventory	26,000 kg
Feed Water Temperature	237.78 ºC

The R5 TH cards numbering (the nodalization scheme) are presented in Table 4-7.

Table 4-7 – R5 TH Nodalization Scheme

Components	Cards Numbers
Loop A Volumes - Primary Side	100 to 149
Loop A Volumes – Secondary Side	150 to 199
Loop B Volumes – Primary Side	200 to 249
Loop B Volumes – Secondary Side	250 to 299
Small Components Volumes	300 to 399
Core and pressurized Volumes	400 to 499
Loop A Junctions – Primary Side	500 to 549
Loop A Junctions – Secondary Side	550 to 599
Loop B Junctions – Primary Side	600 to 699
Loop A Junctions – Secondary Side	650 to 699

Components	Cards Numbers
Small Components Junctions	700 to 799
Core and pressurized Junctions	800 to 899

The R5 TH nodalization, derived from reference [60], is shown in Figure 4-8.

Figure 4-8 – R5 TH model

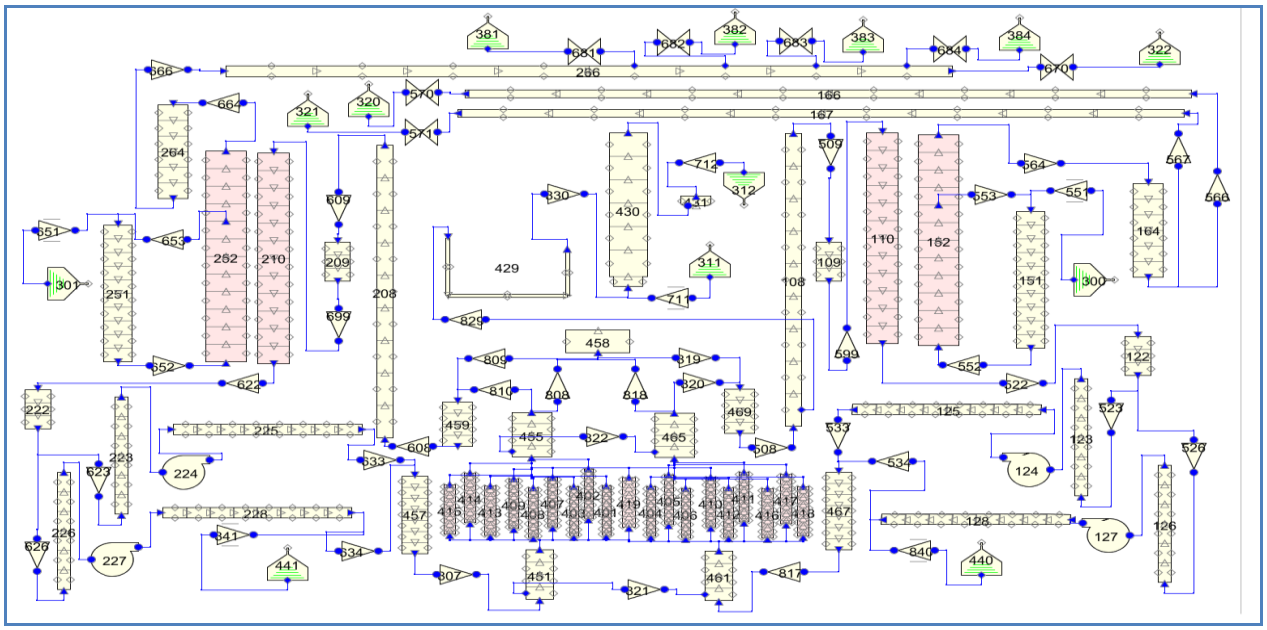

Source: Reference [60]

4.1.4. NPP1 NK/TH Coupling Scheme

The mapping scheme, i.e. the spatial mesh overlays between NK nodes and TH channels is one of the inputs for the P3D/R5 coupled code. The TH and NK models must consider an adequate number of channels and nodes (radial), as well as volumes and regions (axial). A very simple TH mesh together with a very simple NK nodalization (or vice-versa) may not provide an accurate solution.

The TH/NK radial mapping is presented in Figure 4-9. It can be seen there are one NK node per FA and 19 TH channels (each channel with the number of FA presented in Table 4-5). The nodes from 113 to 129 are contained within two distinct channels, with the same geometry. Thus, the weight factor for each node/channel is 0.5 (its sum must be 1).

Figure 4-9–TH/NK Mapping Scheme

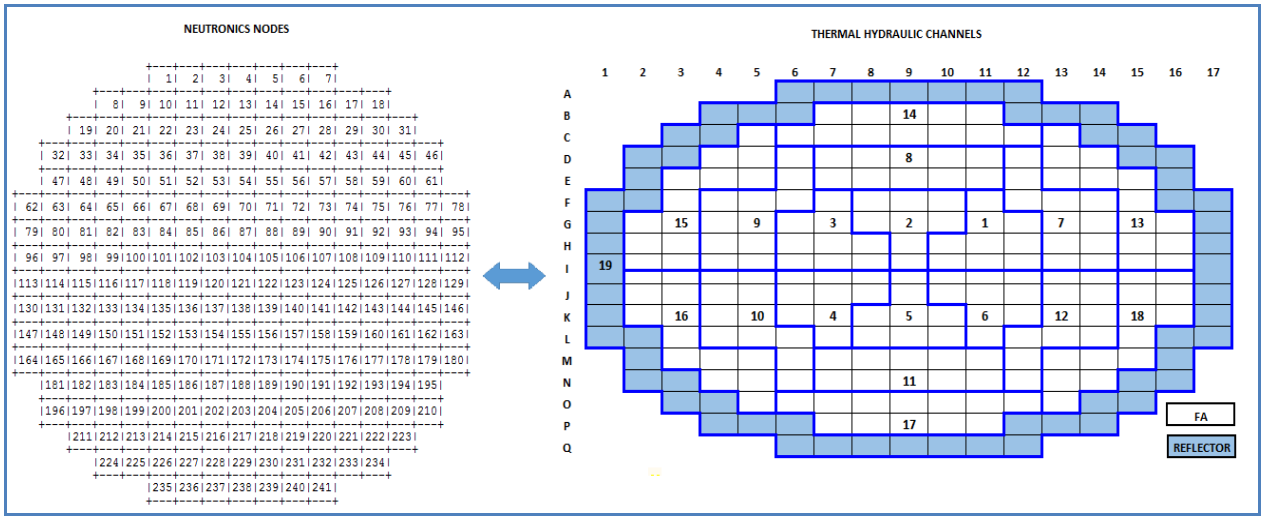

Figure 4-10 shows the axial mapping between the TH channels and the NK cells. The top and bottom cells are the reflectors. The axial TH middle channels (from 2 to 7) contain the NK regions that represent the active core. Although there is a numbering mismatch between both nodalizations, according to the MSLB benchmark exercise [12], each NK region is contained within only one TH volume, which makes the mapping process straight-forward based on the geometry of the TH and NK nodalization. The axial weight factor is then calculated for each TH cell by the equation below:

$$w_{i,j,k} = 1 - \left(\frac{d_j}{h_i} \right) \tag{4-1}$$

where *i* is the inlet TH axial volume; *j* is outlet TH channel; *k* is the inlet or outlet NK region; *d* is the axial distance from the TH inlet/outlet junction to the NK neutronic node and *h* is the inlet/outlet TH cell height. It is assumed that the bottom reflector has no inlet region and the top reflector has no outlet region.

Figure 4-10 – TH/NK Axial Mapping

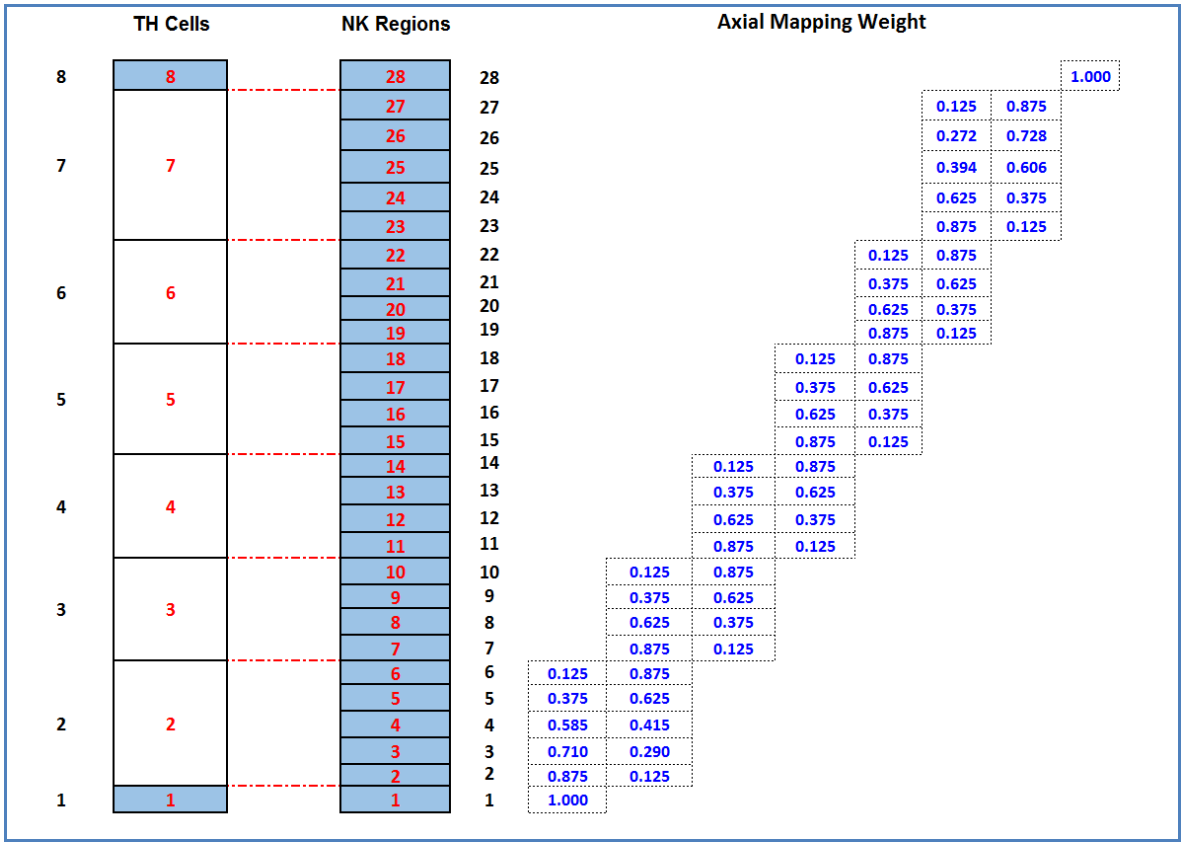

The final weight factors are calculated by the multiplication of the radial and axial weights. It is worth nothing that the weight factor sum for each NK node, radial and axial, must be always one. Last, a MATLAB script generates the Card 1 and Card 2.

4.2. NPP2 Main Modeling Data

The NPP2 core has an 11 by 11 assembly configuration which comes from past design features. There are 113 FA each one of 21.81 cm width (44 reflector assemblies plus 69 FAs – 28 of 69 have control rod assemblies). The core NK and TH axial regions are presented in Figure 4-11. The core active height is 241.30 cm. There is a 14.74 cm height reflector in the top and another one in the bottom of the core, adding to a total height of 270.78 cm.

Figure 4-11–– (a) Axial NK Regions and (b) Axial TH Volumes

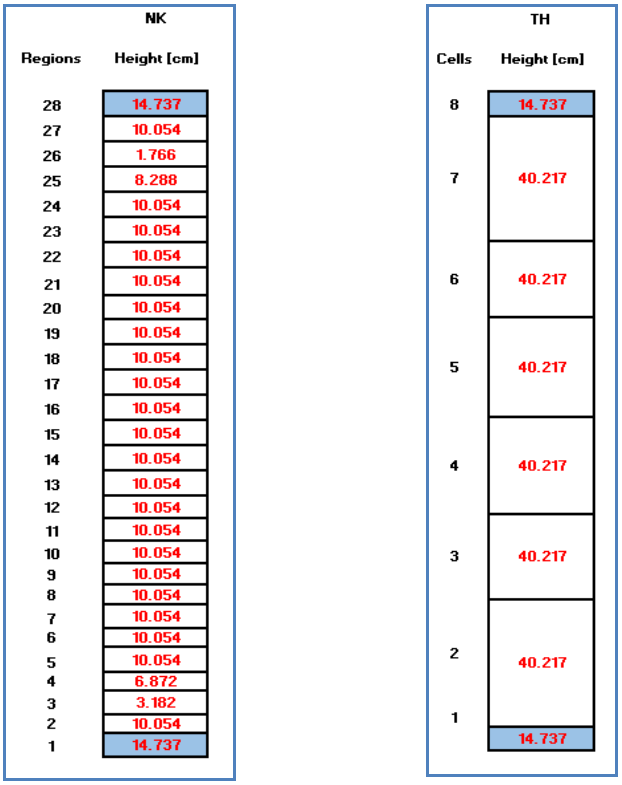

NK	
Regions	Height [cm]
28	14.737
27	10.054
26	1.766
25	8.288
24	10.054
23	10.054
22	10.054
21	10.054
20	10.054
19	10.054
18	10.054
17	10.054
16	10.054
15	10.054
14	10.054
13	10.054
12	10.054
11	10.054
10	10.054
9	10.054
8	10.054
7	10.054
6	10.054
5	10.054
4	6.872
3	3.182
2	10.054
1	14.737

TH	
Cells	Height [cm]
8	14.737
7	40.217
6	40.217
5	40.217
4	40.217
3	40.217
2	40.217
1	14.737

(a) **(b)**

The core radial configuration, compared to the core of NPP1, is presented in Figure 4-12. It can be seen that the number of TH channels was reduced from 19 to 13 (including the bypass region). The CRA assembly locations are show in Figure 4-13, where the numbering indicates the CRA assembly bank.

Figure 4-12–NPP2 Radial Core Configuration Compared to NPP1

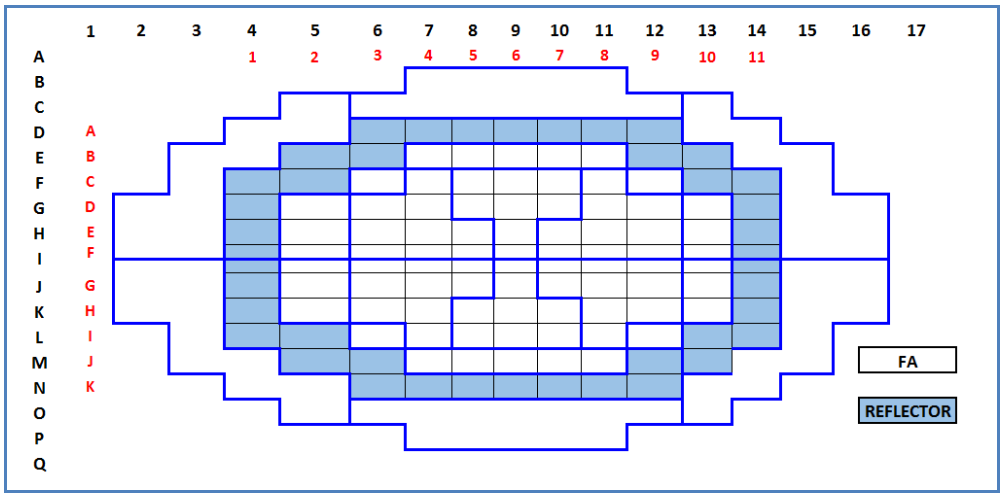

Figure 4-13 – CRA Core Configuration

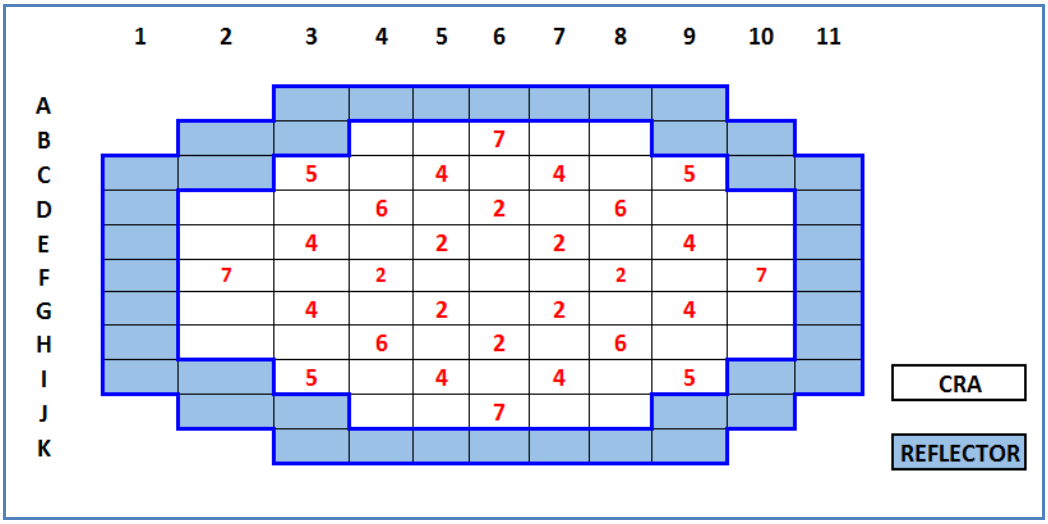

Figure 4-14 presents the radial NK nodes to TH channels mapping. The number of nodes was also reduced to 109 for each NK region. The nodes from 50 to 60 are contained in two different channels each one and, therefore, the weight for each node/channel is 0.5.

The axial mapping between the TH cells and the NK regions follows the same procedure presented in Figure 4-10 (the total height has changed, but the TH cells and NK regions ratios are the same).

Figure 4-14 – Radial NK Nodes to TH Channels Mapping

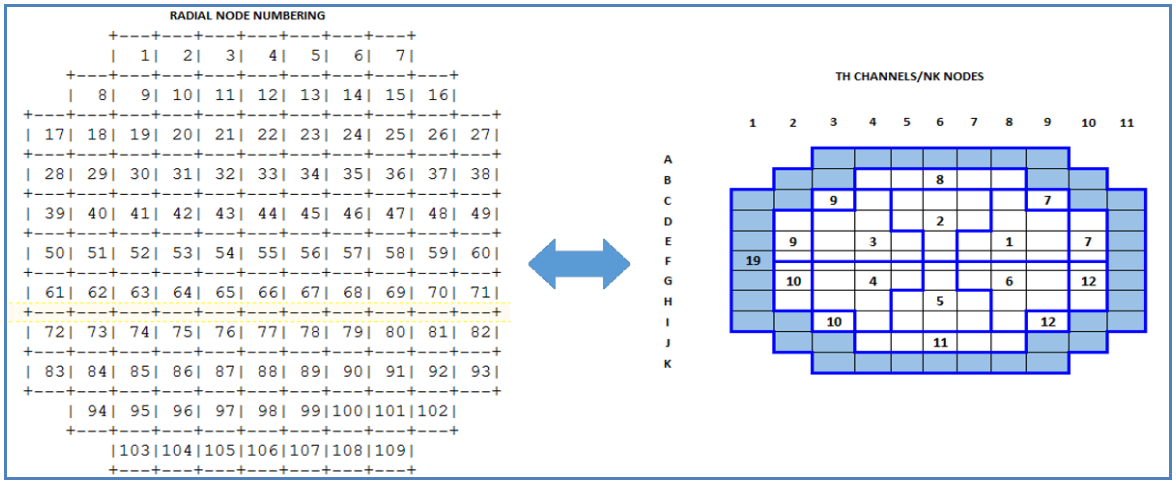

The position of the CRA insertion within the core is given from the bottom of the lower reflector: a height of 256.04 cm means a completely withdrawn CRA and a height of 14.74 cm means a completely inserted CRA. The insertion is measured in steps, each one of 1.13 cm

(0 step is equal to a completely inserted CRA and 228 steps are equal to a completely withdraw CRA). The TH channel areas have changed according to Table 4-8:

Table 4-8 - TH Channels and FA equivalent for NPP2

TH Channel	Number of equivalent FA	Flow Area (m^2)
1	7.5	0.19
2	7.5	0.19
3	7.5	0.19
4	7.5	0.19
5	7.5	0.19
6	7.5	0.19
7	3.5	0.09
8	5	0.13
9	3.5	0.09
10	3.5	0.09
11	5	0.13
12	17.08	0.09
19	17.08	0.45

4.3. NPP3 Main Modeling Data

The NPP3 core has a 13 by 13 assembly configuration. There are 155 FA each one of 21.81 cm width (50 reflector assemblies and 105 FAs – 44 of 105 have control rod assemblies). The core NK and TH axial regions are presented in Figure 4-15. The core active height is 268.73 cm. There is a 16.41 cm height reflector at the top and another one at the bottom of the core, adding to a total height of 301.56 cm.

The position of the CRA insertion is given from the bottom of the lower reflector: a height of 285.14 cm means a completely withdrawn CRA and a height of 16.41 cm means a completely inserted CRA. The insertion is measured in steps, each one of 1.25 cm (0 steps = completely inserted CRA and 228 steps = completely withdraw CRA).

Figure 4-15-– (a) Axial NK Cells and (b) Axial TH Region for NPP3

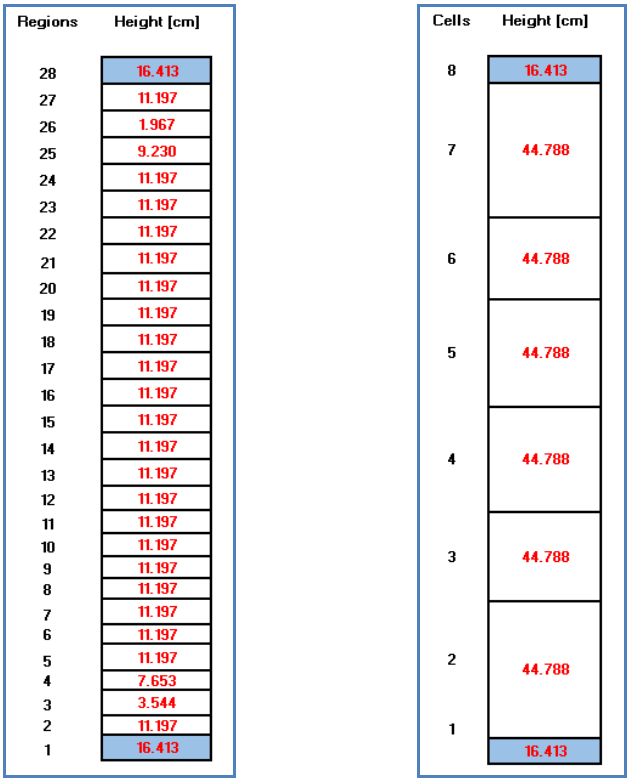

Regions	Height [cm]
28	16.413
27	11.197
26	1.967
25	9.230
24	11.197
23	11.197
22	11.197
21	11.197
20	11.197
19	11.197
18	11.197
17	11.197
16	11.197
15	11.197
14	11.197
13	11.197
12	11.197
11	11.197
10	11.197
9	11.197
8	11.197
7	11.197
6	11.197
5	11.197
4	7.653
3	3.544
2	11.197
1	16.413

Cells	Height [cm]
8	16.413
7	44.788
6	44.788
5	44.788
4	44.788
3	44.788
2	44.788
1	16.413

(a) **(b)**

The core radial configuration, compared to the core of NPP1, is presented in Figure 4-16. It can be seen the number of TH channels was also reduced from 19 to 13 (including the bypass region). The CRA assembly locations are show in Figure 4-17, where the numbering indicates the CRA assembly bank.

Figure 4-16–NPP3 Radial Core Configuration Compared to NPP1

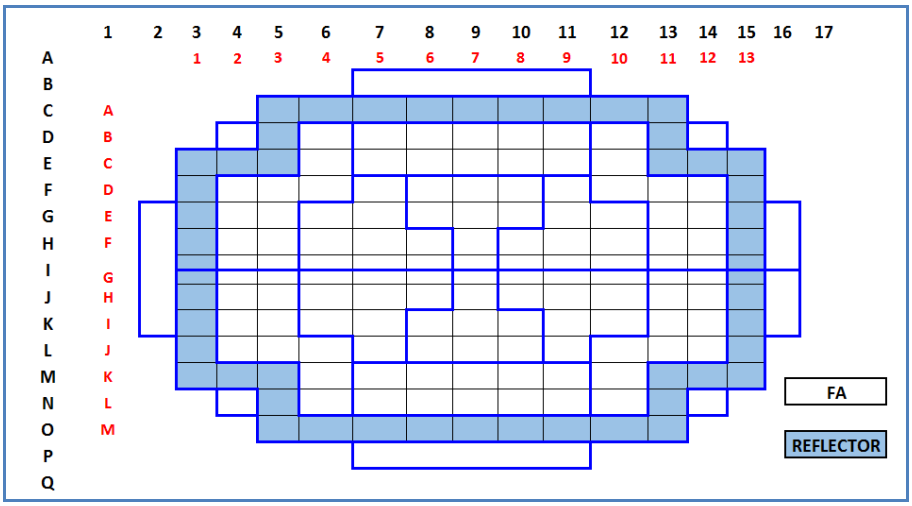

Figure 4-17 – CRA Core Configuration

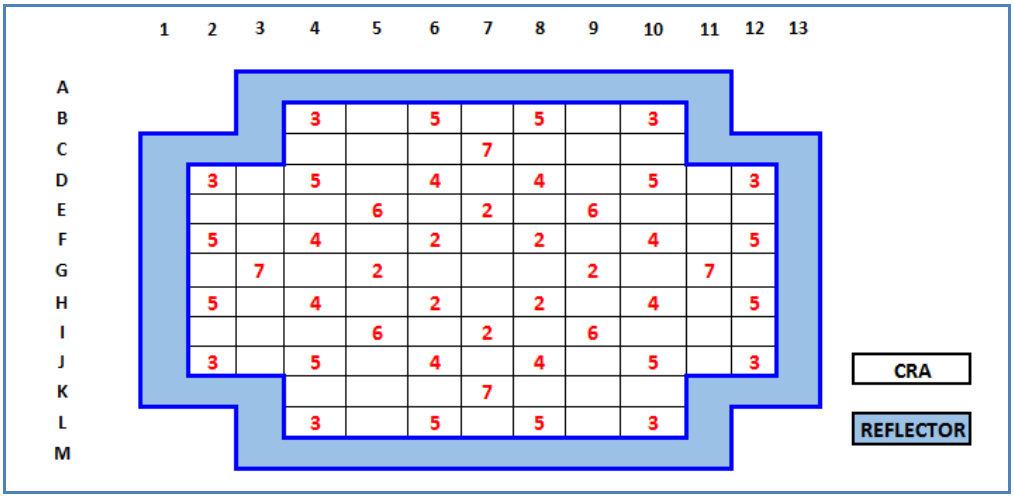

Figure 4-18 presents the radial NK nodes to TH channels mapping. The number or nodes was also reduced to 153 for each NK region. The nodes from 71 to 83 are contained in two different channels each one and, therefore, the weight factor for each node/channel will be 0.5.

Figure 4-18 – Radial NK Nodes to TH Channels Mapping

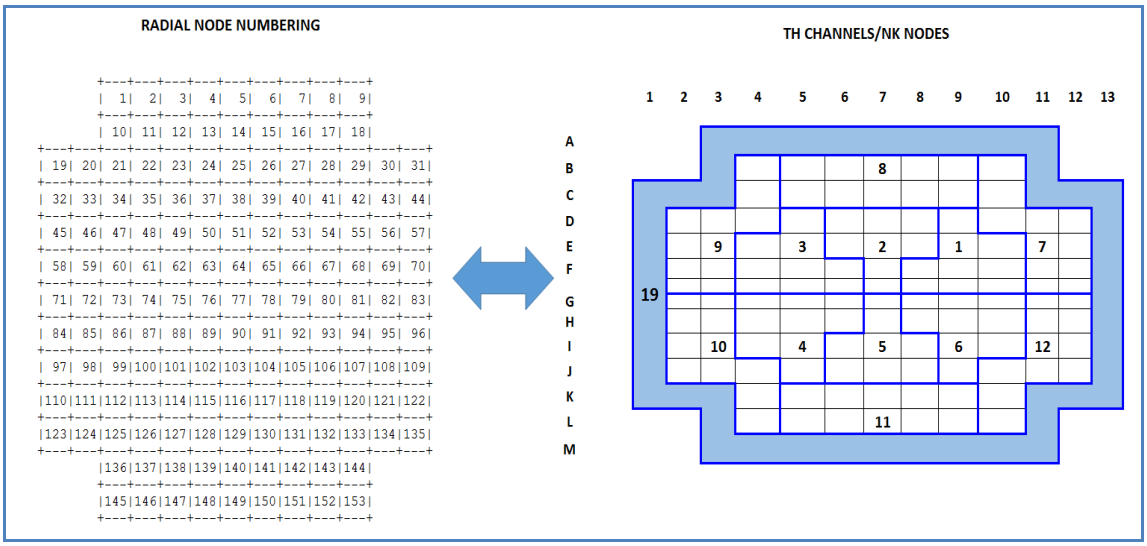

The axial mapping between the TH volumes and the NK regions follows the same procedures presented in Figure 4-10 (the total height has changed, but the TH cells and NK regions ratios are the same). The TH channel areas have also changed according to Table 4-9:

Table 4-9 - TH Channels and FA equivalent

TH Channel	Number of equivalent FA	Flow Area [m2]
1	7.5	0.19
2	7.5	0.19
3	7.5	0.19
4	7.5	0.19
5	7.5	0.19
6	7.5	0.19
7	10.0	0.26
8	10.0	0.26
9	10.0	0.26
10	10.0	0.26
11	10.0	0.26
12	10.0	0.26
19	20.5	0.53

4.4. Chapter Summary

This chapter presented the main NPP1 information and the R5 and P3D modeling changes that lead to NPP2 and NPP3. To summarize, the main core parameters for the NPP2 and NPP3, compared to NPP1, are presented in Table 4-10.

Table 4-10 – Main NPPs Parameters

Parameter	NPP1	NPP2	NPP3
Total Power (MWt)	2,772	530	1,061
Fuel Assembly Power (MWt)	15.66	7.69	10.10
# Cells x and y directions/Core	17 x 17	11 x 11	13 x 13
# Assemblies/Core	241	113	155
# Fuel Assemblies/Core	177	69	105
# Reflectors/Core	64	44	50
Pins per FA	208	208	208

Parameter	NPP1	NPP2	NPP3
Guide Tubes per FA	16	16	16
# of FA types	29	29	29
# FA with CRDMs/Core	60	28	44
Active Height (cm)	357.12	241.30	268.73
# Axial layers	24	24	24
Radial cells width (cm)	21.81	21.81	21.81
# steps CR withdraw	971	228	228
Control Rod step size (cm)	0.35	1.13	1.25
Reactor Coolant Flow Rate (kg/s/pump)	5,668.0	1,083.7	2,169.5
Total Coolant System Flow Rate (kg/s)	17,602.2	3,365.5	6,737.4
Core Flow Rate (kg/s)	16,052.4	3,069.2	6,144.2
Bypass Flow Rate (kg/s)	1,549.8	296.3	593.2

5. EXTENDED KALMAN FILTER ESTIMATION TOOL

The core neutron population drives the nuclear reaction rate, and the resulting power drives the TH behavior in LWR. Therefore, the determination of criticality, i.e. the core multiplication factor, using the measured neutron flux, is among the most significant aspects in nuclear reactor studies. However, the current online reactivity meters use the deterministic IPK method [48] [65], which does not account for the stochastic neutron flux interactions with materials. In addition, the neutron flux determination through signal detectors generates noisy data, which needs to be processed to yield the proper flux values.

State estimation is the method to determine unknown state variables of a dynamical system from an indirect and/or inaccurate series of measurements. One of the best examples of an optimum estimator for linear systems is the KF [66] [67] [68]: an optimal estimator that minimizes the mean square error of the estimated variable if the noise is Gaussian (or the best linear estimator if it is not). The EKF is an extension of the KF for nonlinear systems, which works on a stream of noisy input data to generate a statistically optimal estimation of the variable of interest, keeping a higher level of accuracy [68]. The EKF implementation in this study follows the theory from reference [69] applied to the reactor kinetics model [3].

This work implements an EKF algorithm to estimate the reactivity during a RIA. The EKF algorithm uses simulated data obtained from the coupled code P3D/R5, after the addition of random noise. In order to assess the reliability and consistency of the results, the IPK method is also implemented and both algorithms (EKF and IPK) are compared to the P3D/R5 simulation.

5.1. EKF Implementation

The EKF for a continuous-time nonlinear stochastic system, assuming discrete-time measurement, is implemented using MATLAB by a set of equations that models the estimated plant-sensor system dynamics. The estimated state is calculated according to the EKF block diagram presented in Figure 5-1, where: $F(x(t))$ is the state model; *x(t)* is the state vector; $H(x(t_k),t_k)$ is the observation model and t_k is the *k*-th discrete-time point; *W(t)* is the state noise, which is assumed to be an independent Gaussian white process with zero mean and spectral density *Q'(t); y(t_k)* is the measurement vector and *V(t_k)* is the measurement noise,

which is also assumed to be independent Gaussian white process with zero mean and covariance $R(t_k)$; and T represents the discretization/sampling period according to the time step of the P3D/R5 simulation. The following equations describe the non linear system and the process and measurement noise:

$$\frac{dx(t)}{dt} = F(x(t)) + W(t) \tag{5-1}$$

$$y(t_k) = H(x(t_k), t_k) + V(t_k) \tag{5-2}$$

$$E[W(t)] = 0 \tag{5-3}$$

$$E[W(t) \cdot W^T(\tau)] = Q'(t) \cdot \delta(t - \tau) \tag{5-4}$$

$$E[V(t_k)] = 0 \tag{5-5}$$

$$E[V(t_k) \cdot V^T(t_m)] = R(t_k) \cdot \delta_{km} \tag{5-6}$$

where δ_{km} is the Kronecker delta, i.e.,

$$\delta_{km} = \begin{cases} 1 \text{ if } k = m \\ 0 \text{ otherwise} \end{cases}$$

Denote by $\hat{x}(t_k / t_k)$ the estimated state at time t_k just after processing the measurements taken up to time t_k. In the same way, $P(t_k / t_k)$ denotes the error covariance matrix of the estimated state. The pair $\hat{x}(t_k / t_k)$ and $P(t_k / t_k)$ represent the EKF state at time t_k.

Consider a reference trajectory obtained by integrating:

$$\dot{\bar{x}}(t) = F(\bar{x}(t)) \tag{5-7}$$

in the interval [t_k , t_{k+1}] with initial conditions

$$\bar{x}(t_k) = \hat{x}(t_k / t_k) \tag{5-8}$$

Defining:

$$\delta x(t) = x(t) - \bar{x}(t) \tag{5-9}$$

and considering that it is sufficiently small, the following linear approximation can be taken:

$$\dot{\delta x}(t) = \left.\frac{\partial F}{\partial x}\right|_{\bar{x}(t)} \cdot \delta x(t) + W(t) \tag{5-10}$$

The integration of the previous equation in the interval [t_k , t_{k+1}] winds up:

$$\delta x(t_{k+1}) = \Phi(t_{k+1}, t_k) \cdot \delta x(t_k) + W(t_{k+1}) \tag{5-11}$$

where $\Phi(t_{k+1}, t_k)$ is the state transition matrix associated to the linearized system (5-10), which can be computed by integrating the equation:

$$\frac{\partial}{\partial t}\Phi(t, t_k) = \left.\frac{\partial F}{\partial x}\right|_{\bar{x}(t)} \Phi(t, t_k) \tag{5-12}$$

in the interval [t_k , t_{k+1}] with initial conditions

$$\Phi(t_k, t_k) = I \tag{5-13}$$

$W(t_{k+1})$ is a white Gaussian stochastic process with zero mean and covariance given by

$$Q(t_{k+1}) = \int_{t_k}^{t_{k+1}} \Phi(t_{k+1}, \tau) \cdot Q'(\tau) \cdot \Phi^T(t_{k+1}, \tau) d\tau \tag{5-14}$$

Consider the nominal measurement defined by:

$$\bar{y}(t_k) = H(\bar{x}(t_k)) \tag{5-15}$$

and let $\delta y(t_k)$ be

$$\delta y(t_k) = y(t_k) - \bar{y}(t_k) \tag{5-16}$$

Then the linearized measurement equation can be written as

$$\delta y(t_k) = M(t_k) \cdot \delta x(t_k) + V(t_k) \tag{5-17}$$

where

$$M(t_k) = \left.\frac{\partial H}{\partial x}\right|_{\bar{x}(t_k)} \tag{5-18}$$

Hence, KF in its original linear form [68] [67] can be applied to the problem given by equations (5-11) and (5-17) giving thus rise to the EKF, which can be summarized by:

i. Take the measurement $y(t_{k+1})$ and compute $\delta y(t_{k+1})$ by using equation (5-16);
ii. Apply the KF to estimate $\delta\hat{x}(t_{k+1}/t_{k+1})$ of $\delta x(t_{k+1})$; and
iii. Add ii to $\bar{x}(t_{k+1})$ to obtain $\hat{x}(t_{k+1}/t_{k+1})$.

In other words, given the filter state ($\hat{x}(t_k/t_k)$, $P(t_k/t_k)$) at time t_k and the measurement $y(t_{k+1})$ taken at t_{k+1}, the EKF computes the filter state at t_{k+1} by applying the following steps:

a. Prediction Step

a.1) Compute the predicted value $\hat{x}(t_{k+1}/t_k)$ by integrating

$$\dot{\bar{x}} = F(\bar{x}(t)) \tag{5-19}$$

in the interval t_k to t_{k+1} with initial condition $\bar{x}(t_k) = \hat{x}(t_k/t_k)$.

a.2) Compute the predicted error covariance matrix:

$$P(t_{k+1}/t_k) = \Phi(t_{k+1}/t_k) \cdot P(t_k/t_k) \cdot \Phi^T(t_{k+1}/t_k) + Q(t_{k+1}) \tag{5-20}$$

b. Update Step

b.1) Compute the EKF gain matrix:

$$K(t_{k+1}) = P(t_{k+1}/t_k) \cdot M^T(t_{k+1}) \cdot \left[M(t_{k+1}) \cdot P(t_{k+1}/t_k) \cdot M^T(t_{k+1}) + R(t_{k+1})\right]^{-1} \tag{5-21}$$

b.2) Process the measurement $y(t_{k+1})$ and compute the updated estimated state:

$$\hat{x}(t_{k+1}/t_{k+1}) = \hat{x}(t_{k+1}/t_k) + K(t_{k+1}) \cdot \left[y(t_{k+1}) - H(\hat{x}(t_{k+1}/t_k))\right] \tag{5-22}$$

b.3) Compute the updated error covariance matrix

$$\begin{aligned} P(t_{k+1}/t_{k+1}) = {} & [I - K(t_{k+1}) \cdot M(t_{k+1})] \cdot P(t_{k+1}/t_k) \cdot [I - K(t_{k+1}) \cdot M(t_{k+1})]^T + \\ & + K(t_{k+1}) \cdot R(t_{k+1}) \cdot K^T(t_{k+1}) \end{aligned} \tag{5-23}$$

The EKF initial state at time t_0, namely, $(\hat{x}_0, P_0)$ is assumed to be given. Hence

$$\hat{x}(t_0/t_0) = \hat{x}_0 \tag{5-24}$$

$$P(t_0/t_0) = P_0 \tag{5-25}$$

Figure 5-1 – EKF Block Diagram

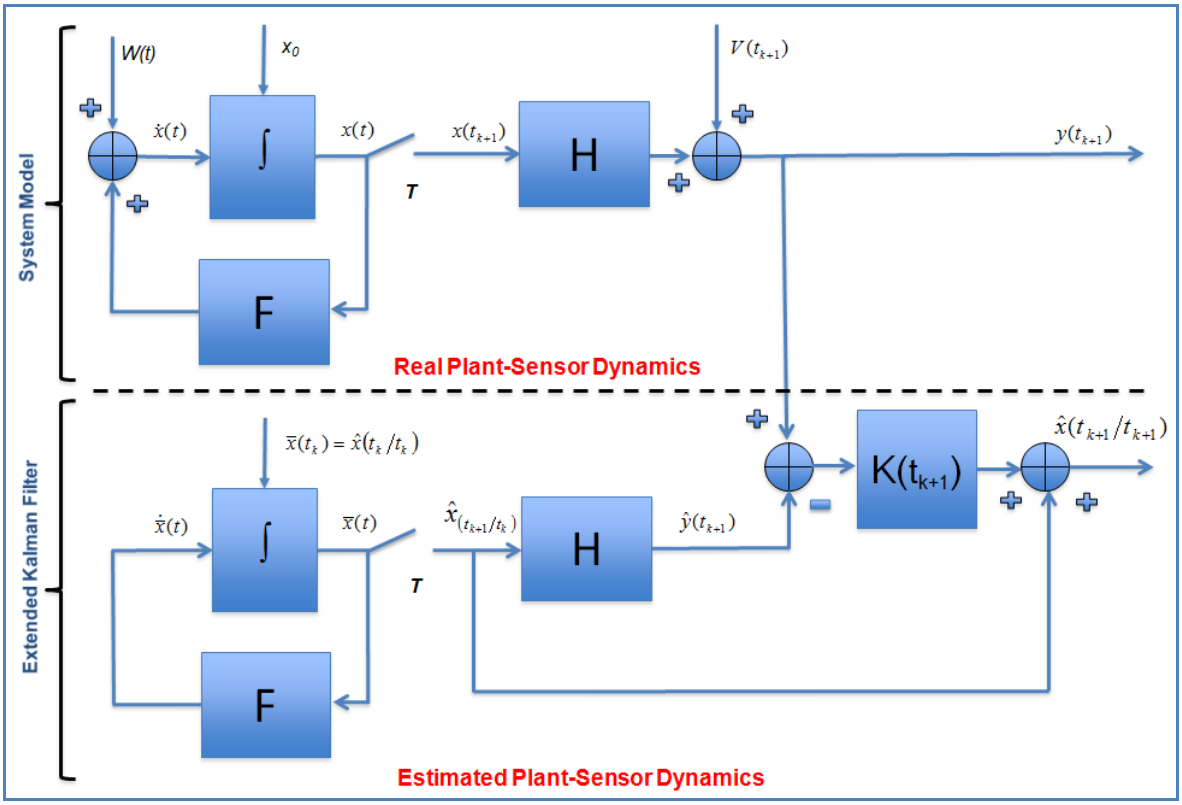

By implementing the algorithm above, which works for a continuous-time dynamical system with discrete measurements taken at discrete times, the state is estimated at each time step according to the scheme shown in Figure 5-2:

Figure 5-2 – Prediction and Update Cycles Block Diagram

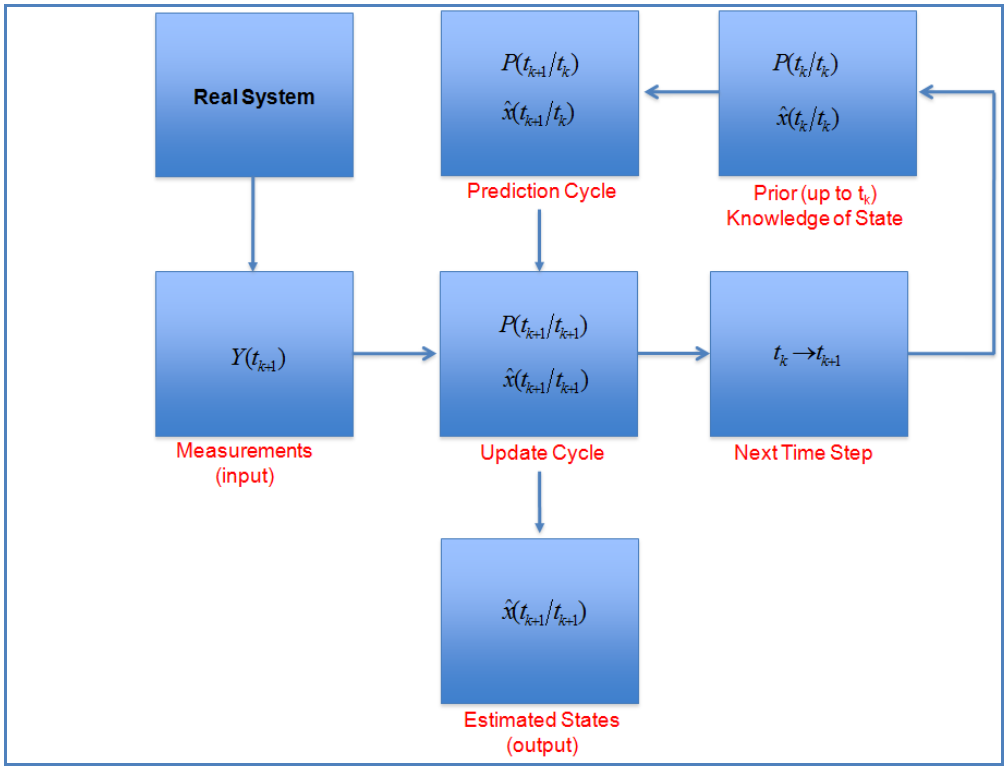

5.2. Simulation Strategy

This work evaluates the EKF compared to IPK algorithm for reactivity estimation using the power output from the P3D/R5 NPPs simulations results. The cases under investigation are shown in Table 5-1.

Table 5-1 – EKF Evaluation: Cases under Investigation

Case	Core Conditions	Rod Worth ($)
a	CRA ejection under HFP	0.2
b	CRA under HZP	0.4
c	CRB ejection under HZP	1.3

The input for both algorithms is the reactor power $P(t_k)$ generated by the P3D/R5 coupled code under RIA conditions, after the addition of random noise $V(t_k)$. The benchmark strategy is presented in Figure 5-3. The EKF reactivity is found by applying the stochastic EKF method, the IPK reactivity is the result of a direct application of the deterministic IPK

algorithm, and the P3D/R5 reactivity is the result of the CRE evaluated using the coupled code P3D/R5. The reference time for all reactivity calculations is the same. The IPK and the estimation tool are based on the point kinetics reactor equations (PKRE) and are implemented using the MATLAB simulation environment.

Figure 5-3 – Benchmark Strategy

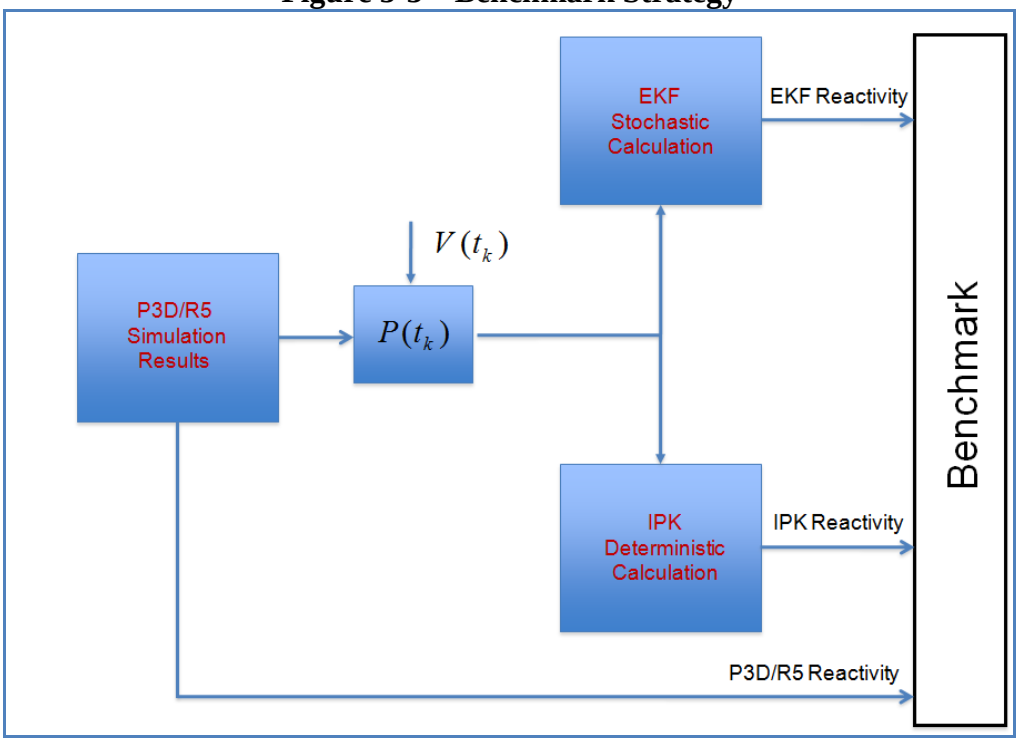

5.3. Point Kinetics Reactor Equation

The PKRE are simple ordinary differential equations, which relate the neutron density and delayed neutron precursor concentration. These equations are usually solved using a six delayed precursor groups [70] [71] [72]: enough to provide an adequately degree of accuracy. The PKRE are:

$$\frac{dn(t)}{dt} = \left[\frac{\rho(t)-\beta}{\Lambda}\right] n(t) + \sum_{i=1}^{6} \lambda_i C_i(t) \qquad (5\text{-}26)$$

$$\frac{dC_i(t)}{dt} = \frac{\beta_i}{\Lambda} n(t) - \lambda_i C_i(t) \qquad 1 \le i \le 6 \qquad (5\text{-}27)$$

where:

- $\rho(t)$ is the reactivity at time *t;*
- *n(t)* is the time dependent neutron density*;*
- $C_i(t)$ the effective concentration of delayed neutron of group *i;*
- β is the total effective delayed neutron fraction. Thus

$$\beta = \sum_{i=1}^{6} \beta_i \; ;$$

- β_i is the effective delayed neutron fraction of group *i;*
- λ_i is the effective decay constant of group *i;*
- Λ is the mean neutron generation time, which is defined as

$$\Lambda = \frac{\ell}{k(t)} = \ell \cdot (1-\rho) \; ;$$

- ℓ is the mean lifetime of a neutron in the a reactor; and
- *k(t)* is the multiplication factor.

The delayed neutron precursor initial concentration is given by:

$$C_i(t=0) = \frac{\beta_i}{\lambda_i \Lambda} P(0) \qquad 1 \le i \le 6 \qquad (5\text{-}28)$$

5.4. IPK Reactor Equation

The IPK reactor equation correlates the reactivity $\rho(t)$ as a function of the time dependent power level *P(t)*. Therefore, it may be used to calculate the reactivity from a specific power profile. The IPK is derived directly from equations 5-26 and 5-27 after simple manipulation [3]:

$$\rho(t) = \beta + \Lambda \frac{d}{dt}\left[\ln P(t)\right] - \beta \int_0^\infty D(\tau) \frac{P(t-\tau)}{P(t)} d\tau \qquad (5\text{-}29)$$

where $D(\tau)$ is defined as the "*Delayed Neutron Kernel*":

$$D(\tau) = \sum_{i=1}^{6} \frac{\lambda_i \beta_i}{\beta} e^{-\lambda_i \tau} \tag{5-30}$$

5.5. State-Space Model of the PKRE for the EKF

The implementation of the EKF estimation tool depends on the adequate mathematical modeling of the phenomenon, according to the following state space form:

$$\frac{dx(t)}{dt} = F(x(t)) + W(t) = A_n x(t) + B_n + W(t) \tag{5-31}$$

The representation of the reactivity as a state variable, similar to the work on references [3] and [8], uses the following modeling equations:

$$\rho(t) = \alpha + w \cdot t \tag{5-32}$$

$$\frac{d\rho(t)}{dt} = w \tag{5-33}$$

$$\frac{dw(t)}{dt} = 0 \tag{5-34}$$

$$S = \frac{-\rho_0 \cdot n_0}{\ell} \tag{5-35}$$

where α and w stand for the stochastic reactivity jump and slope, respectively, and S is the neutron source modeled as a function of the initial reactivity and neutron density. The state is defined as:

$$x = \begin{bmatrix} n & C_1 & C_2 & C_3 & C_4 & C_5 & C_6 & \rho & w \end{bmatrix}^T, \tag{5-36}$$

where the superscript T denotes the transpose.

After simple manipulation of previous equations, we build up the matrices A_n, B_n and the Jacobian $A = \frac{\partial F}{\partial x}$:

$$A_n = \begin{bmatrix} -\frac{\beta}{\ell} & \lambda_1 & \lambda_2 & \lambda_3 & \lambda_4 & \lambda_5 & \lambda_6 & 0 & 0 \\ \frac{\beta_1}{\ell} & -\lambda_1 & 0 & 0 & 0 & 0 & 0 & 0 & 0 \\ \frac{\beta_2}{\ell} & 0 & -\lambda_2 & 0 & 0 & 0 & 0 & 0 & 0 \\ \frac{\beta_3}{\ell} & 0 & 0 & -\lambda_3 & 0 & 0 & 0 & 0 & 0 \\ \frac{\beta_4}{\ell} & 0 & 0 & 0 & -\lambda_4 & 0 & 0 & 0 & 0 \\ \frac{\beta_5}{\ell} & 0 & 0 & 0 & 0 & -\lambda_5 & 0 & 0 & 0 \\ \frac{\beta_6}{\ell} & 0 & 0 & 0 & 0 & 0 & 0 & -\lambda_6 & 0 \\ 0 & 0 & 0 & 0 & 0 & 0 & 0 & 0 & 1 \\ 0 & 0 & 0 & 0 & 0 & 0 & 0 & 0 & 0 \end{bmatrix} \tag{5-37}$$

$$B_n = \begin{bmatrix} \frac{\rho n}{\ell} + S & 0 & 0 & 0 & 0 & 0 & 0 & 0 & 0 \end{bmatrix}^T \tag{5-38}$$

$$A = \begin{bmatrix} \frac{\rho - \beta}{\ell} & \lambda_1 & \lambda_2 & \lambda_3 & \lambda_4 & \lambda_5 & \lambda_6 & \frac{n}{\ell} & 0 \\ \frac{\beta_1}{\ell} & -\lambda_1 & 0 & 0 & 0 & 0 & 0 & 0 & 0 \\ \frac{\beta_2}{\ell} & 0 & -\lambda_2 & 0 & 0 & 0 & 0 & 0 & 0 \\ \frac{\beta_3}{\ell} & 0 & 0 & -\lambda_3 & 0 & 0 & 0 & 0 & 0 \\ \frac{\beta_4}{\ell} & 0 & 0 & 0 & -\lambda_4 & 0 & 0 & 0 & 0 \\ \frac{\beta_5}{\ell} & 0 & 0 & 0 & 0 & -\lambda_5 & 0 & 0 & 0 \\ \frac{\beta_6}{\ell} & 0 & 0 & 0 & 0 & 0 & 0 & -\lambda_6 & 0 \\ 0 & 0 & 0 & 0 & 0 & 0 & 0 & 0 & 1 \\ 0 & 0 & 0 & 0 & 0 & 0 & 0 & 0 & 0 \end{bmatrix} \tag{5-39}$$

The system is nonlinear due to the term $\frac{\rho \cdot n}{\ell} + S$.

5.6. Chapter Summary

This chapter presented the stochastic EKF algorithm, the PKRE and the IPK deterministic method. The EKF formulation and structure of update/predict and measurement/corrects equations, which are adequate to online real time data processing, are applied to reactivity estimation.

The EKF and IPK algorithms use the power profile, obtained from the coupled code P3D/R5, as an input after the addition of random noise. To assess the reliability and consistency of the results, both algorithms (EKF and IPK) outputs are compared to the P3D/R5 reactivity. Besides the P3D/R5 coupled package, MATLAB is used to add random noise to the power profile and to implement the IPK and the EKF algorithms. The application of the stochastic EKF, its sophisticate implementation, and its features add innovation to the task of calculation of reactivity during RIA conditions and under noisy measurements.

6. REACTIVITY WORTH IDENTIFICATION

In this chapter, the standalone P3D code is used for reactivity worth identification and to establish the CRA/CRB to be ejected for each case shown in Table 3-3. Therefore a first set of P3D HFP all rods out (ARO) and HZP all rods in (ARI) are performed to find the CRA initial conditions, with similar reactivity worth, that leads to criticality. Then, the rod worth identified by the P3D standalone steady-state case, R5 standalone case and P3D/R5 coupled transient case, are compared. Furthermore, the reactivity coefficients needed for the R5 standalone simulations are calculated.

6.1. Control Rod Assembly Worth

The effectiveness of a control rod depends on the ratio of neutron flux at the location of the control rod to the average core neutron flux. The control rod worth, i.e. the changes in the reactivity caused by a control rod motion, is maximum when it is fully inserted [5]. The HZP ARI control rod worth is calculated by first running the steady-state P3D models for all CRA inserted, and then for one CRA fully withdrawn. The rod worth is calculated by:

$$\rho = \frac{\Delta\rho}{\beta} = \left(\frac{k_{eff2} - k_{eff1}}{k_{eff2}} \right) \cdot \frac{1}{\beta} \qquad (6\text{-}1)$$

k_{eff1} = k effective with all CRA inserted.

$k_{eff\,2}$ = k effective with all control rods fully inserted, but CRA#8 fully withdrawn.

β is the fraction of delayed neutrons.

A similar procedure is followed to calculate the rod worth ($k_{eff\,1}$ and $k_{eff\,2}$ calculations) for HFP ARO: first, all rods are out for the $k_{eff\,1}$ calculations. Then, for the $k_{eff\,2}$ calculations, all control rods are out, but CRA# 8 is fully inserted.

After the control rod worth in the HFP and HZP simulations are run, the CRA# 8, the rod that holds similar worth among the three NPPs, is identified. Then, a set of P3D

simulations is performed to choose a suitable critical initial condition, i.e. the control rod assembly's initial condition that allows $k_{eff} \cong 1$ just before the transient. Although the k_{eff} just before the transient changes for different core coolant flow rate and inlet temperature, the control rod worth does not.

6.1.1. NPP1 Control Rod Worth

The NPP1 HFP ARO P3D simulation suggests that the control rod assemblies located in positions (9, E) and (13, I) are the CRA with the highest rod worth (0.23$), as can be seen in Figure 6-1 (due to core symmetry, only quarter of the core is showed here), all of them belong to the CRA bank #7 in the figure. Therefore, CRA #8 is taken to be the one located in position (13,I).

Figure 6-1–NPP1 HFP Control Rod Assembly Worth (1/4 core shown)

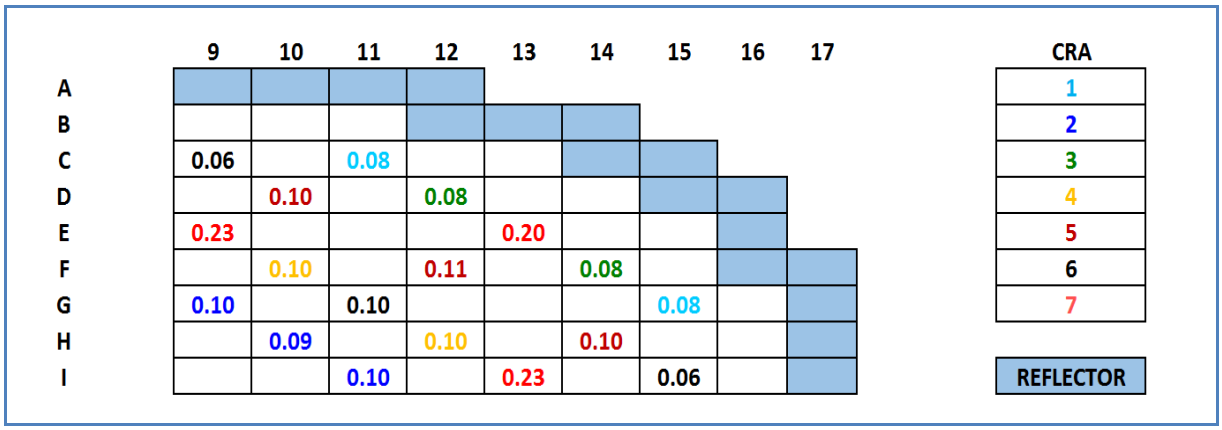

The results for the HZP ARI P3D simulations are shown in Figure 6-2. The control rod assemblies located in positions (5, E), (13, E), (5, M) and (13, M) (CRA bank # 7) are the ones with higher reactivity worth (0.43$). Nevertheless, the CRA#8 is assumed to be the one located in position (13, E).

Figure 6-2–NPP1 HZP Control Rod Assembly Worth (1/4 core shown)

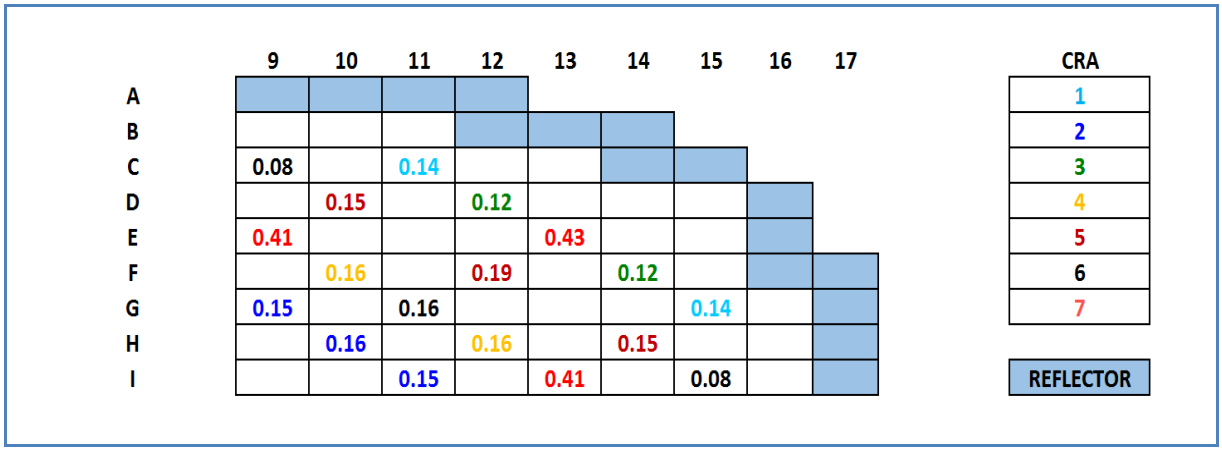

The NPP1 bank reactivity worth identification is summarized in Table 6-1. Based on these results, the control rod bank #2 is chosen to be ejected (defined as CRB#8) due to its reactivity worth closer to 1.5$ (case *c*), its position within the thermal hydraulic core inner ring and its safety purpose.

Table 6-1 – NPP1 CRA Bank Reactivity

CRA Bank #	**ARO HFP** ($)	**ARI HZP** ($)
1	0.69	0.87
2	0.68	1.51
3	0.67	0.78
4	1.00	1.01
5	1.31	1.68
6	0.66	0.82
7	1.90	2.26

Next, a set of P3D simulations is performed to find the control rods assembly initial conditions that lead to criticality just before the ejection of the CRA/CRB#8, i.e. $k_{eff} \cong 1$ at t=0 second, for both HFP and HZP (the CRA#8 is assumed to be fully inserted at time t=0 second). Table 6-2 shows the criticality initial conditions and the CRA/CRB# 8 rod worth when applying these initial conditions. It must be noted that an accurate set of control rods' initial conditions is very important to performing an adequate and consistent simulation.

Table 6-2– NPP1 P3D Criticality Initial Conditions

Case	Core Conditions	CRA#1 to #7 at t=0	k_{eff}	CRA/CRB#8 Rod Worth
a	HFP	CRA # 1, 3, 4, 6 and 7: fully withdraw CRA #2 and 5: 520 steps withdraw	1.00005	0.24
b	HZP	CRA # 1, 3, 4, 6 and 7: fully inserted CRA #2 and 5: 770 steps withdraw	1.00008	0.41
c	HZP	CRA # 1, 2, 3, 4, 6 and 7: fully inserted CRA #5: 720 steps withdraw	1.00002	1.32

6.1.2. NPP2 Control Rod Worth

The control rod worth NPP2 identification follows a similar procedure to item 6.1.1. Nevertheless, the simulation results presented in Figure 6-3 and Figure 6-4 indicate that the CRA with the highest rod worth are the ones in positions (5,E), (7,E), (5G) and (7,G) - all of them belonging to CRA#2. However, to compare the reactivity worth among NPP1, NPP2 and NPP3, the CRA#8 is assumed to be the one in position (8,D) for both HFP (0.22$) and HZP (0.44$).

Figure 6-3 – NPP2 HFP Control Rod Assembly Worth (1/4 core shown)

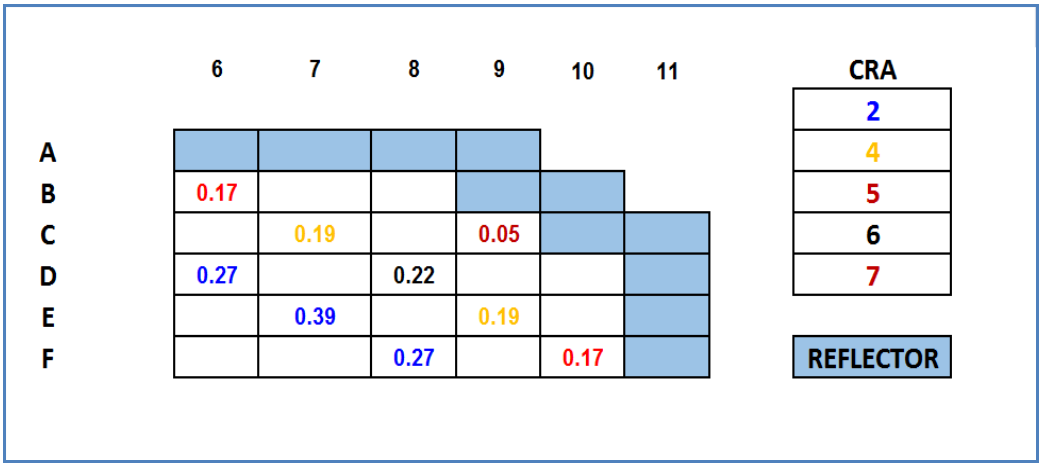

Figure 6-4 – NPP2 HZP Control Rod Assembly Worth (1/4 core shown)

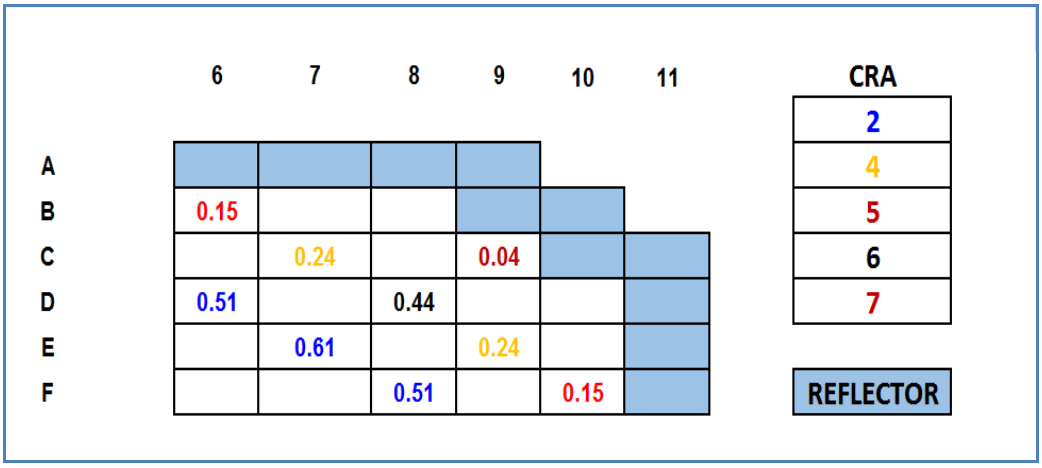

In addition, the NPP2 CRA bank reactivity worth is presented in Table 6-3. Based on these results, the control rod bank #4 (defined as CRB#8) is chosen to be ejected due to its reactivity worth closer to 1.5$.

Table 6-3 – NPP2 CRA Bank Reactivity

Bank Number	ARO HFP ($)	ARI HZP ($)
2	2.87	3.85
4	1.62	1.51
5	0.18	0.20
6	1.01	1.01
7	0.34	0.39

Next, a set of P3D simulations is performed to find the control rods assembly's initial configuration, as can be seen in Table 6-4.

Table 6-4– NPP2 P3D Criticality Initial Conditions

Case	Core Conditions	CRA#2 to 7 at t=0	k_{eff}	CRA/CRB #8 Rod Worth
a	HFP	CRA #2, 5 and 7: fully withdraw CRA #4: 90 steps withdraw CRA # 6: 98 steps withdraw	1.00041	0.24

Case	Core Conditions	CRA#2 to 7 at t=0	k_{eff}	CRA/CRB #8 Rod Worth
b	HZP	CRA #4, 5 and 7: fully inserted CRA #2 and 6: 100 steps withdraw	1.00091	0.42
c	HZP	CRA # 4, 5, 6 and 7: fully inserted CRA #2: 200 steps withdraw	1.00004	1.33

6.1.3. NPP3 Control Rod Worth

The results presented in Figure 6-5 and Figure 6-6 indicate that the control rod assemblies with the highest reactivity worth are the ones in position (11,G) for the HFP (0.25$), and position (8,F) for the HZP (0.43$). Due to their reactivity worth closer to the ones found in item 6.1.1 and item 6.1.2, these control rod assemblies are also assumed to be the CRA#8 in the NPP3 case.

Figure 6-5 – NPP3 HFP Control Rod Assembly Worth (1/4 core shown)

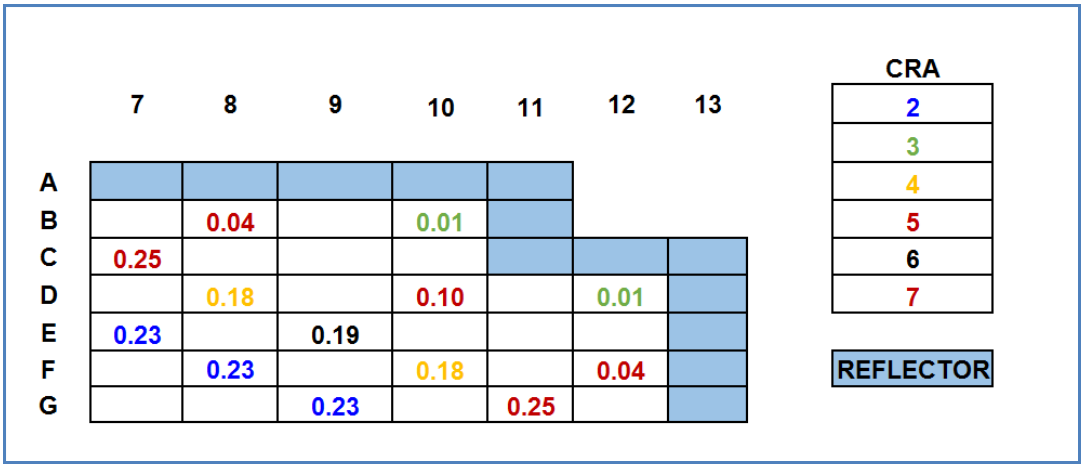

The NPP3 CRA bank reactivity worth is presented in Table 6-5. The control rod bank #4 is chosen to be ejected for case *c* due to its reactivity worth of 1.52$ (defined as CRB#8).

Figure 6-6 – NPP3 HZP Control Rod Assembly Worth (1/4 core shown)

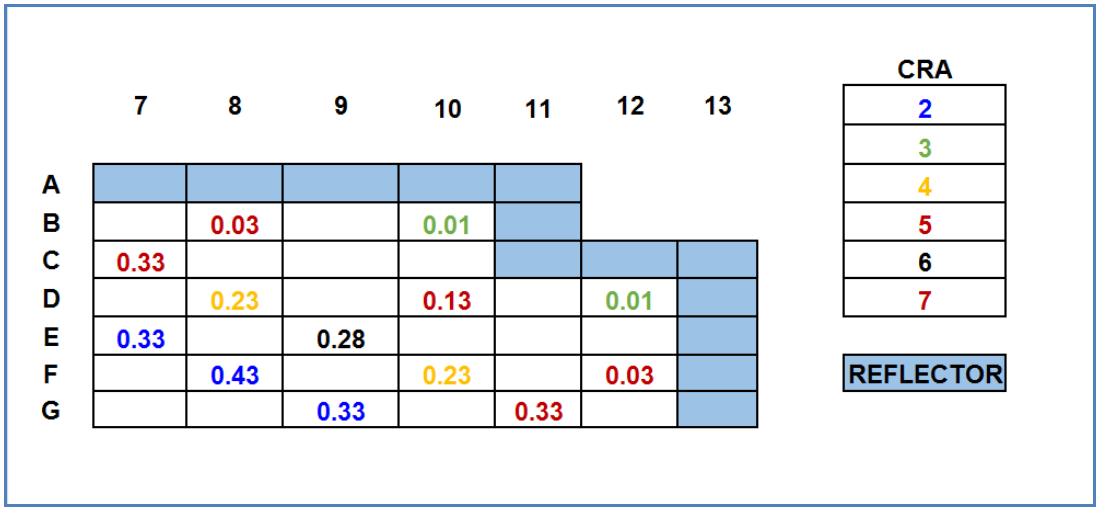

Table 6-5 – NPP3 CRA Bank Reactivity

Bank Number	ARO HFP ($)	ARI HZP ($)
2	1.84	3.05
3	0.10	0.07
4	1.56	1.52
5	0.74	0.67
6	0.99	0.99
7	1.20	1.15

After that, a set of P3D simulations is performed to find the control rod assemblies' initial configuration and k_{eff}, as can be seen in Table 6-6.

Table 6-6– NPP3 P3D Criticality Initial Conditions

Case	Core Conditions	CRA#2 to 7 at t=0	k_{eff}	CRA/CRB #8 Rod Worth
a	HFP	CRA # 3, 5, 6 and 7: fully withdraw CRA #2: 180 steps withdraw CRA# 6: 165 steps withdraw	1.00004	0.26
b	HZP	CRA # 2, 5 and 7: fully inserted	1.00006	0.40

Case	Core Conditions	CRA#2 to 7 at t=0	k_{eff}	CRA/CRB #8 Rod Worth
		CRA #4: 200 steps withdraw CRA# 6: 176 steps withdraw		
c	HZP	CRA # 2, 3, 4, 5, 6 and 7: fully inserted CRA #2: 176 steps withdraw	1.00006	1.34

6.2. Reactivity Coefficients Identification

The R5 model requires, besides the NPP geometric and thermal hydraulic data, information regarding the core neutronic behavior. The reactivity coefficients, plugged into the temperature and density reactivity tables in the R5 models, are based on P3D simulation results from items 6.1.1, 6.1.2 and 6.1.3. The R5 solves the space-independent point reactor kinetics and a complete set of reactor kinetics data for transient calculations must always be plugged in the code [54].

The reactivity $\rho(t)$ is a quantity that measures the deviation of the effective neutron multiplication factor $k(t)$ from unity ($k(t)$ is ratio of the number of new fission neutrons to the number of neutrons leaking from the core or being absorbed), as represented by the equation:

$$\rho = \frac{k(t)-1}{k(t)} \tag{6-2}$$

Therefore, a positive reactivity (insertion of reactivity) means an increase in the number of neutrons and a negative reactivity indicates a decrease in the neutron population. Although during normal operation the reactivity can be controlled by moving the control rods or adding/removing neutrons absorber in the moderator, it is also affected by changes in the fuel and moderator temperatures and in the moderator void content. Therefore, during a CRE RIA, the amount of reactivity added by a rod ejection will be limited. The rate of reactivity change is shown by the following equation [5]:

$$\dot{\rho} = \dot{\rho}_{CS} + \frac{\partial \rho}{\partial T_F}\dot{T}_F + \frac{\partial \rho}{\partial T_M}\dot{T}_M + \frac{\partial \rho}{\partial \alpha_M}\dot{\alpha}_M \tag{6-3}$$

where $\dot{\rho}_{CS}$ is the reactivity rate of change due the control systems, $\dot{T}_F$ is the rate of change in the fuel temperature, $\dot{T}_M$ is the rate of change in the moderator, and $\dot{\alpha}_M$ is the rate of change for the steam volume fraction (void fraction). The term $\partial\rho/\partial T_F$ is known as the Doppler coefficient and it is always negative – hence, an increase in the fuel temperature provides a negative reactivity feedback. The terms $\partial\rho/\partial T_M$ and $\partial\rho/\partial\alpha_M$ may be positive or negative, depending on the reactor design and operating conditions. The Doppler and moderator reactivity coefficients for the various cases are presented in Table 6-7. They are the results of P3D simulations assuming the initial conditions presented in Table 6-2, Table 6-4 and Table 6-6.

Table 6-7 –Reactivity Coefficients

NPP	Case	Doppler Coefficient ($/k)	Moderator Coefficient ($/kg/m^3)
1	a	-4.91E-03	5.38E-02
	b	-5.69E-03	5.65E-02
	c	-5.67E-03	5.56E-02
2	a	-5.02E-03	5.64E-02
	b	-5.69E-03	5.68E-02
	c	-5.76E-03	5.47E-02
3	a	-5.05E-03	5.41E-02
	b	-5.73E-03	5.60E-02
	c	-5.73E-03	5.37E-02

Furthermore, the volume weighting factors needed for the R5 models are calculated by:

$$w = \frac{1}{n_{AR}} \cdot \frac{1}{n_{FA}} \tag{6-4}$$

where n_{AR} is number of axial regions and n_{FA} is the number of FAs.

Finally, R5 calculates the reactor kinetics feedback accounting for the moderator fluid density, void fraction moderator fluid temperature and volume average fuel temperature. In addition, the code calculates fission products decay plus actinide decay calculations. The ANS-79 is taken as a decay heat standard model [54], as indicated by reference [12].

6.3. Chapter Summary

The standalone P3D code is used for ARO and ARI simulations, which allows the identification of the rod locations with similar reactivity rods, and the highest ones in the cores. Based on the simulation results, the CRA/CRB is defined and the core initial condition, for each case and NPP under investigation, is set. The reactivity coefficients needed for R5 neutronic feedback calculations are also calculated. Table 6-8 presents a summary of reactivity worth identification.

Table 6-8 – Summary of Reactivity Worth Identification

NPP	Case	CRA/CRB#8 Position	ARI/ARO ($)	Steady-State $k_{eff} \cong 1$ ($)
1	a	(13, I)	0.23	0.24
	b	(13, E)	0.43	0.41
	c	Bank #2	1.51	1.32
2	a	(8,D)	0.22	0.24
	b	(8,D)	0.44	0.42
	c	Bank #4	1.51	1.33
3	a	(11,G)	0.25	0.26
	b	(8,F)	0.43	0.40
	c	Bank #4	1.52	1.34

7. NPP TOTAL POWER AND REACTIVITY ASSESSMENT

The analysis presented here suggests that either R5 or P3D alone may not adequately represent feedback effects during transients. In fact, the simulation results indicate that the use of coupled codes may lead to less conservative outcomes, particularly as the core size shrinks. Although the exchange of offline parameters among the two standalone codes, e.g. the use of the P3D reactivity coefficients in the TH system codes, can improve the quality of the results, the use of the P3D/R5 coupled package allows a more complete analysis of the NPP system.

It was found that the predicted power response and reactivity behavior during the RIA are very different among the three cases under investigation:

- case *a* has a fast increase in the reactivity, a power peak of about 25% due to the lack of reactivity control, and a slow power return to steady-state;
- case *b* has a very slow power dynamics; and
- case *c* has a sharp power peak.

Nevertheless, in this chapter session 7.1 presents the NPP1 relative power and total reactivity assessment, according to Table 3-3 using the codes P3D & R5 and the P3D/R5 package, to analyze the effectiveness of the standalone codes compared to the coupled one under RIA conditions. Session 7.2 presents P3D/R5 total power and reactivity simulation results to investigate the consequences of reducing the core size. Session 7.3 discuss the effect of increase the NPP2 output level.

7.1. Total Reactivity and Power Assessment by the Three Codes

7.1.1. Case a: CRA#8 HFP (Initial NPP Power at 100%)

It can be seen in Figure 7-1 and Figure 7-2 that in case *a* the relative power first goes up as the reactivity increases from zero to 0.16$ (P3D), 0.17$ (R5) and 0.15$ (P3D/R5) within 0.1 seconds. Then, the power falls off as the temperature feedback effect takes place. The total power simulation results for the three codes have similar behavior, with a maximum power of 127% (P3D), 125% (R5), and 124% (P3D/R5). All simulation results present the same power and reactivity trends. However, the coupled package steady-state power stays at 92.5% of the

nominal power (R5 stays at 110% and P3D stays at 104%) due to the stronger Doppler and moderator feedback effects.

Figure 7-1 – NPP1 Case *a* Power

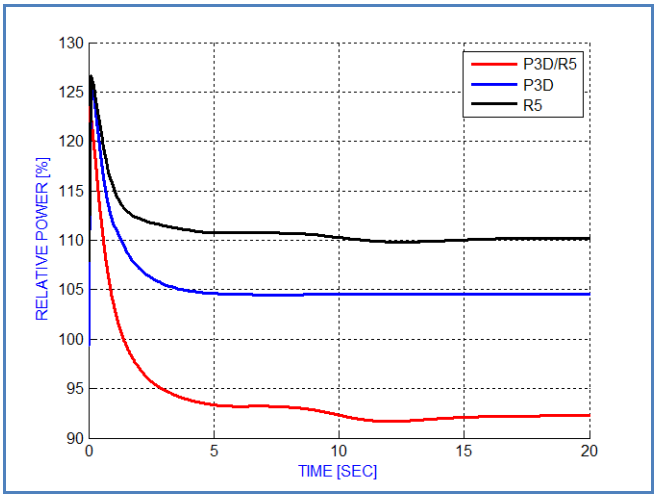

Figure 7-2 – NPP1 Case *a* Total Reactivity Distribution

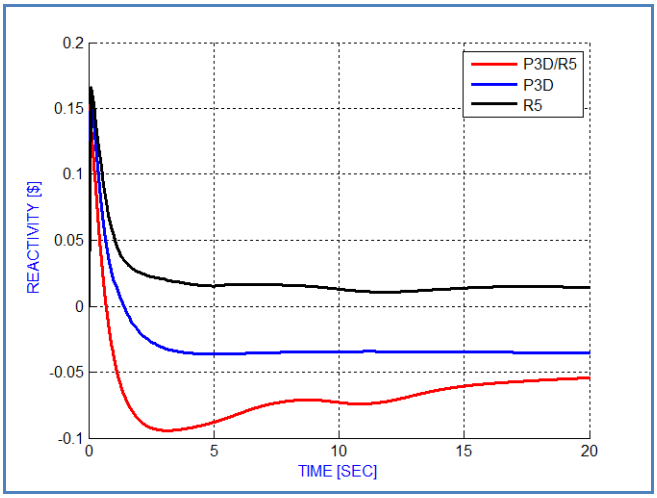

The P3D, R5 and P3D/R5 predicted total, Doppler, control rod and moderator reactivities are shown in Figure 7-3, Figure 7-4 and Figure 7-5. As seen, the results indicate that the use of coupled codes leads to less conservative transients from the total power point of view.

Figure 7-3 – NPP1 Case *a* P3D Reactivity

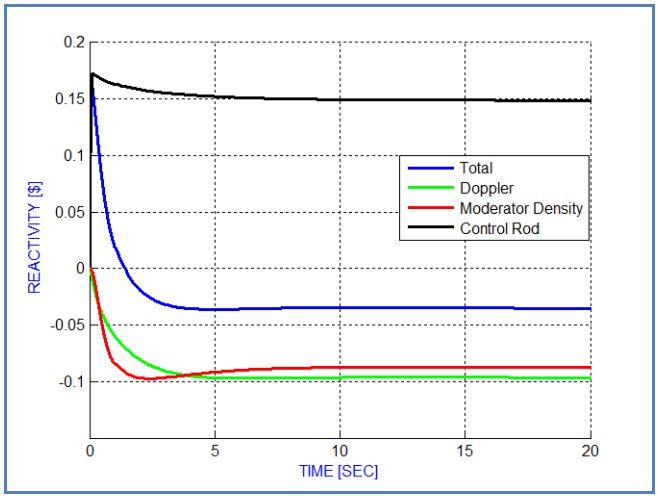

Figure 7-4 – NPP1 Case *a* R5 Reactivity

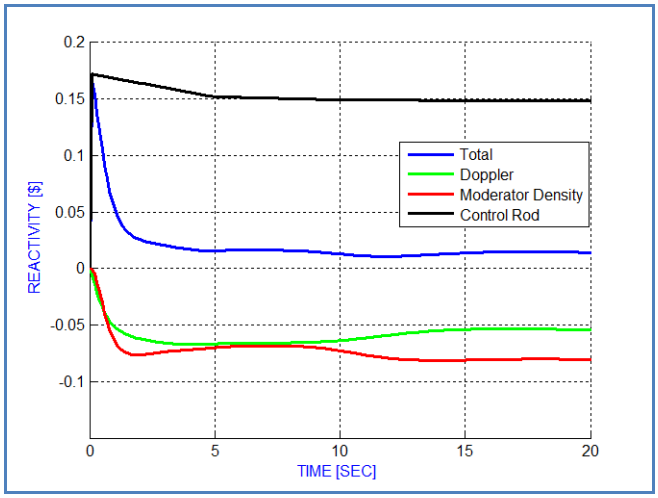

Figure 7-5 – NPP1 Case *a* P3D/R5 Reactivity

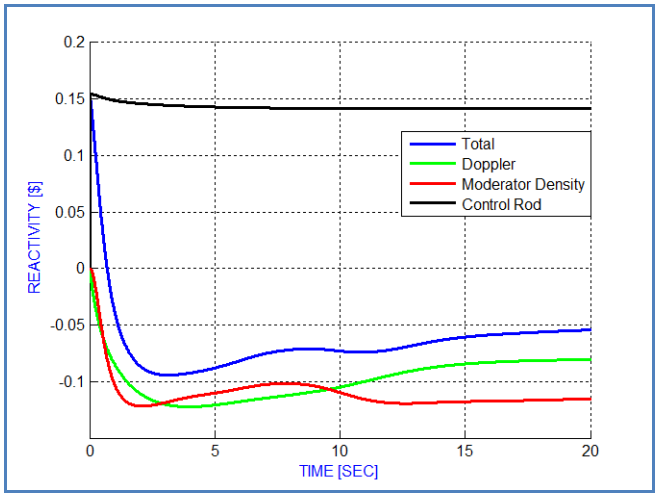

7.1.2. Case *b:* CRA#8 HZP (NPP Initial Power at 0.01%)

For the same core, HZP initial conditions and rod worth (case *b*), the P3D total power simulation does not reproduce the same behavior that the R5 and P3D/R5 predict, as shown in Figure 7-6 - the respectively total reactivity results are shown in Figure 7-7. In Figure 7-7, the total reactivity is the sum of the reactivity due to Doppler feedback, moderator feedback and control rods. However, the total reactivity used for power calculations in PARCS also includes a null reactivity term that encompasses numerical errors associated with the calculations of each component of reactivity. This numerical error is often insignificant, such as the case for the P3D/R5 coupled simulations. However, for the P3D case shown in Figure 7-6, the null reactivity is actually significant and the total reactivity reaches zero by 200 seconds. This is due to the fact that P3D uses a very simplified thermal hydraulics model that affects the cross section interpolation such that the numerical error (e.g. null reactivity) associated with estimation of the reactivity components is significant (the initial power is very small in this case).

Figure 7-6 – NPP1 Case *b* Power

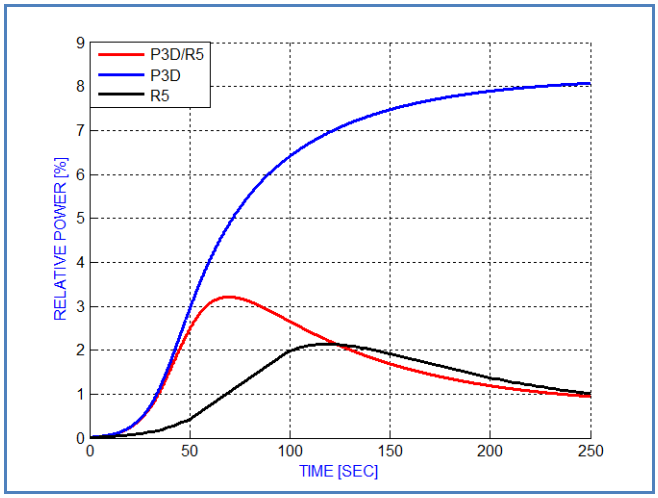

It must be noted that within 0.1 seconds, the total reactivity jumps from 0 to 0.29$ (relative power jumps to 0.02% within the same time frame) and keeps rising slowly for more than 15 second. The small initial power explains why it takes longer for the power to rise and then eventually to fall off. The control rod, Doppler and Moderator reactivities are presented in Figure 7-8, Figure 7-9 and Figure 7-10, for each code (P3D, R5 and P3D/R5) respectively.

Figure 7-7 – NPP1 Case *b* Total Reactivity Distribution

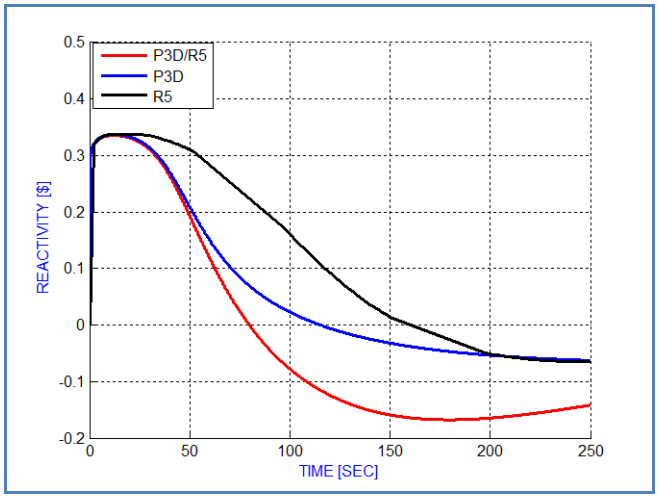

Figure 7-8 – NPP1 Case *b* P3D Reactivity

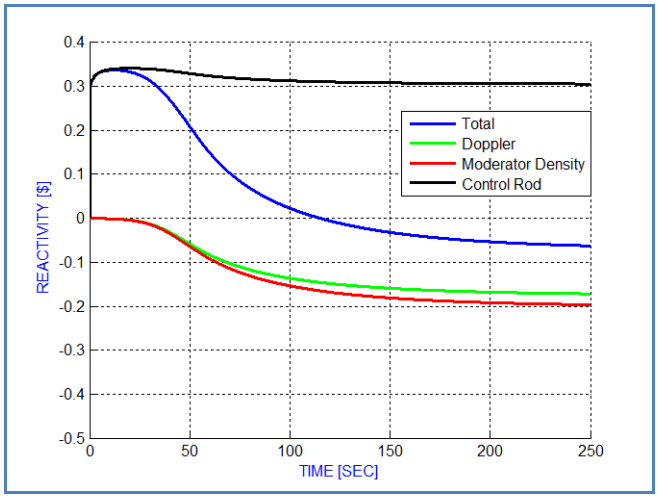

Figure 7-9 – NPP1 Case *b* R5 Reactivity

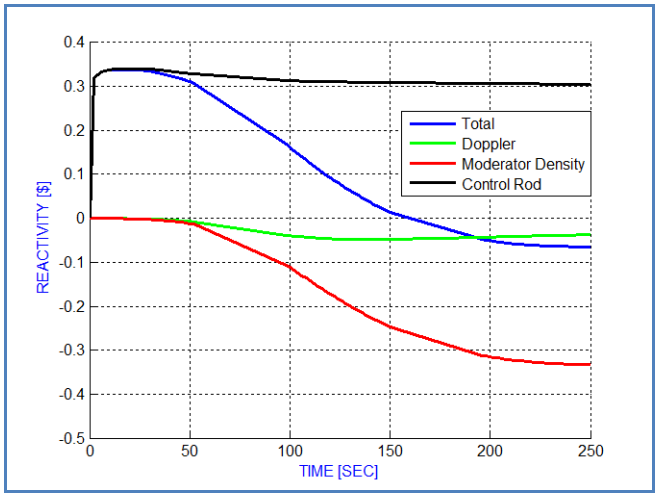

Figure 7-10 – NPP1 Case *b* P3D/R5 Reactivity

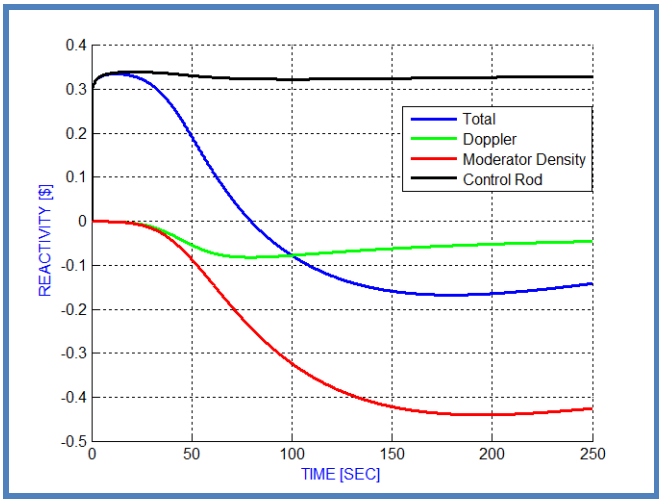

Thus, the use of the P3D standalone code leads to the conclusion the total power increases from 0.01% of the nominal to more than 8% and never sharply decreases - a relative power increase of more than 800 times within 250 sec. The HZP power, without cross section Boron dependence, takes longer for the power to reach its peak and the steady-state, even for the coupled code

7.1.3. Case *c:* NPP1 CRB#8 HZP

The total power behavior and reactivity due to the CRB ejection (case *c*) is presented in Figure 7-11 and Figure 7-12.

Figure 7-11 - Case *c* NPP1 Power

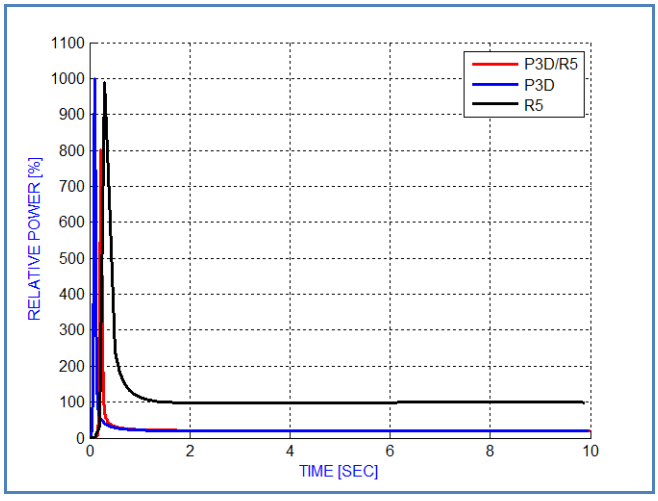

Figure 7-12 - Case *c* Total Reactivity

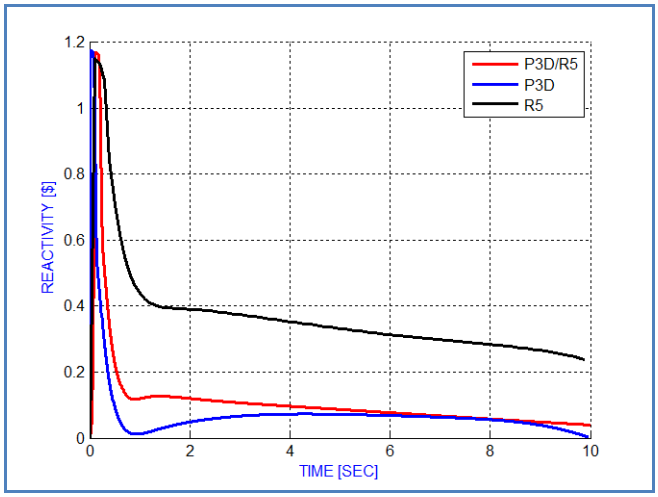

The reactivity worth of the ejected rod is as high as 1.18$, as presented in section 6.1. As a consequence, a fast power peak is expected just after the CRB ejection. The reactivity trend using the three codes is very similar: the high reactivity worth dominates the power behavior, thus the total power increases very fast and subsequently decreases deeply in a short time. It must be noted the power peak reaches 1000 (P3D), 980 (R5) and 800 (P3D/R5) times the nominal power. Furthermore, the use of the P3D/R5 codes presents a less conservative result with a lower peak and lower steady-state value are reached

Figure 7-13- NPP1 Case *c* P3D Reactivity

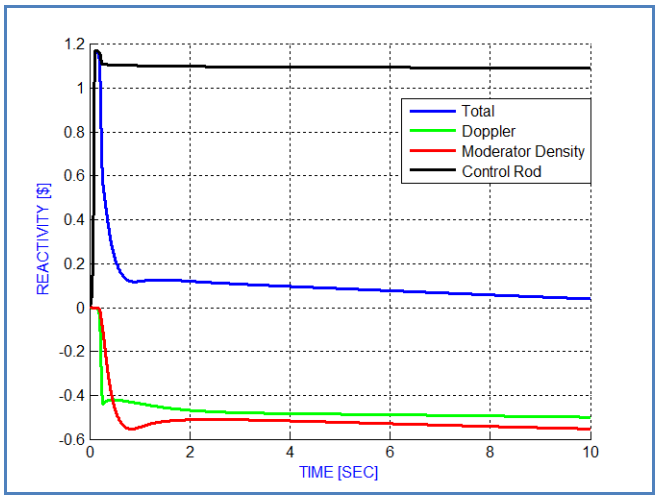

Figure 7-14 – NPP1 Case *c* R5 Reactivity

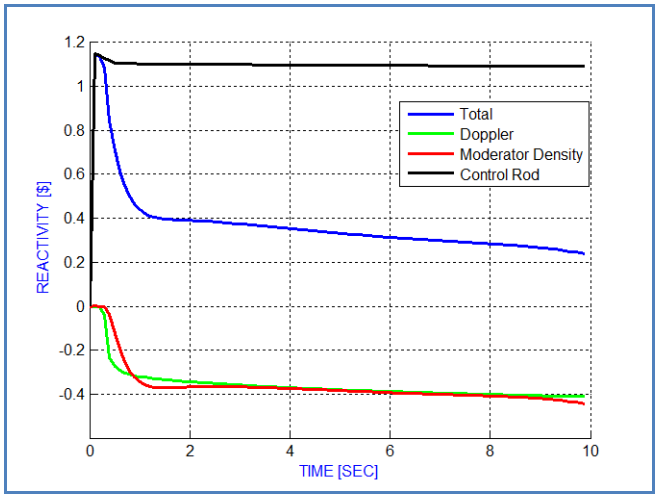

Figure 7-15 – NPP1 Case *c* P3D/R5 Reactivity

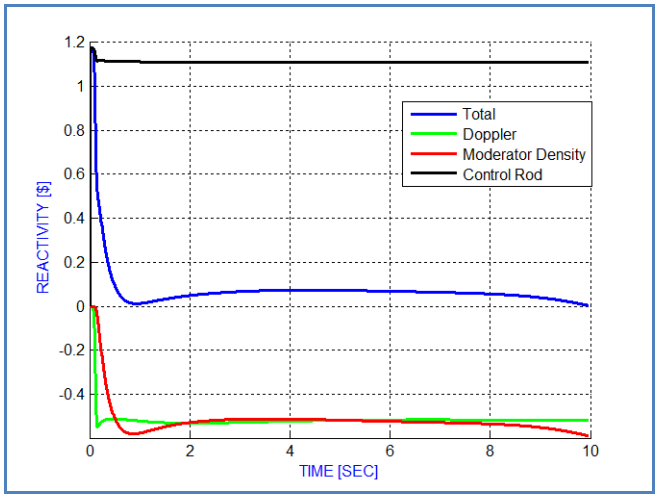

7.2. P3D/R5 Total Power and Reactivity Assessment for the Three Plants

The simulation of distinct plant sizes combines similarities in the NPP1, NPP2 and NPP3 core designs, e.g. the fuel assembly's enrichment, the use of inner fuel assembly ring, the axial fuel distribution (see section 4 for details), to assess the total power and reactivity behavior, as well as the 3D power distribution, simulated by the P3D/R5 coupled package. Therefore, the effect of reducing the core power from 2,772 MWt to 1,061 and to 530 MWt is addressed by ejecting a CRA/CRB that presents similar reactivity worth.

7.2.1. Case *a:* CRA#8 HFP (Initial NPP Power at 100%) for the Three Plants

As shown in Figure 7-16, by applying the same case *a* assumptions and initial conditions, the relative power reaches its peak at 125% (NPP1), 121% (NPP2) and 123% (NPP3) - the small differences among the peaks are not significant. However, the reactor power at steady-state (after 15 seconds) is lower for the smaller cores: 94% (NPP1), to 64% (NPP3) and to 51% (NPP2). This trend is consistent with the total reactivity behavior shown in Figure 7-17. In addition, the averaged fuel and coolant temperatures are lower for NPP2 as shown in Figure 7-18 and Figure 7-19.

Figure 7-16 – Case *a* Relative Nuclear Power

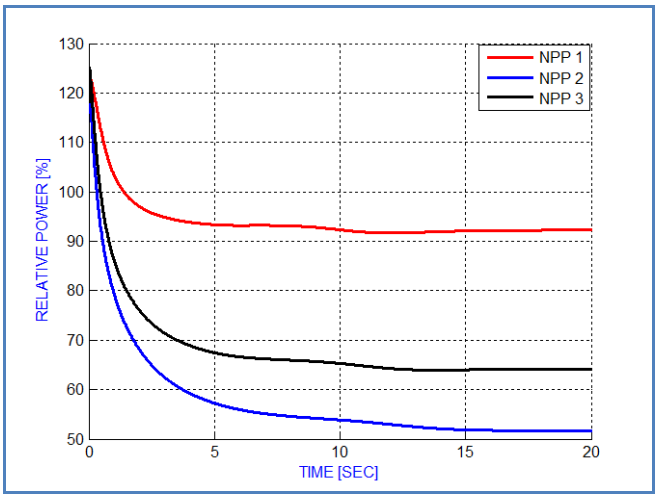

Figure 7-17 – Case *a* Total Reactivity

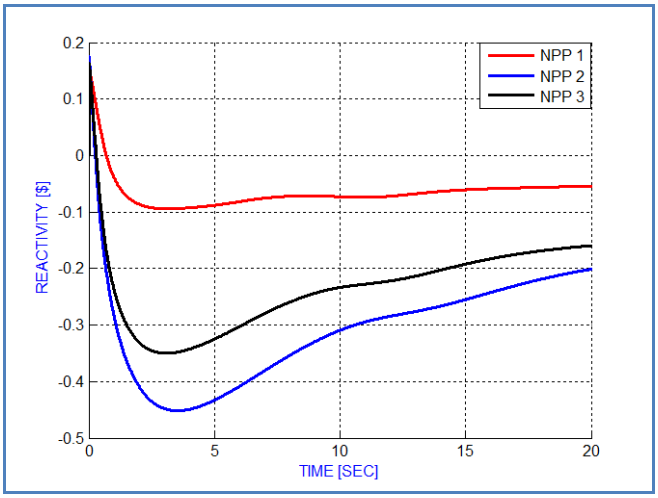

Figure 7-18 – Case *a* Averaged Fuel Temperature

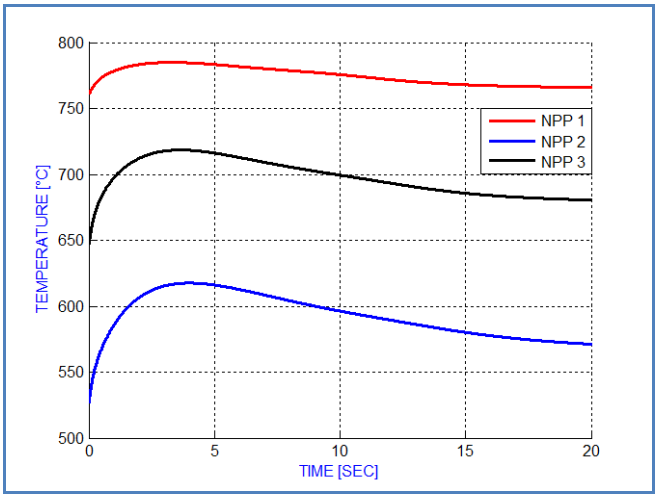

Figure 7-19 – Case *a* Averaged Coolant Temperature

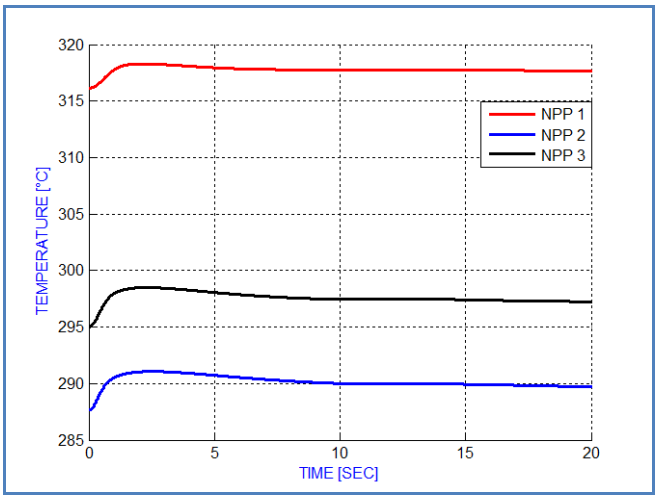

7.2.2. Case *b:* CRA#8 HZP (Initial NPP Power at 0.01%)

A similar behavior can be seen in Figure 7-20 for case *b*. Although the HZP simulation is very conservative from the accident analysis point of view, the core is critical at very low power and the ejection of the control rods introduces large positive reactivity compared to case *a*, as shown in Figure 7-21, that lead to a higher relative power: NPP1 has a peak of about 475 times the initial power, NPP2 about 327 times and NPP3 about 374 times the initial power. However, the relative power peak is limited to less than 4.8% (NPP1), 3.2% (NPP2) and 3.8% (NPP3) of the nominal power. The results are consistent with the total reactivity

behavior. The NPP2 expected maximum reactivity of 0.42$, presented in Table 6-4, is close to the NPP1 (0.41$) and the NPP3 (0.40$).

Figure 7-20 – Case *b* NPP Power

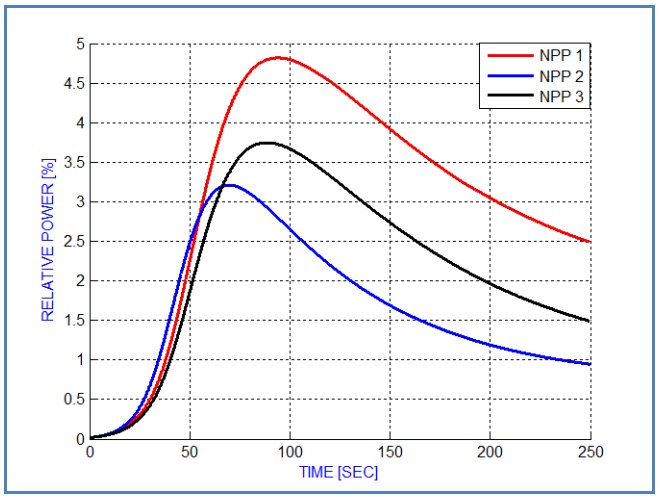

Figure 7-21 – Case *b* Total Reactivity

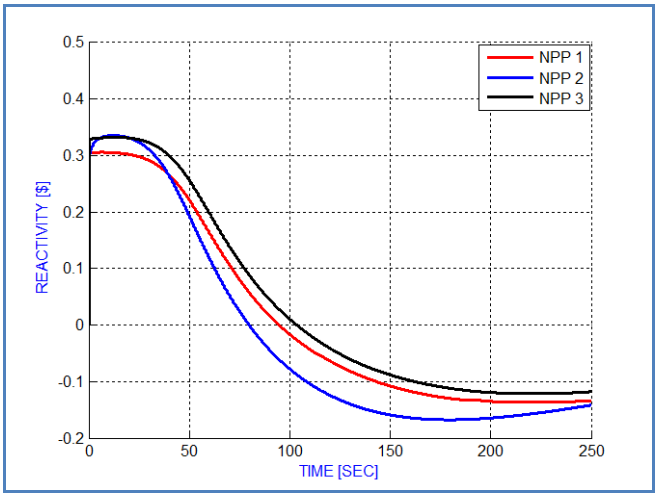

As a consequence, the NPP2 case *b* core averaged fuel temperature and coolant averaged temperature, presented in Figure 7-22 and Figure 7-23, are lower than the ones for NPP1 and NPP3.

Figure 7-22 – Case *b* Averaged Fuel Temperature

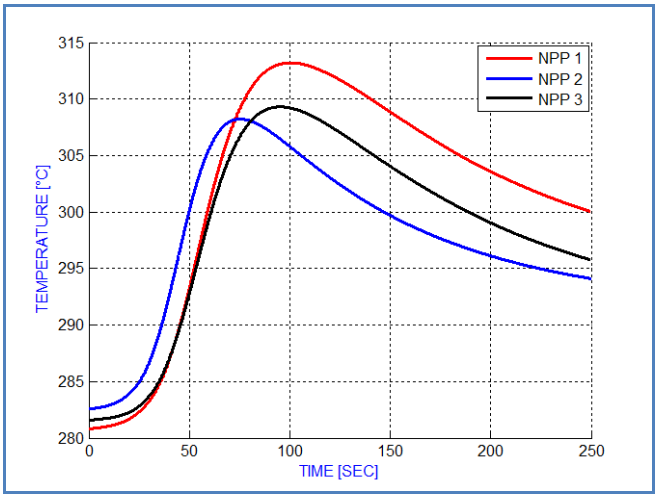

Figure 7-23 – Case *b* Averaged Coolant Temperature

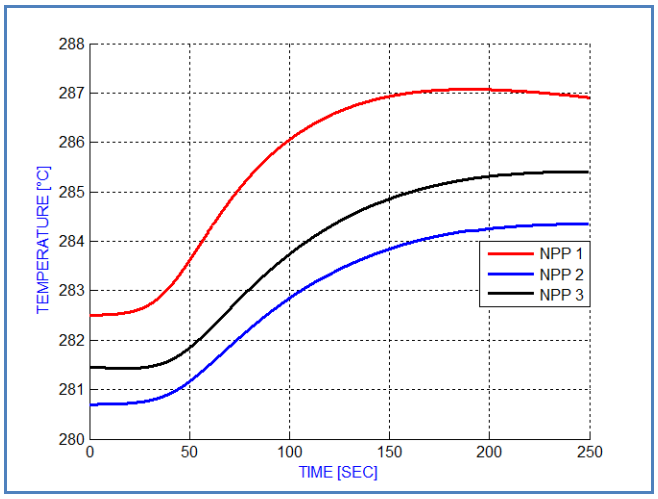

7.2.3. Case *c:* CRB#8 HZP (Initial NPP Power at 0.01%)

The CRB (case *c*) presents a peculiar behavior, as can be seen in Figure 7-24. Besides the lower total power peak of 400% (NPP2), compared to 600% (NPP3) and 1,000 (NPP1), the simulation results indicate that the peak is also delayed. The large positive reactivity inserted, as can be seen in Figure 7-25, after the rod ejection is also delayed by 0.08 second (NPP1), 0.16 seconds (NPP2) and 0.11 seconds (NPP3), which explains this behavior. The steady-state relative power is about 20% of the full power for the three NPPs.

Figure 7-24 – Case *c* NPP Power

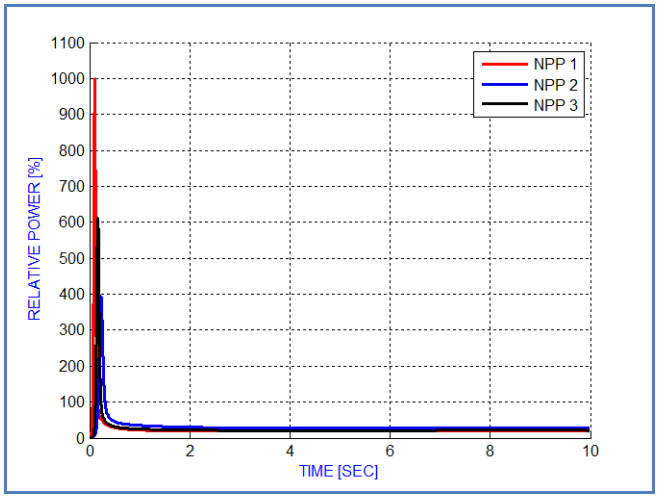

Figure 7-25 – Case *c* Total Reactivity

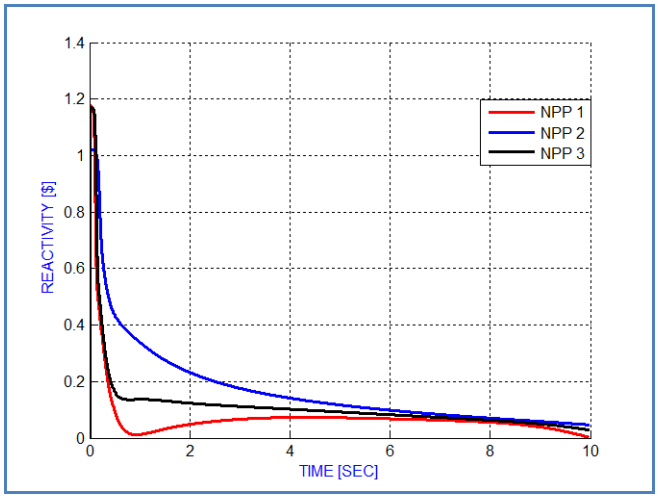

Figure 7-26 and Figure 7-27 present the case *c* average fuel and coolant temperature. In general, the higher reactivity worth results in higher moderator and fuel temperature, as expected due to negative fuel and void reactivity feedback.

Figure 7-26 – Case *c* Averaged Fuel Temperature

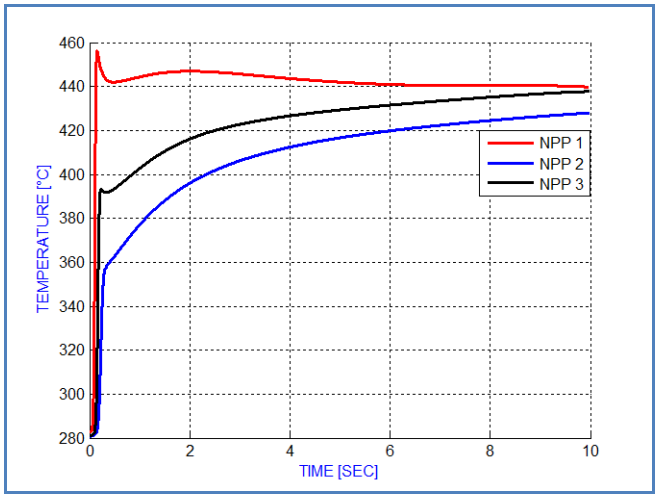

Figure 7-27 – Case *c* Averaged Coolant Temperature

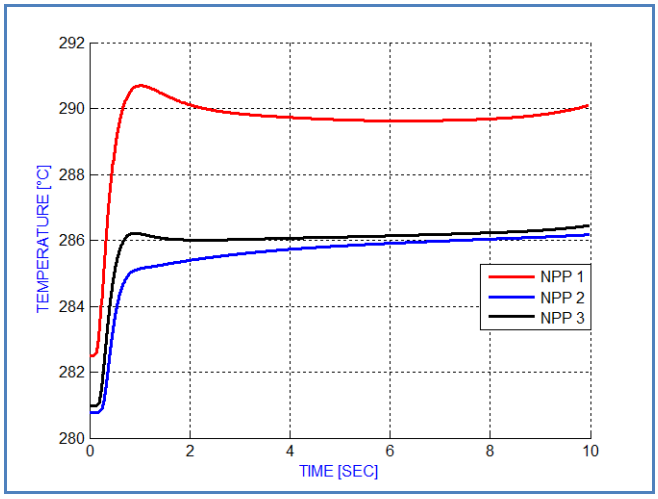

7.3. Total Power and Reactivity Assessment for NPP2a

The reactivity coefficients listed in Table 6-7 are similar (up to 5% difference) among the three NPPs core output levels and the RIA occurs within 0.1 second. Therefore, it is expected that the core size dominates the total power behavior. To confirm that the small difference on the moderator and Doppler coefficients does not interfere with the overall simulation conclusions, the linear heat generation rate (LHGR) of NPP2 was changed in both P3D and R5 models/codes to match the 15 kW/m NPP#1 LHGR (from this point, it is identified as NPP2a) by increasing the power level to 730 MWt.

The new NPP2a Doppler and moderator reactivity are presented in Table 7-1. It is worth noting that there is a large reactivity coefficient difference between the NPP2 and NPP2a for case *a* but small differences for case *b* and case *c*. These results are consistent to the coefficients presented in Table 6-7.

Table 7-1 –Reactivity Coefficients of NPP2a for similar NPP1 LHGR

	Doppler Coefficient ($/k)			**Moderator Coefficient ($/kg/m$^{3)}$**		
Case	**NPP 2**	**NPP 2a**	**Diff. (%)**	**NPP 2**	**NPP 2a**	**Diff. (%)**
a	-5.02E-03	-4.78E-03	4.86	5.64E-02	5.39E-02	4.50
b	-5.69E-03	-5.70E-03	-0.08	5.68E-02	5.68E-02	-0.05
c	-5.76E-03	-5.72E-03	0.83	5.47E-02	5.43E-02	0.63

Next, a new set of simulation leads to the identification of the CRA/CRB#8, as it can be seen in Table 7-2

Table 7-2 – NPP2a CRA/CRB#8 Identification

Case	**CRA/CRB#8 Position**	**ARI/ARO ($)**	**Steady-State $k_{eff} \cong 1$ ($)**
a	(8,D)	0.23	0.25
b	(8,F)	0.46	0.42
c	Bank #4	1.48	1.32

Following, after new set of simulations, the initial conditions are chosen, as shown in Table 7-3, to guarantee that the K_{eff} of unity for each NPP just before the occurrence of the RIA.

Table 7-3 – NPP2a P3D Criticality Initial Conditions

Case	**CRA#2 to 7 at t=0**	**k_{eff}**
a	CRA # 4, 5 and 7: fully withdraw CRA # 2 and 7: 135 steps withdraw CRA # 6: 98 steps withdraw	1.00017
b	CRA #2, 5 and 7: fully inserted CRA #4 and 6: 190 steps withdraw	1.00001

Case	CRA#2 to 7 at t=0	k_{eff}
c	CRA # 4, 5 and 7: fully inserted CRA #2 and 6: 155 steps withdraw	1.00003

Then, the NPP2a P3D/R5 coupled simulations are performed according to Table 3-3 conditions. Therefore, as it can be seen from Figure 7-28 to Figure 7-33, the reactivity and total power responses are consistent with previous results as the power level of NPP#2 is updated to 730 MWt to accommodate the changes in the LGHR. P3D and R5 use an internal temperature calculation scheme based on the input power. During the steady-state run, the fuel and moderator temperature are calculated and a restart file is generated: this file contains the starting points for the transient calculations.

Figure 7-28 – Case *a* P3D/R5 Total Power

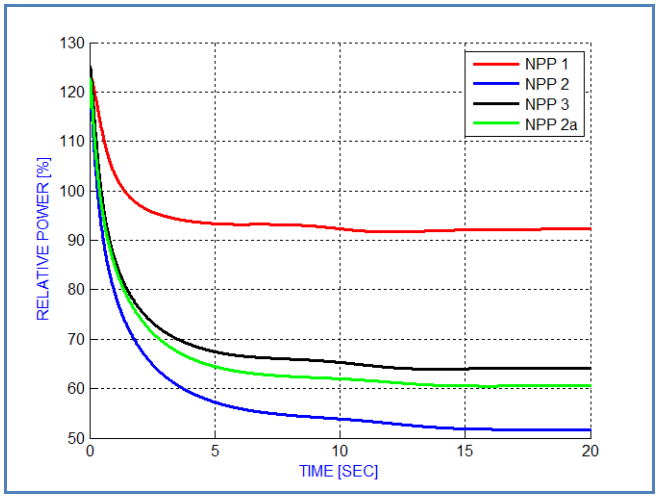

Figure 7-29 – Case *a* P3D/R5 Total Reactivity

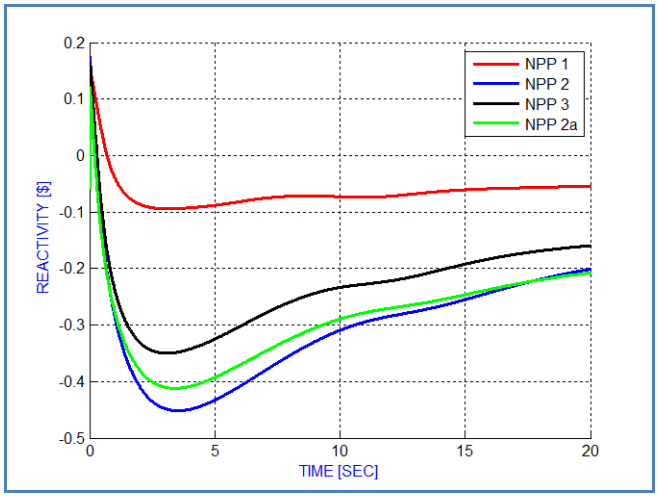

Figure 7-30 – Case b P3D/R5 Total Power

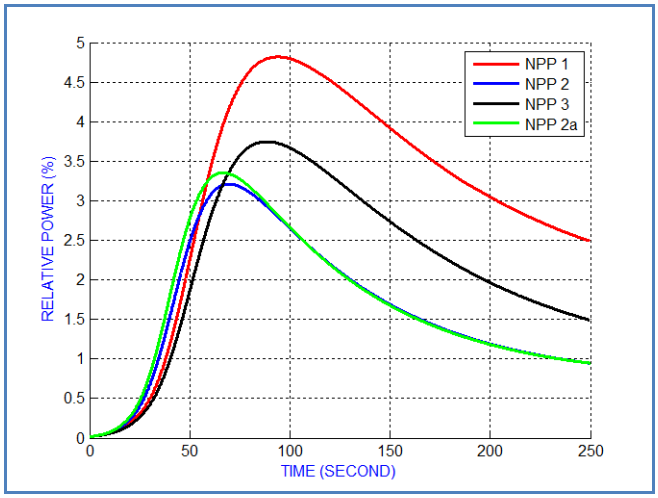

Figure 7-31 – Case *b* P3D/R5 Total Reactivity

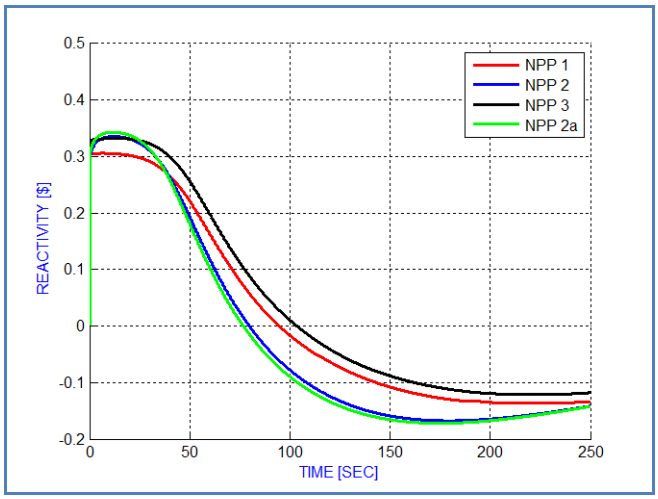

Figure 7-32 – Case *c* P3D/R5 Total Power

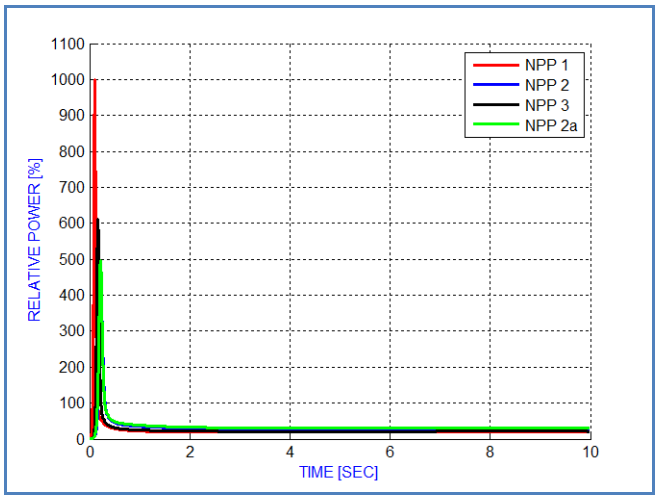

Figure 7-33 – Case *c* P3D/R5 Total Reactivity

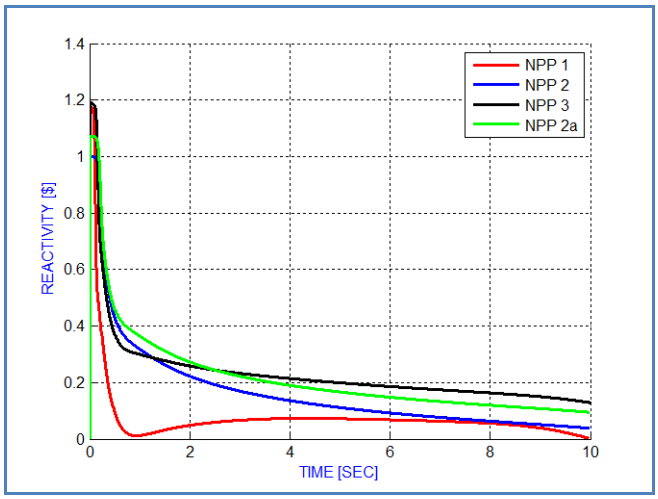

7.4. Chapter Summary

The use of a thermal hydraulic and/or a neutronic code may present similar results if simulated data from one code is plugged in the other code. However, this procedure demands many interactions and it is time demanding. On the other hand, the coupled codes use the best of each code and it is less time consuming, allowing automatically code interactions. For both cases, accurate simulation results imply good understanding of the problems and the code. Furthermore, the use of coupled codes leads to less conservative transients' outcomes, from the design point of view, as the core shrinks.

To benchmark simulation results among the three NPPs, the comparison of initial and maximum reactivity among the cases and codes is presented in Table 7-4. As can be seen, from the design point of view, the P3D/R5 transient simulation typically predicts lower peak reactivity than the standalone simulations. The magnitude of reduction in prediction of peak reactivity becomes larger as the core shrinks. Furthermore, the P3D steady-state simulation is also conservative and does not correspond to the expected peak in reactivity due to the ejection of CRA.

Table 7-4 – Comparison of Initial and Maximum Reactivity Simulation Data

Case	NPP	Initial ($)	Maximum Transient Peak ($)		
		P3D	P3D	R5	P3D/R5
a	1	0.24	0.16	0.17	0.15
	2	0.24	0.18	0.19	0.16
	3	0.26	0.18	0.17	0.15
b	1	0.41	0.33	0.34	0.33
	2	0.42	0.31	0.35	0.31
	3	0.40	0.36	0.33	0.32
c	1	1.34	1.20	1.19	1.18
	2	1.32	1.10	1.11	1.09
	3	1.32	1.22	1.16	1.15

Table 7-5 presents the maximum P3D/R5 averaged fuel and coolant temperatures. In general, the higher reactivity worth results in higher moderator and fuel temperature, as expected due to negative fuel and void reactivity feedback.

Table 7-5 – P3D/R5 maximum Fuel and Coolant Temperature

Case	NPP	Averaged Fuel Temperature (°C)	Averaged Coolant Temperature (°C)
a	1	780	318
	2	615	291
	3	720	298

b	**1**	314	287
	2	307	284
	3	309	285
c	**1**	460	292
	2	425	286
	3	440	287

8. 3D CORE POWER DISTRIBUTION ASSESSMENT

The use of P3D coupled with R5 allows a 3D assessment of the power distribution during a RIA. At the beginning of the simulation, the core is at steady-state with the CRA/CRB#8 fully inserted and the power being generated relatively uniformly within all the fuel assemblies (within the normal distributions of radial neutron flux variations, the peak to average assembly power is typically less than 1.5). However, after the RIA, the 3D power distribution can have high peaking factor that is different among the various cases, but it does not depend on the size of the core (under the stated assumptions of similar core designs):

a. Case *a*: after the insertion of reactivity, the power surrounding the control rod being ejected increases, but after 10 seconds of simulation the power returns to the relatively uniform distribution;
b. Case *b*: after the insertion of reactivity, the power surrounding the control rod being ejected increases significantly from its initial value and does not return to a uniform distribution. The area surrounding the ejected CRA stays hotter than the remaining assemblies. Therefore, as expected, an ejection of a CRA under HZP core conditions may have a worse effected within the fuel assembly surrounding the CRA#8 during and after the transient; and
c. Case *c*: after the insertion of reactivity, there is a very fast rise in the power distribution within the fuel assemblies surrounded by the bank being ejected. In this case, the insertion of a higher reactivity may keep the core hotter for longer period of time.

The 3D core power distribution represents the assembly peaking factor, i.e. the assembly power divided by the average assembly power in the core, which is the reactor total power divided by the number of fuel assemblies.

8.1. NPP1 3D Power Distribution

At the beginning of the case *a* simulation, i.e. t = 0 seconds, the core is at steady-state, but the power is not being generated uniformly due to the insertion of the CRA#8. After the ejection, the faster increase in the reactivity, as discussed in item 7, leads to an increase in the power surrounding of the control rod being ejected. Therefore, the power distribution

surrounding the rod FA in the position (13,I) increases 212.36% just after the CRE. After the transient, it returns closer (105.18%) to the initial power, as can be seen in Figure 8-1, Figure 8-2 and Figure 8-3. Thus, Figure 8-4 indicates that the power is again uniformly distributed at t=10.0 seconds.

Figure 8-1 - NPP1 Case *a* 3D Power Distribution at t=0 sec

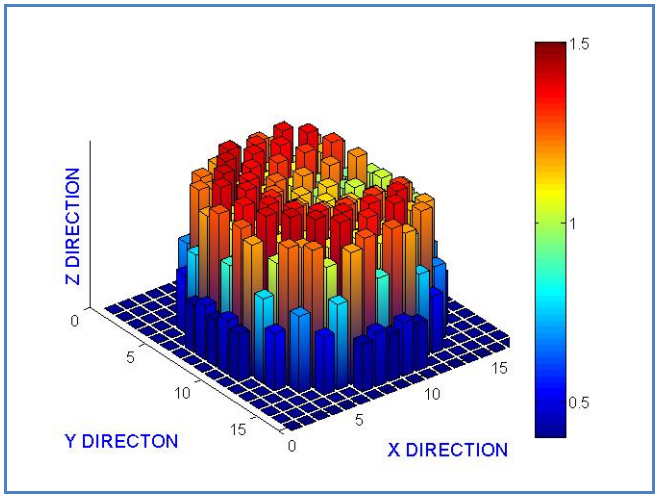

Figure 8-2 - NPP1 Case *a* 3D Power Distribution at t=0.10 sec

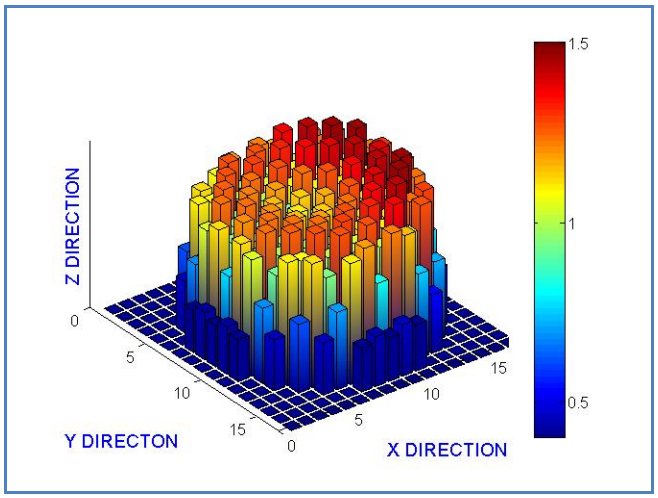

Figure 8-3 - NPP1 Case *a* 3D Power Distribution at t=10.0 sec

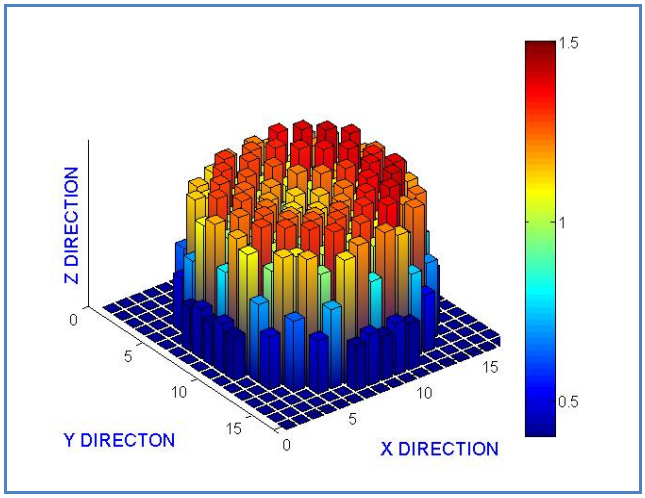

Figure 8-4 - NPP1 Case *a* Radial Power Distribution at t=10.0 sec

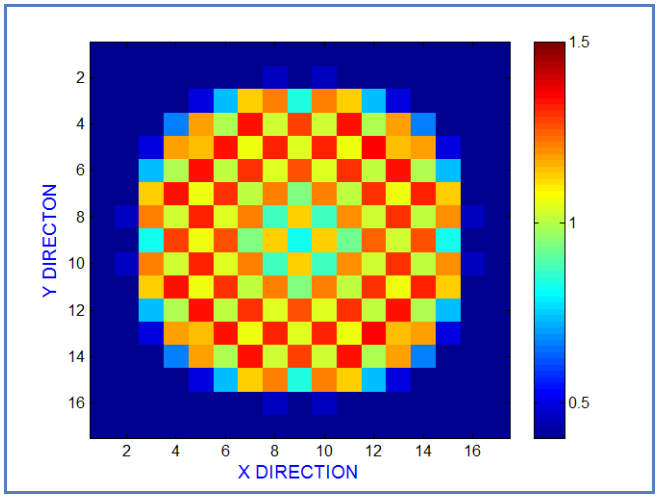

The case *b* 3D power distribution is presented in Figure 8-5, Figure 8-6 and Figure 8-7. The simulation results indicate that at time t=0 seconds the power is well distributed due to the very small reactor power (only 0.01% of the nominal power). Then, after the CRE, there is an increase of 243.6% in the power surrounding the CRA#8 (the total relative maximum power is only 3.2% of the nominal power, as indicated by session 7.2).

Figure 8-5 - NPP1 Case *b* 3D Power Distribution at t=0 sec

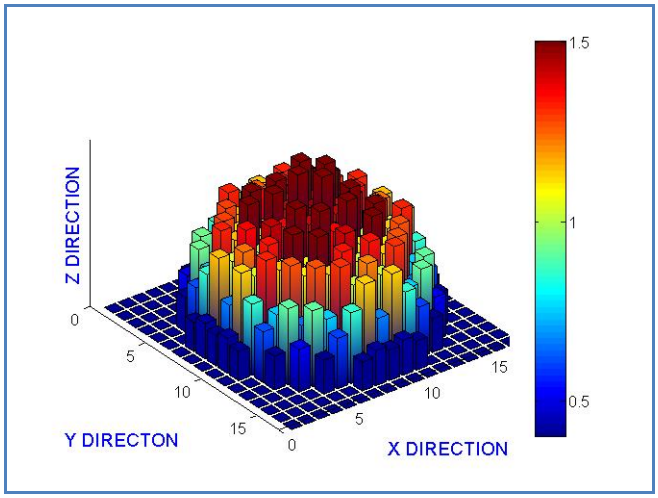

Figure 8-6 - NPP1 Case *b* 3D Power Distribution at t=0.1 sec

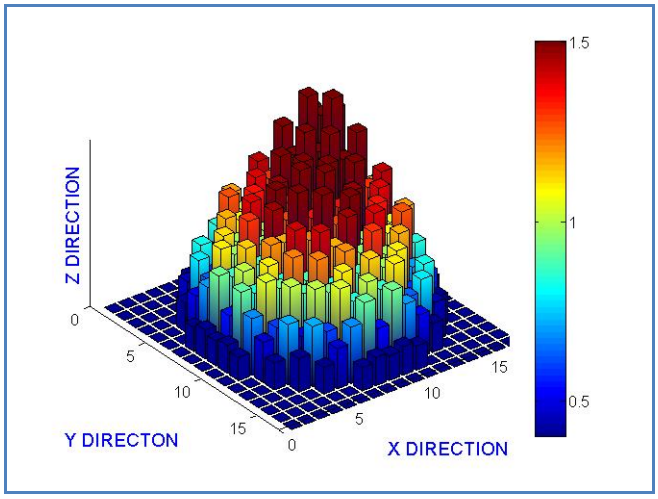

Moreover, after the transient (t=200 seconds) the power is not uniformly distributed. The area surrounding the ejected CRA stays hotter than the remaining assemblies: the power distribution in the surroundings of the CRA#8 is 201.07% higher. Therefore, as expected, a CRA ejection of under HZP core conditions may have a worse effect within the FA surrounding the CRA#8 during and after the transient. Figure 8-8 presents the radial power distribution at t=200 seconds. It can be seen that the power peak occurs within the assemblies surrounding the CRA#8.

Figure 8-7 - NPP1 Case *b* 3D Power Distribution at t=200.0 sec

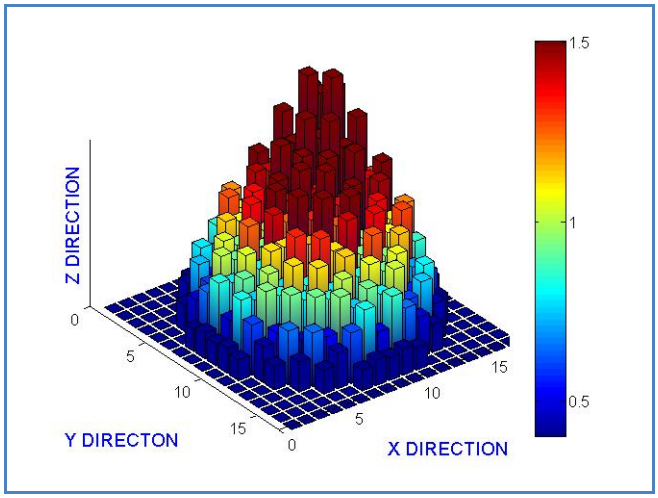

Figure 8-8 - NPP1 Case *b* Radial Power Distribution at t=200.0 sec

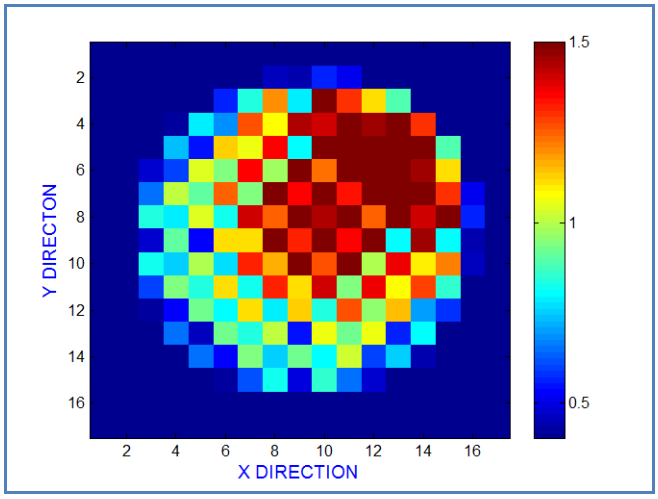

The CRB#8, case *c*, 3D power distribution is presented in Figure 8-9, Figure 8-10 and Figure 8-11. It can be seen that at t=0 seconds the power is well distributed among the FAs due to the CRB#8 symmetry. Then, at t=0.1 seconds there is a 183.68% rise in the power distribution within the FAs surrounded by the bank being ejected. However, after the transient (i.e. after t=10 seconds), the power distribution is still 151.82% higher than at t=0 seconds (this trend does not occur for the HFP: the power is uniformly distributed just after the reactor reaches steady-state). This result indicates that, although the chance of this accident looks small, the insertion of a higher reactivity under a HZP core conditions may keep the core hotter for longer time.

Figure 8-9 - NPP1 Case *c* 3D Power Distribution at t=0 sec

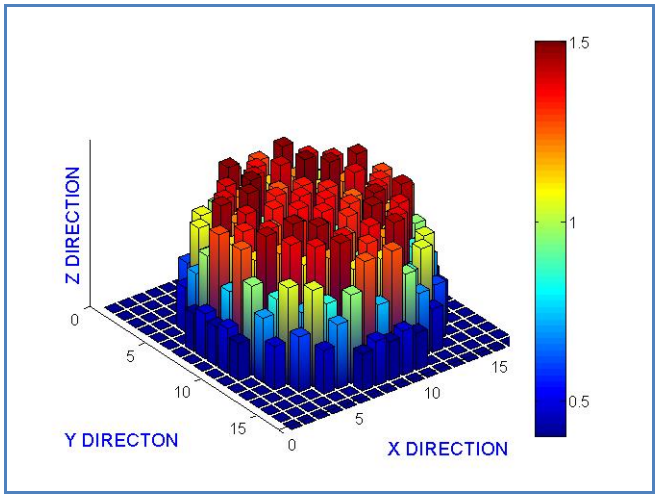

Figure 8-10 - NPP1 Case *c* 3D Power Distribution at t=0.1 sec

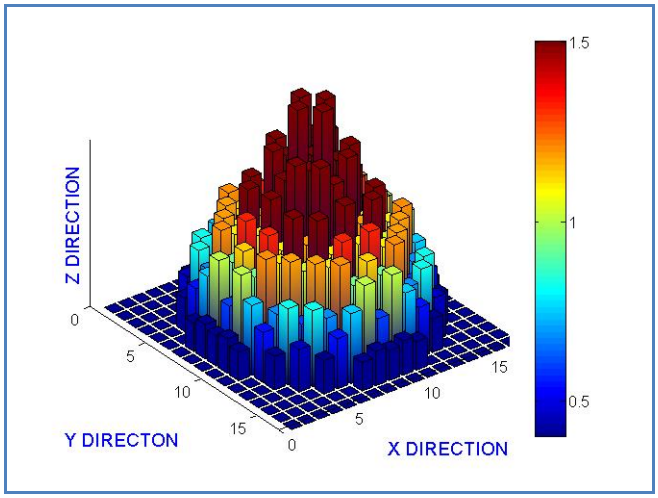

Figure 8-12 shows the radial power distribution after the transient. It can be seen that the power is uniformly distributed within the core center. Although the power response and the feedback due to the reactivity insertion are very fast, the core power remains significantly higher.

Figure 8-11 - NPP1 Case *c* 3D Power Distribution at t=10.0 sec

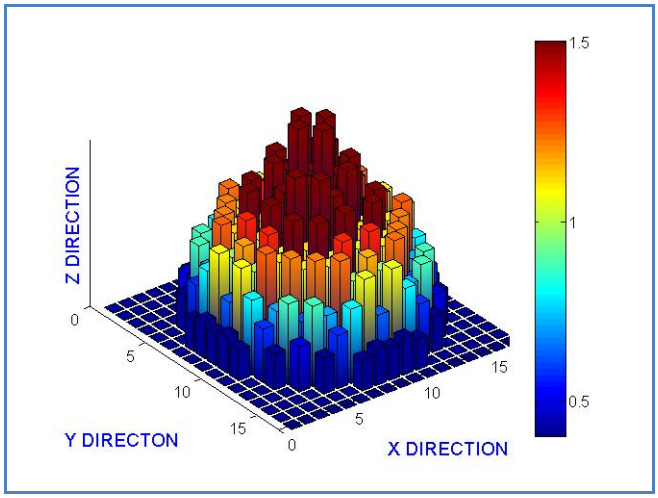

Figure 8-12 - NPP1 Case *c* Radial Power Distribution at t=10.0 sec

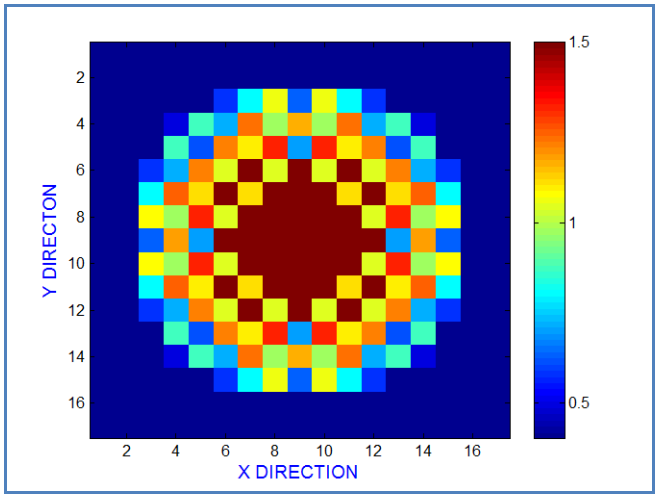

8.2. NPP2 3D Power Distribution

The case *a* control rod assembly ejection causes a fast rising in the 3D power distribution within the FAs located nearby the CRA#8, as revealed by Figure 8-13 and Figure 8-14. However, as the core goes small keeping the same design, the power increasing is only 135.55% compared to 212.36% (NPP1).

After the peak in the 3D power distribution, the coolant mass flow rate increases removing the extra heat. Therefore, the power returns closer to its original value, as it can be seen in Figure 8-15, very fast: after the transient (i.e. t=10.0 seconds), it stays at 103.32% of the initial power.

Figure 8-13 – NPP2 Case *a* Power Distribution at t=0 sec

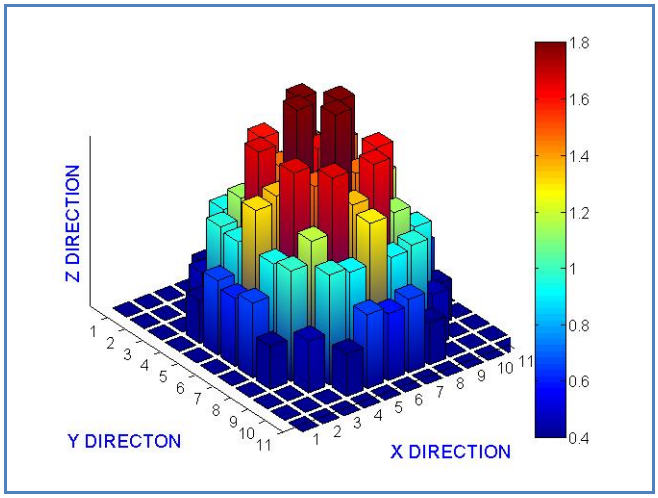

Figure 8-14 – NPP2 Case *a* Power Distribution at t=0.065 sec

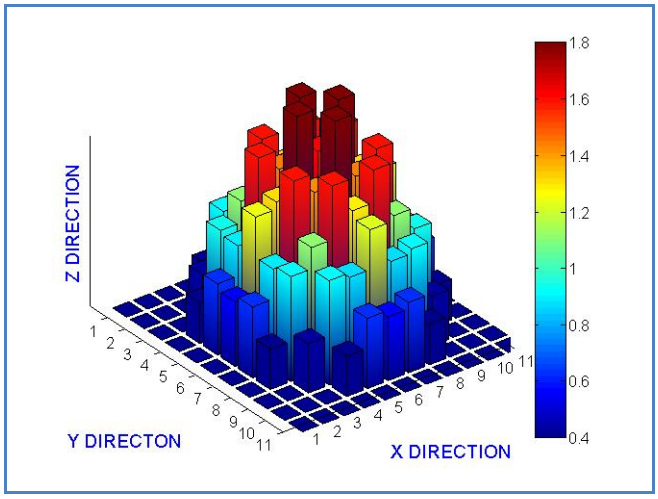

Figure 8-16 presents the radial power distribution after the transient. It can be seen that the power is also uniformly distributed compared to the distribution at t=0 seconds.

Figure 8-15 – NPP2 Case *a* Power Distribution at t=10.0 sec

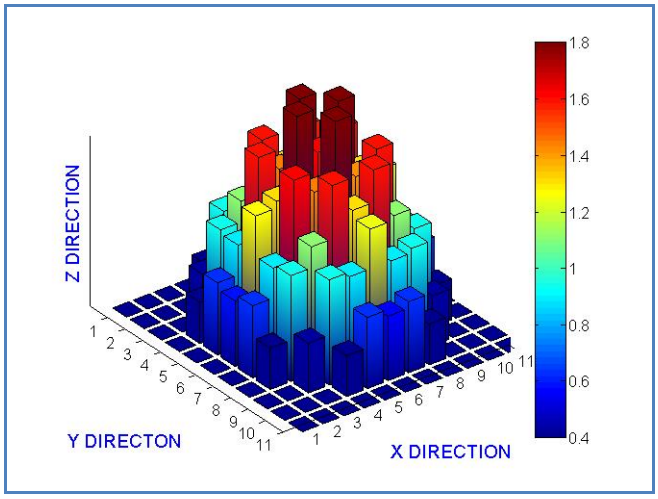

Figure 8-16 – NPP2 Case *a* Radial Power Distribution at t=10.0 sec

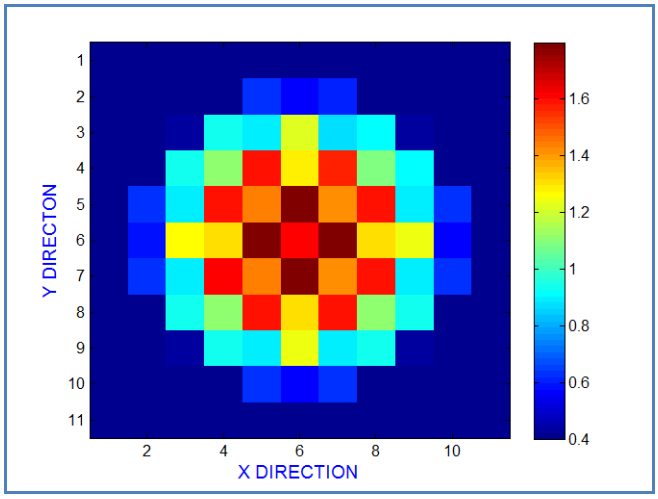

The case *b* simulation results are presented in Figure 8-17, Figure 8-18 and Figure 8-19. Besides the increase of 142.82% in the power surrounding the CRA#8 (it is significantly small compared to 243.66% for NPP1), the core stays hotter longer than for the HFP (after t=200.0 sec, the power is 123.12%). The radial power distribution is uniformly distributed, as can be seen in Figure 8-20.

Figure 8-17 – NPP2 Case *b* Power Distribution at t=0 sec

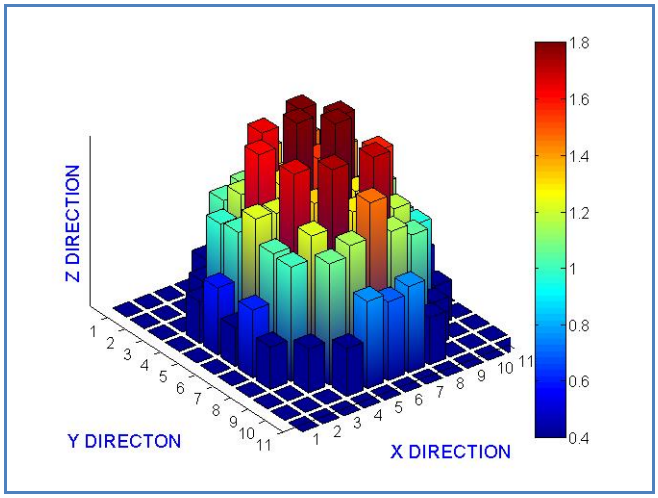

Figure 8-18 – NPP2 Case *b* Power Distribution at t=0.065 sec

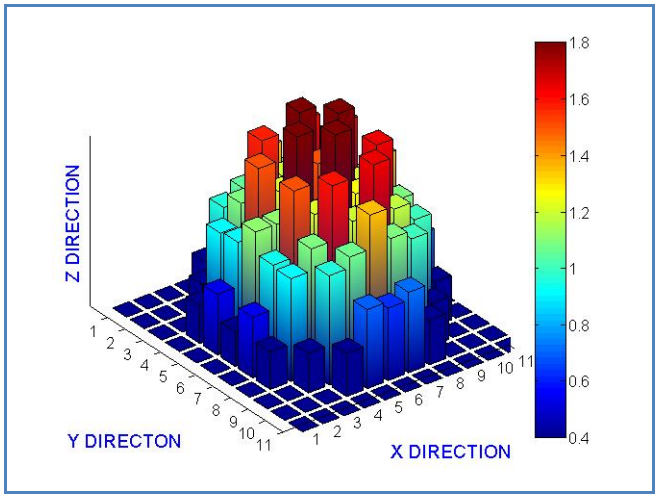

Figure 8-19 – NPP2 Case *b* Power Distribution at t=200.0 sec

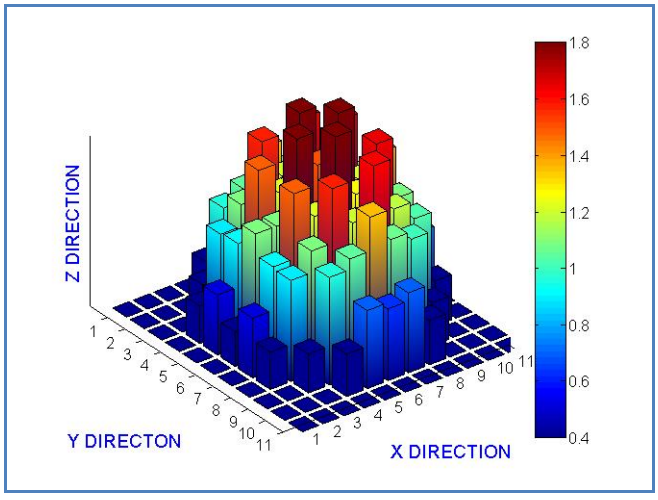

Figure 8-20 – NPP2 Case *b* Radial Power Distribution at t=200 sec

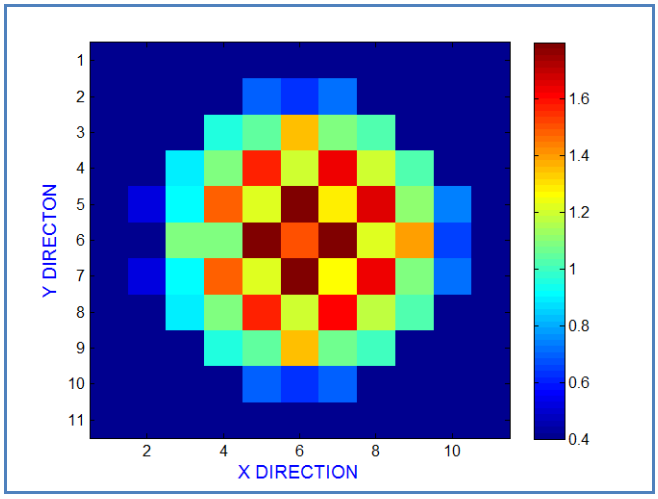

The case *c* CRB ejection simulation results are shown in Figure 8-21, Figure 8-22 and Figure 8-23. It can be noted that due to reactivity worth higher than 1$, the power also changes fast within the core central fuel assemblies and it stays higher after the end of the transient. However, as the core shrinks, the power distribution is lower: 124.30% at t=0.065 seconds and 113.47 % at t=10 seconds. Figure 8-24 shows the radial power distribution at t=10.0 seconds.

Figure 8-21 – NPP2 Case *c* Power Distribution at t=0 sec

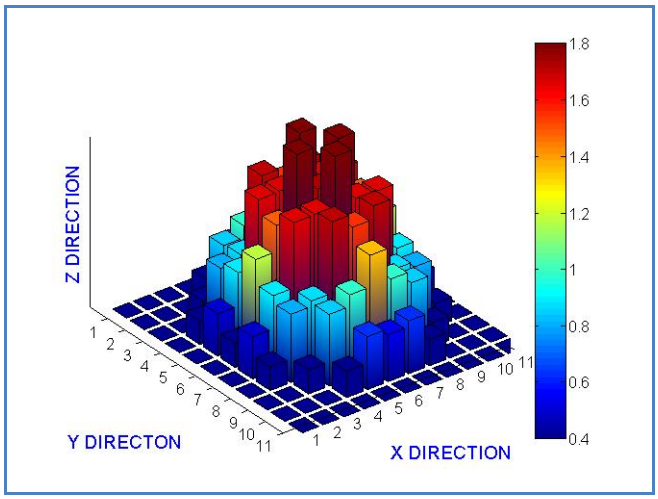

Figure 8-22 – NPP2 Case *c* Power Distribution at t=0.065 sec

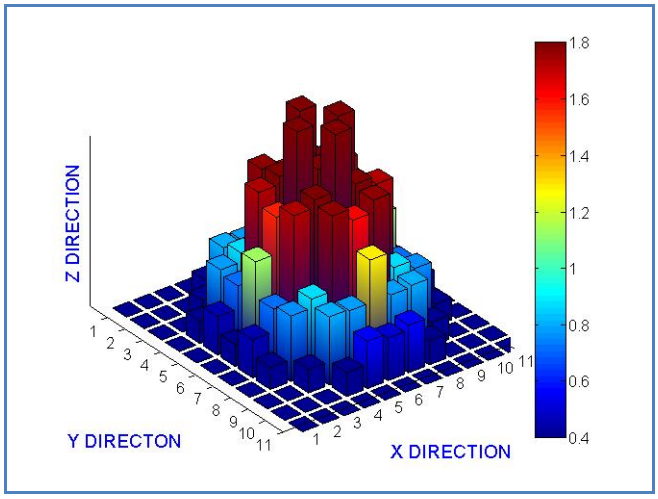

Figure 8-23 – NPP2 Case *c* Power Distribution at t= 10.0 sec

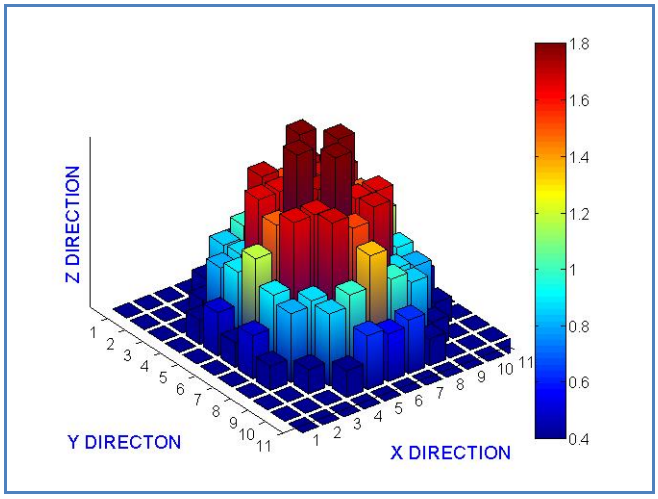

Figure 8-24 – NPP2 Case *c* Radial Power Distribution at t=10.0 sec

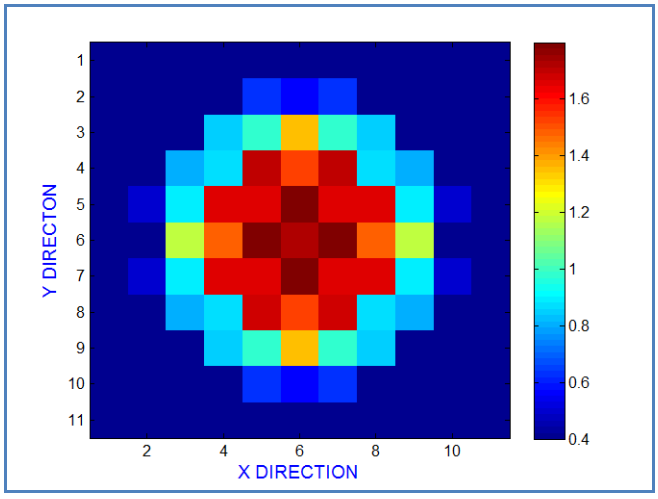

8.3. NPP3 3D Power Distribution

The core size reduction, assuming otherwise similar core design, has a small impact on the case *a* 3D power distribution, as can be seen from Figure 8-25 to Figure 8-27. The power surrounding the control rod being ejected increases and then turns back to its original value very fast. Under the assessed reactivity, the CRA#8 ejection causes an increase in the power of 176.20% at t=0.075 sec. After the transient, the power is only 104.13% (i.e. after t=10.0 sec).

It can be seen in Figure 8-28 that the power is well distributed just after the transient.

Figure 8-25 – NPP3 Case *a* Power Distribution at t=0 sec

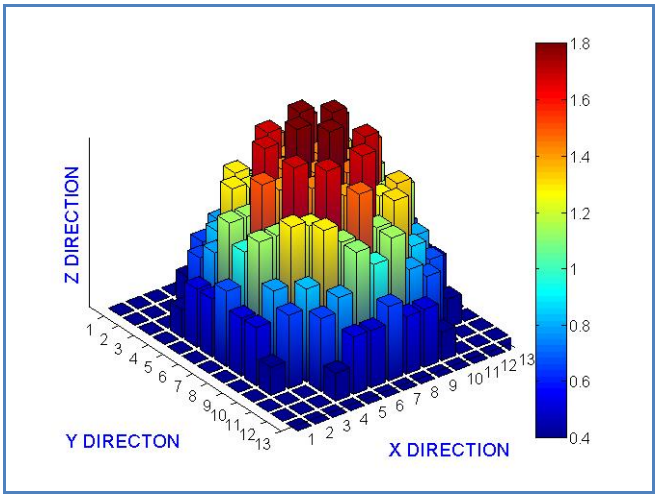

Figure 8-26 – NPP3 Case *a* Power Distribution at t=0.075 sec

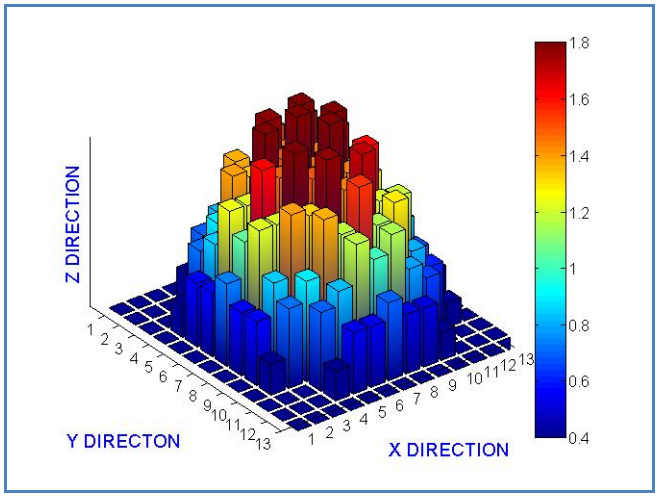

Figure 8-27 – NPP3 Case *a* Power Distribution at t=10.0 sec

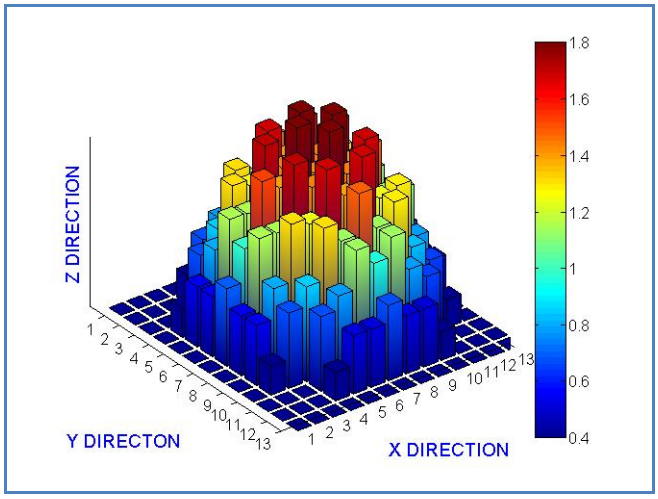

Figure 8-28 – NPP3 Case *a* Radial Power Distribution at t=10.0 sec

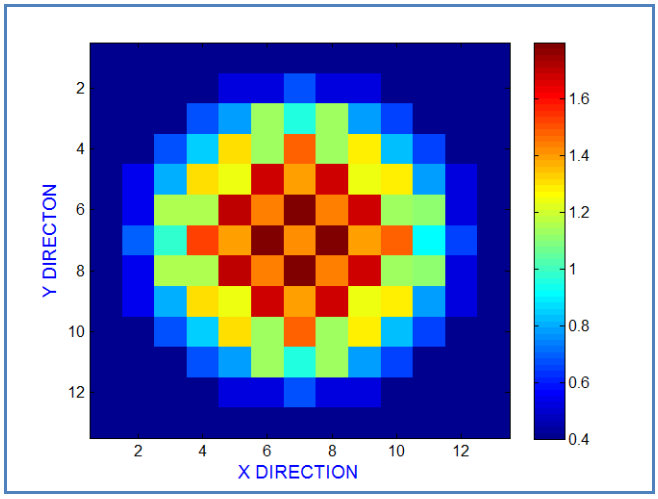

The case *b* simulation results are presented from Figure 8-29 to Figure 8-31. Besides the initial power increasing, the core condition stays hotter longer than for case *a*. Also, it can be seen that there is no significant impact on the 3D power distribution regarding the core size: at t=0.075 second, the power surrounding the CRA#8 increases to 147.63% and at t= 200 seconds it is 136.61%. As it can be seen in Figure 8-32, there is a hot spot nearby the CRB#8 in radial power distribution at t=200 seconds.

Figure 8-29 – NPP3 Case *b* Power Distribution at t=0 sec

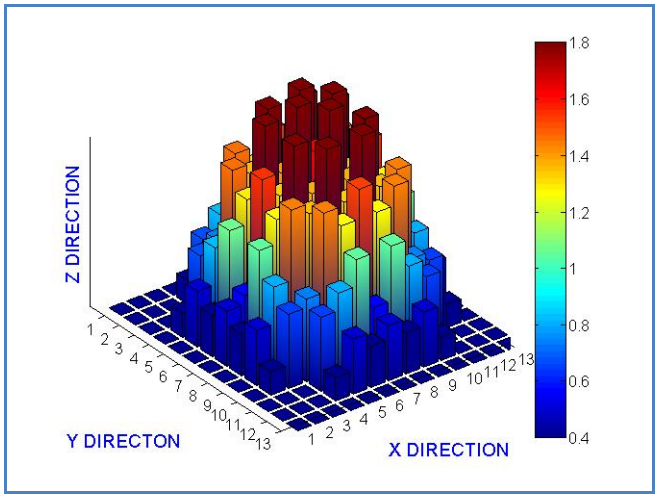

Figure 8-30 – NPP3 Case *b* Power Distribution at t=0.075 sec

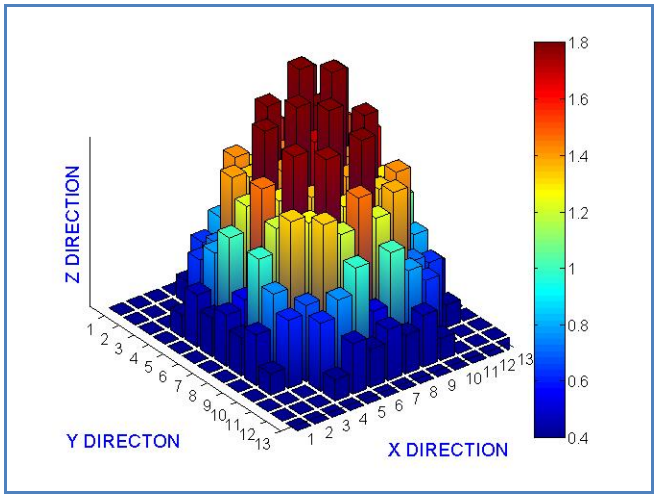

Figure 8-31 – NPP3 Case *b* Power Distribution at t=200 sec

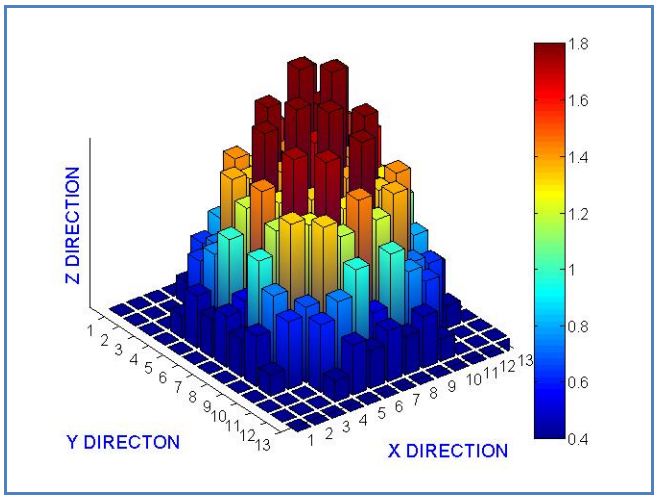

Figure 8-32 – NPP3 Case *b* Radial Power Distribution at t=200 sec

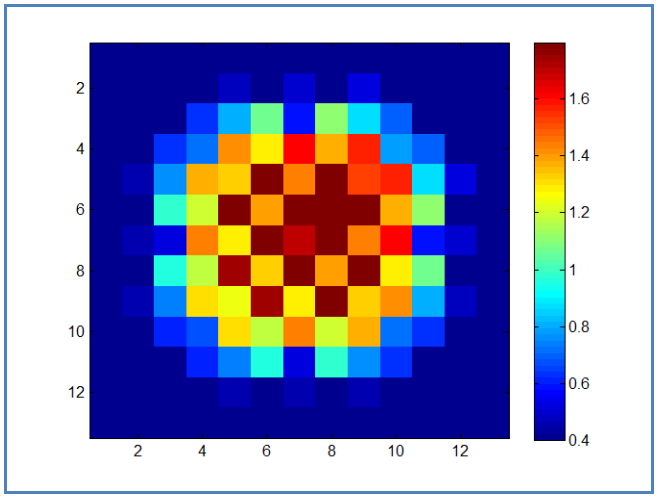

The case *c* simulation results are presented from Figure 8-33 to Figure 8-35. The power at the center assembly increases to 131.55% within t=0.075 sec. After the transient, the power comes down to 117.10%. Figure 8-36 presents the radial power distribution at t=10 sec.

Figure 8-33 – NPP3 Case *c* Power Distribution at t=0 sec

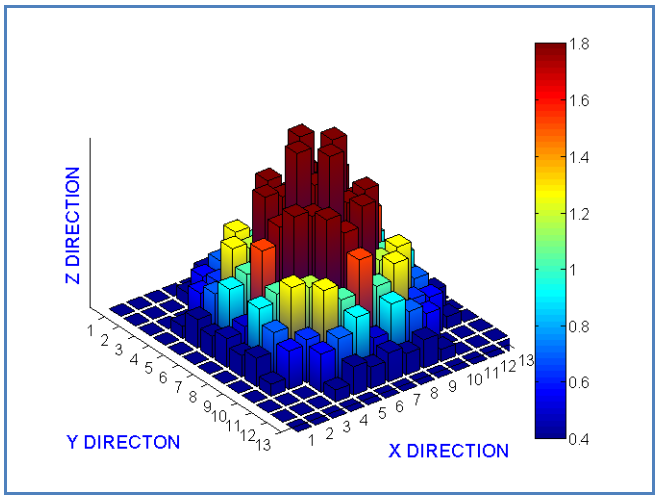

Figure 8-34 – NPP3 Case *c* Power Distribution at t=0.075 sec

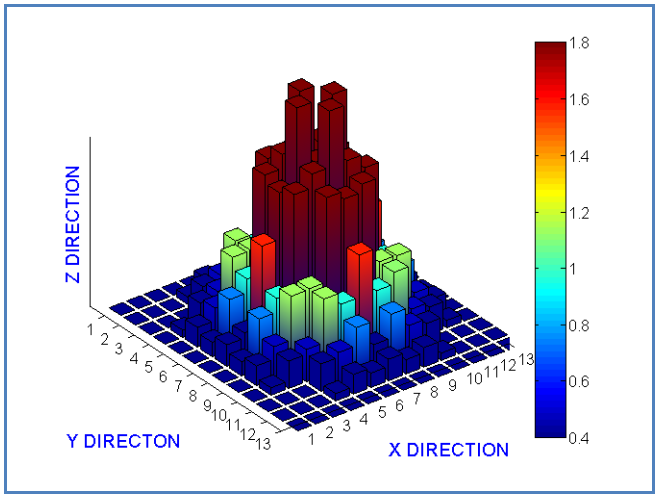

Figure 8-35 – NPP3 Case *c* Power Distribution at t=10.0 sec

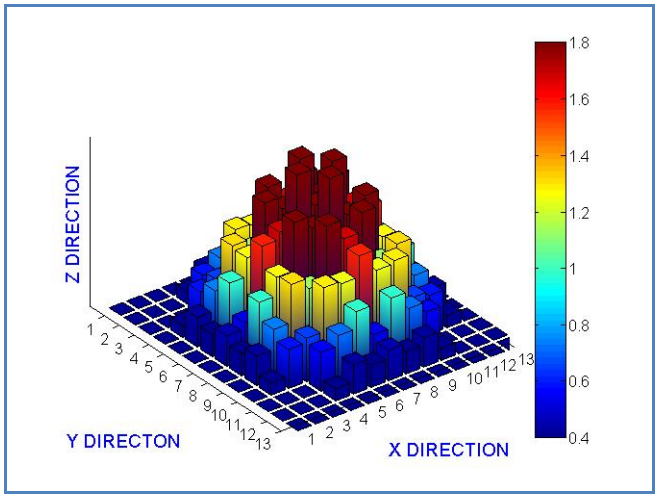

Figure 8-36 – NPP3 Case *c* Radial Power Distribution at t=10.0 sec

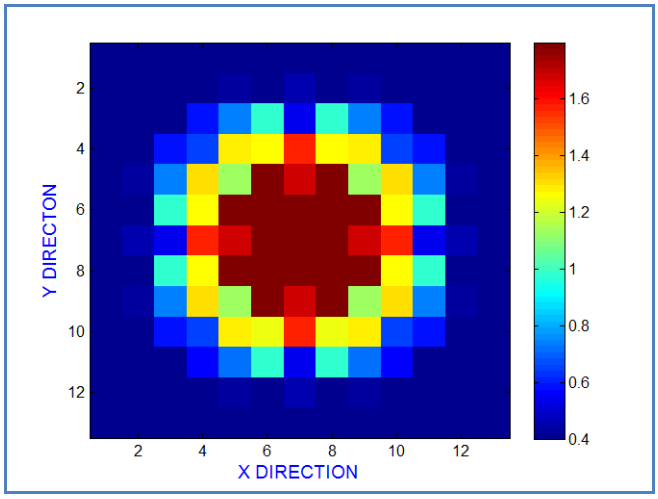

8.4. Chapter Summary

The simulation results indicate that the 3D power distribution depends on the reactivity worth due to the rod ejection, as expected, but also on the core initial condition. The core size reduction from NPP1 to NPP2 and NPP3, assuming similar core design, has a small impact on the power distribution, with the core power increasing locally in the area surrounding the rod/bank being ejected. The 3D analysis also indicates that the power under HFP core conditions becomes uniformly distributed just after the transient, while under HZP the area surrounding the CRA ejection stays hot longer for all core sizes.

To summarize, a comparison of 3D power distributions during the transient and at the post-transient steady-state surrounding the CRA/CRB#8 among the three cases and codes is presented in Table 8-1 (the reference point is the power at time t=0 seconds). It can also be seen that the peak assembly power gets lower as the NPPs shrinks.

Table 8-1 – Summary of the Ratio of Peak Assembly Power over the Peak Assembly of the Initial Steady-State, During and Post Transient

Case	NPP	CRA/CRB#8 Transient Power Factor	CRA/CRB#8 Post Transient Steady-State Power Factor
a	1	2.12	1.05
	2	1.35	1.03
	3	1.76	1.04
b	1	2.43	1.91
	2	1.42	1.23
	3	1.47	1.36
c	1	2.03	1.51
	2	1.24	1.13
	3	1.31	1.17

9. REACTIVITY ASSESSMENT USING THE EKF AND IPK METHODS

This study has implemented the EKF to estimate the nuclear reactor reactivity behavior under a RIA. The coupled P3D/R5 code generated the reactor power profile and a MATLAB script added random noise to the simulated power. For comparison, the IPK deterministic method was also implemented (see Figure 5-3 for details). The EKF and IPK performance are assessed by the convergence of the algorithm and by the reactivity standard deviation (SD). It is worth noting that the implementation of both methods is based on the PKRE. It was found that the EKF method presents better results compared to the IPK method.

Nevertheless, this implementation includes the following features:

a) The reactor goes supercritical upon initiation of RIA;
b) The system is described by continuous time nonlinear stochastic differential equations;
c) The power measurement occurs at discrete times;
d) The system initial conditions are the same independent of the case under analysis;
e) The tuning of the filter goes automatically up to the simulation first time step; and
f) The covariance matrix of the state noise is updated at each time step.

9.1. EKF Tuning

The EKF tuning process includes the task of selecting the filter initial condition and also the appropriate values for the matrices Q' and R [69]. The matrix Q' is symmetric, positive semi-definite, and it models the noise existing in the following state variables: neutron flux, delayed neutron precursor concentrations, reactivity and its slope. The neutron flux is the main source of noise fluctuations [48]. The evaluation of the error covariance matrix relies basically on the evaluation of the $\Phi(t_{k+1}/t_k)\cdot P(t_k/t_k)\cdot\Phi^T(t_{k+1}/t_k)$ term of equation 5-20. This evaluation winds up with a $1/\ell$ dependence of elements (1,1) and (8,8), where $1/\ell$ is a very large number. In addition, element $Q'(9,9)$ is directly related to the reactivity slope. Therefore, only the elements directly related (see equation 5-11) to the neutron flux/reactivity, which are $Q'(1,1)$, $Q'(8,8)$ and $Q'(9,9)$, are assumed to be nonzero. This assumption was also proved to be correct by simulations.

The initial *Q'(i,i)*-entries are chosen based on a representative change in the variables [68] during the time step Δt, i.e. by assuming that the state variable is likely to change by an amount Δy over the interval of interest Δt:

$$Q'_{ii} = \frac{(\Delta y_i)^2}{\Delta t} \tag{9-1}$$

Due to the fast flux response to the insertion of reactivity and the distinct power trend among the three cases under evaluation, these *Q'* entries are calculated using their variation up to the first time step. The covariance matrix *R* represents the measurement error due to the flux sensor meter uncertainty per output channel (this work takes a single sensor). The measurement error is assumed to be 3% [48]. The initial value of the slope is assumed to be *w=0* for the three cases under analysis. The time step is obtained automatically from the P3D/R5 simulation. The matrix *Q* is updated at each time step and it represents the independent stochastic fluctuations in the state variables. In addition, a sensitivity analysis for five different 3% error noise loads, and for 1%, 2% and 3% uncertainties, are performed.

9.2. Reactivity Assessment for Different-Core Sizes

The application of both IPK and EKF methods for the three NPPs under analysis shows similar results independent of the core size, as expected (see Table 9-1 for details). Nevertheless, to guarantee the completeness of the analysis, the NPP1, NPP2 and NPP3 simulation results are presented in this section.

9.2.1. NPP1 Estimated Reactivity Assessment

The power response (and the reactivity behavior) during the RIA are very different among the three cases under investigation: case *a* has a fast increase in the reactivity, a power peak of about 25% due to the lack of reactivity control, and a slow power return to steady-state (Figure 9-1); case *b* has a very slow power dynamics (Figure 9-5); and case *c* has a sharp power peak (Figure 9-10). These different trends are explained by the reactivity worth and the core initial conditions for each case. Nevertheless, the random noise fluctuates stochastically

around the reactor power, as shown in Figure 9-2 (both time and relative power scale zooms for better noise visualization).

Figure 9-1 –Case *a* P3D/R5 Power Distribution With and Without Noise

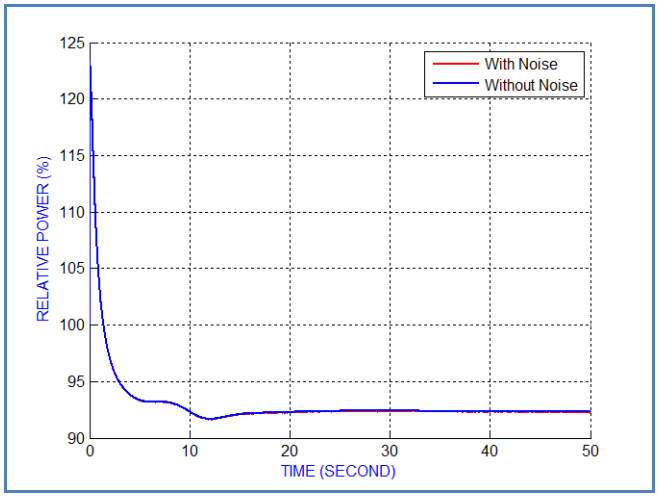

Figure 9-2 –Case *a* P3D/R5 Power Distribution With and Without Noise Zoom

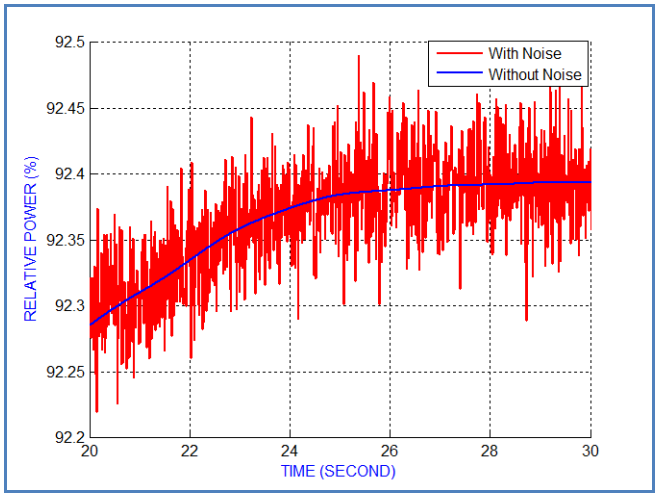

Figure 9-3 and Figure 9-4 show that for the smallest (0.2$) but fast reactivity insertion, which is followed by a moderate feedback effect, both IPK and EKF algorithms converge. However, the SD is higher for the IPK simulation results due to its deterministic method of solving the point kinetics equations, as it is seen in Table 9-1. Also, the steady-state EKF reactivity is closer to the P3D/R5 results compared to the IPK reactivity.

Figure 9-3 – Case *a* P3D/R5 and EKF Reactivity

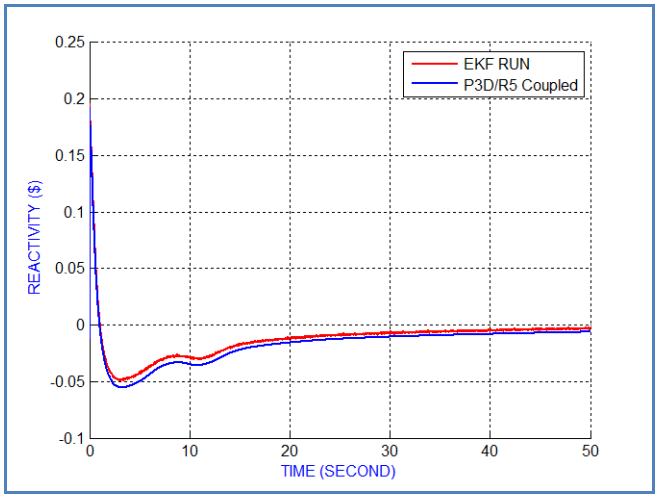

Figure 9-4 – Case *a* P3D/R5 and IPK Reactivity

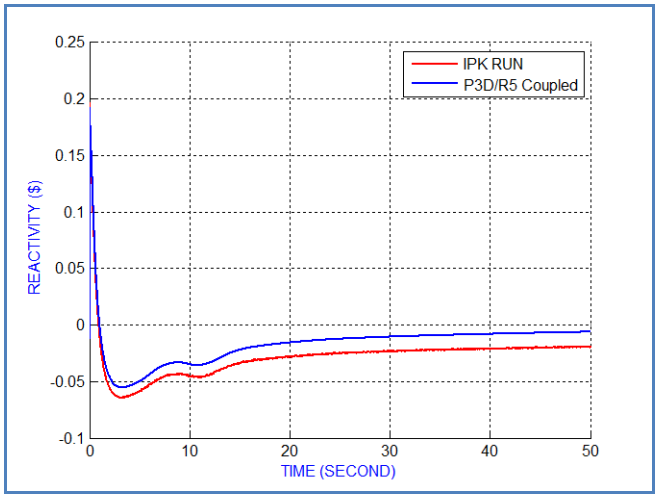

On the other hand, a HZP insertion of 0.4$ (case *b*) has a very slow power response together with power increase from its initial value to more than 480 times within 100 seconds, as can be seen in Figure 9-5. For this case, the EKF presents superior results compared to the IPK because:

i) The IPK reactivity varies from positive to negative (from -120$ to 78$) within 12 seconds of simulation, as presented in Figure 9-7 and Figure 9-8 (reactivity zoom scale), due to the noise in the measurement and the deterministic nature of IPK algorithm – this magnitude depends on the noise load, as can be seen in Figure 9-38. This may add extra difficulty to the task of controlling the reactor based on the deterministic method. While EKF overpredicts the peak reactivity by 30% , it

matches the P3D/R5 reactivity prediction during most of the simulation time as shown in Figure 9-6; and

ii) The reactivity's SD is higher for the IPK method.

It is worth noting that the use of IPK is more effective during normal operation, when noise detectors are less sensitive to reactor parameters and more immune to noise content in the measured signals [65].

Figure 9-5 –Case *b* P3D/R5 Power Distribution With and Without Noise

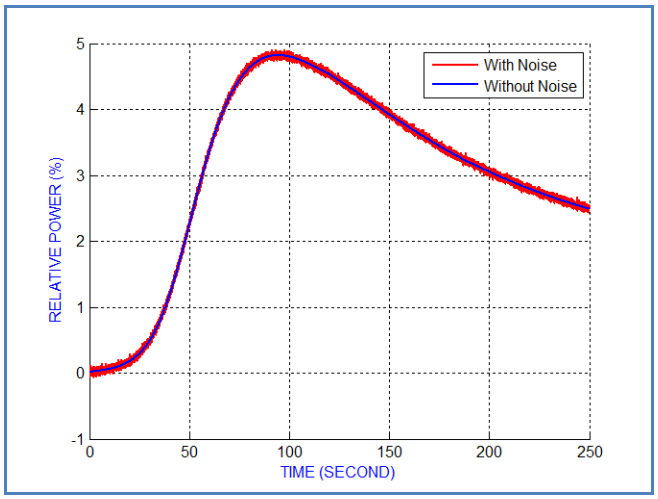

Figure 9-6 – Case *b* P3D/R5 and EKF Reactivity

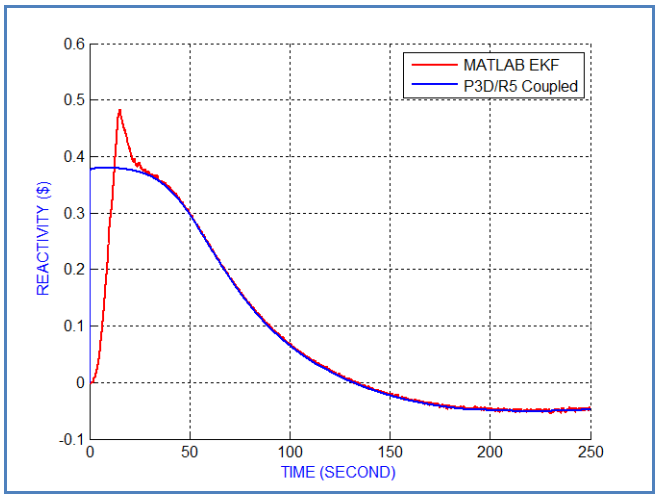

Figure 9-7 – Case *b* P3D/R5 and IPK Reactivity

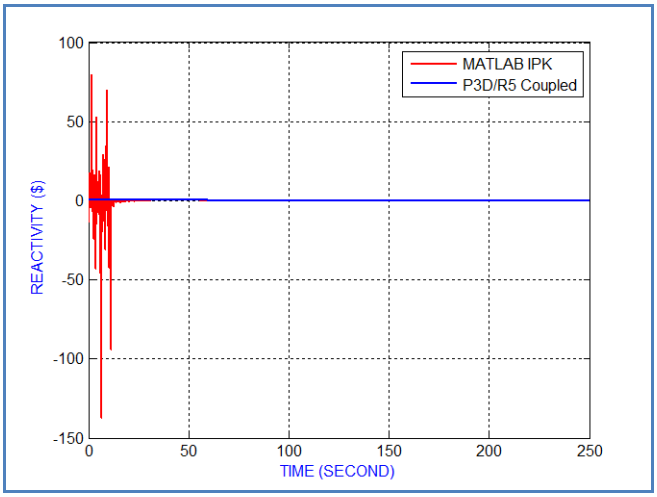

Figure 9-8 – Case *b* P3D/R5 and IPK Reactivity Zoom

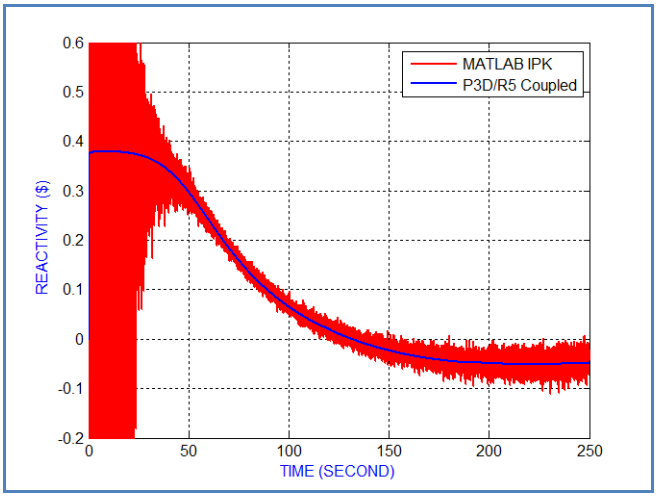

The EKF, as can be seen in Figure 9-6, underpredicts the reactivity during the initial few seconds of simulation. This is due to the *w* (reactivity slope) initial guess $w_{(t=0)}$=0. The simulations for the three cases under investigations (see Table 5-1) assume the same set of initial conditions to compare the results independent of the power and reactivity dynamics. Nevertheless, the initial *w* guess dictates how long it takes the EKF reactivity to follow the P3D/R5 simulation results. The *w=0* initial condition proved to be the best guess independent of the case being simulated. Nevertheless, Figure 9-9 presents simulation results for $w_{(t=0)}$=0.01, which leads to a EKF SD of 0.04$ (see Table 9-1 for SD comparison). It can be seen that the initial delay between the P3D/R5 and the EKF reactivity was significantly reduced.

Figure 9-9 – Case *b* P3D/R5 Reactivity for w=0.01

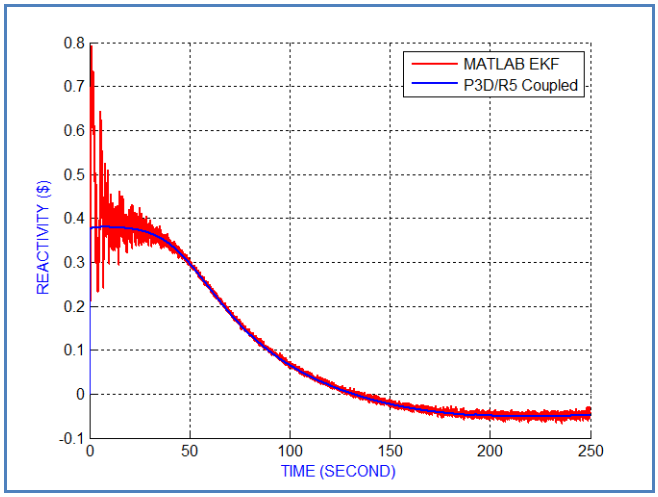

The application of EKF and IPK to the RIA starting from HZP with reactivity insertion of up 1.3$ (case *c*) is shown in Figure 9-10 to Figure 9-13, where a very sharp peak in reactivity and power are simulated (the effect of a sudden increase in power, which could probably damage the fuel, has not been covered within this work). In this case, the simulation results of both IPK and EKF present similar behavior, although the IPK reactivity SD is higher, as show in Table 9-1.

Figure 9-10 – Case *c* P3D/R5 Power Distribution With and Without Noise

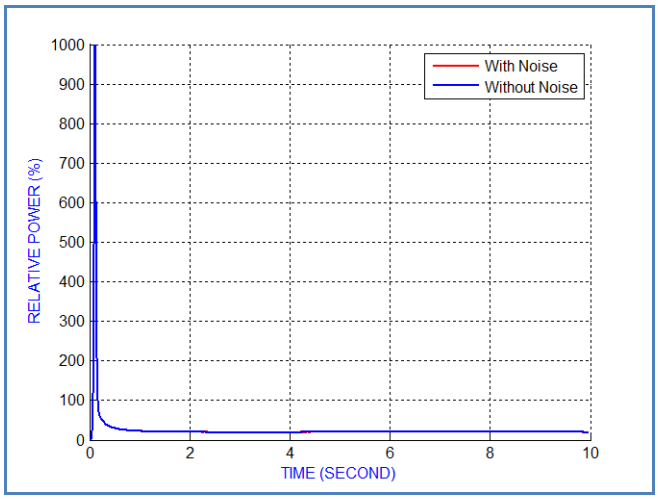

Figure 9-11 –Case *c* P3D/R5 Power Distribution With and Without Noise Zoom

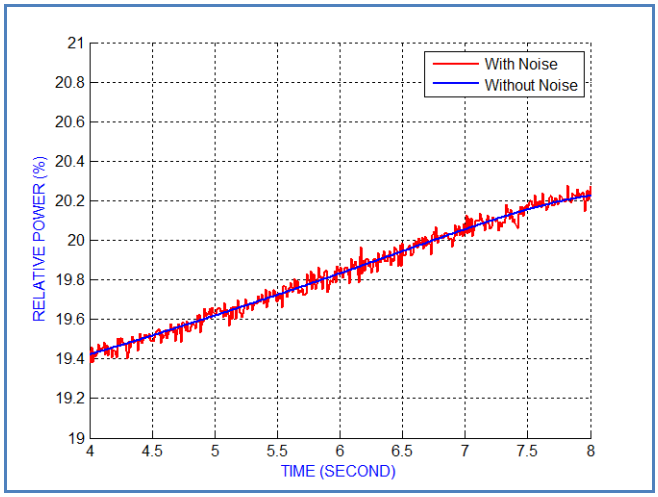

Figure 9-12 – Case *c* P3D/R5 and EKF Reactivity

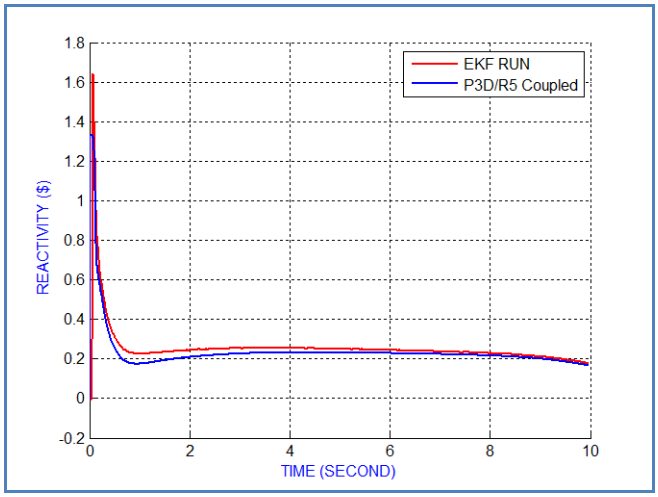

Figure 9-13 –Case *c* P3D/R5 and IPK Reactivity

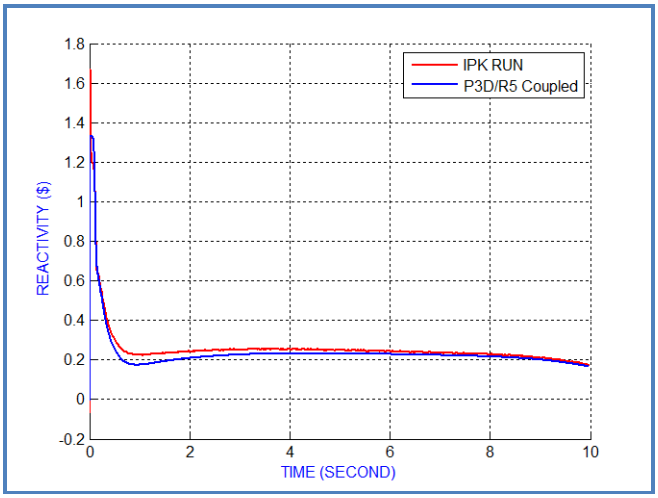

9.2.2. NPP2 Reactivity Assessment

A similar procedure is applied to NPP2. As expected, the results are very similar to those obtained for NPP1. It can be seen from Figure 9-14 to Figure 9-16 (due to the power scale, the noise is not seen in Figure 9-14) that both the IPK and the EKF presents high accuracy during HFP.

Figure 9-14 – Case *a* P3D/R5 Power Distribution With and Without Noise

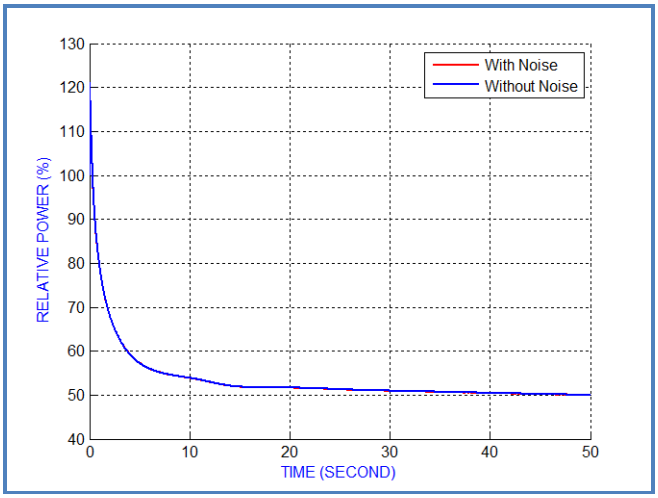

Figure 9-15 - Case *a* P3D/R5 and EKF Reactivity

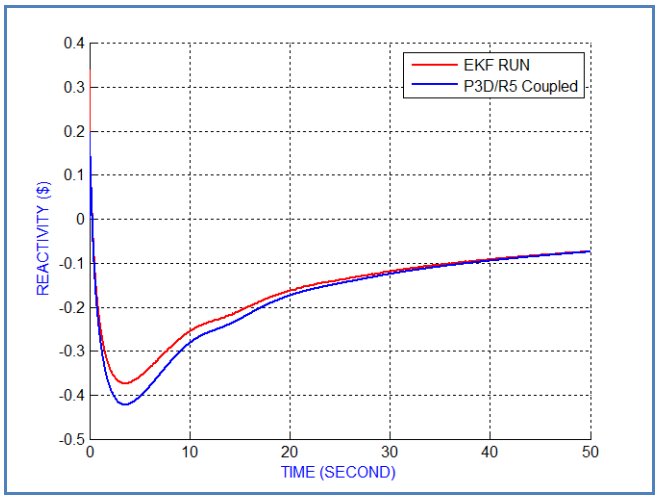

Figure 9-16 – Case *a* P3D/R5 and IPK Reactivity

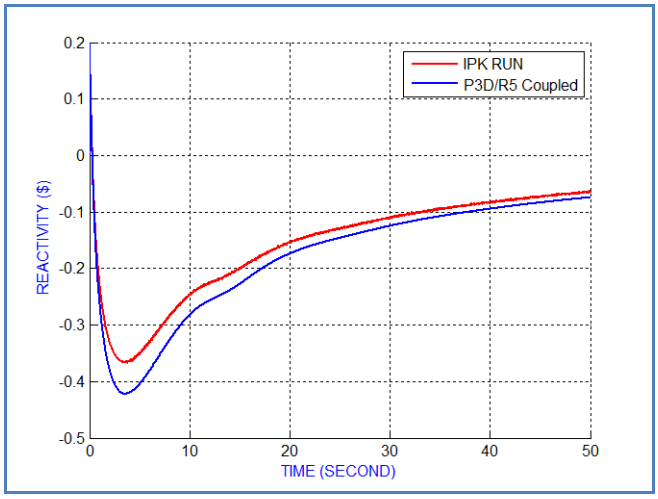

The HZP NPP2 simulation results (case *b*), as can be seen in Figure 9-17, Figure 9-18 and Figure 9-19, are similar to the ones obtained for NPP1. As expected, the core size produces no significant difference in the results. The application of EKF and IPK depends on the power profile and on the noise measurement. The SD comparison among the cases and NPPs is shown in Table 9-1.

The NPP2 case *c* simulations also present similar results for the EKF and IPK just after the RIA initiation. The IPK is more sensitive to the noise and, therefore, the reactivity fluctuate up to t=0.1 second, before following the P3D/R5 trend, as shown from Figure 9-20 to Figure 9-22 (due to the power scale, the noise is not seen in Figure 9-20).

Figure 9-17 – Case *b* P3D/R5 Power Distribution With and Without Noise

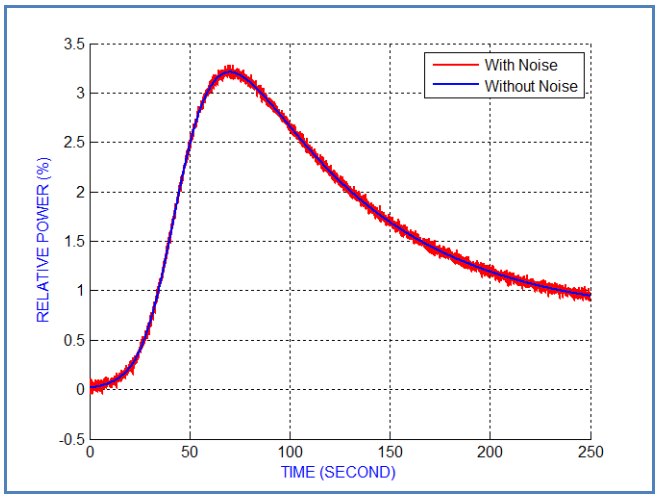

Figure 9-18 – Case *b* P3D/R5 and EKF Reactivity

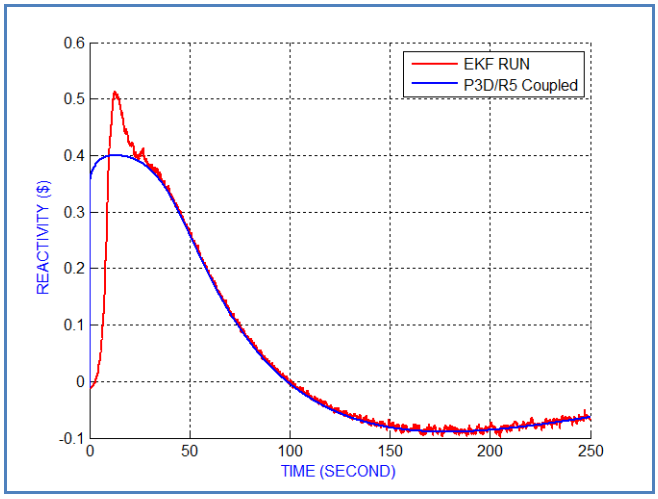

Figure 9-19 – Case *b* P3D/R5 and IPK Reactivity

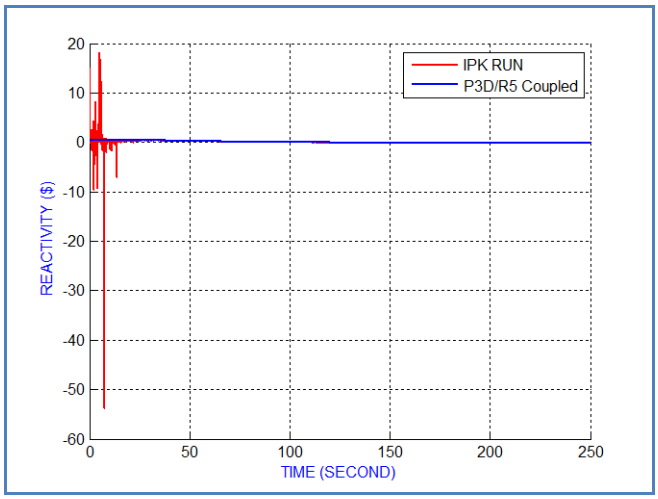

Figure 9-20 – Case *c* P3D/R5 Power Distribution With and Without Noise

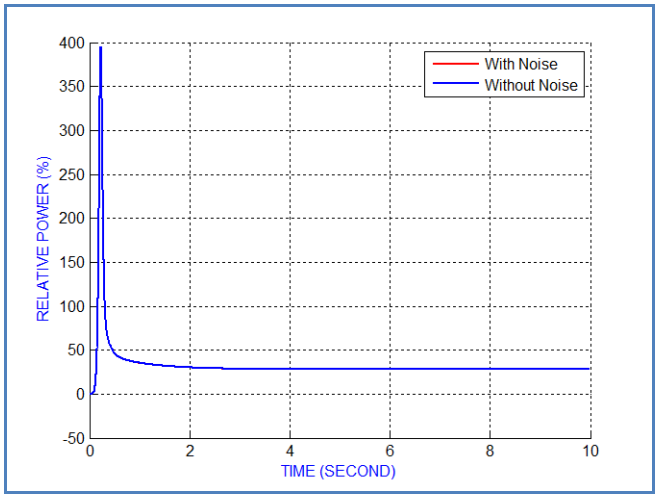

Figure 9-21 – Case *c* P3D/R5 and EKF Reactivity

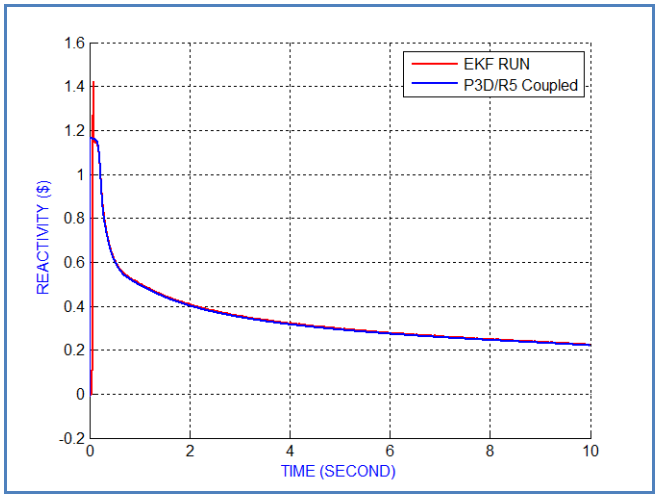

Figure 9-22 – Case *c* P3D/R5 and IPK Reactivity Zoom

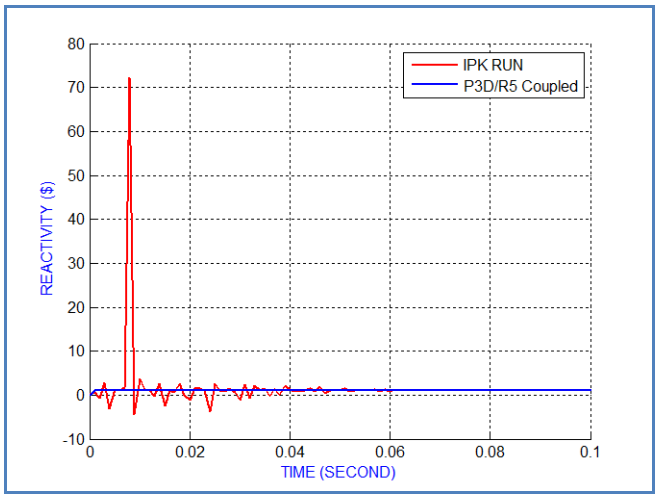

9.2.3. NPP3 Reactivity Assessment

The simulation results for NPP3 are not different from the NPP1 and NPP2, as can be seen from the case *a*, case *b* and case *c* simulation results presented from Figure 9-23 to Figure 9-31 (due to the power scale, the noise is not seen in Figure 9-23 and Figure 9-29). The comparison among the cases and NPPs is shown in Table 9-1.

Figure 9-23 – Case *a* P3D/R5 Power Distribution With and Without Noise

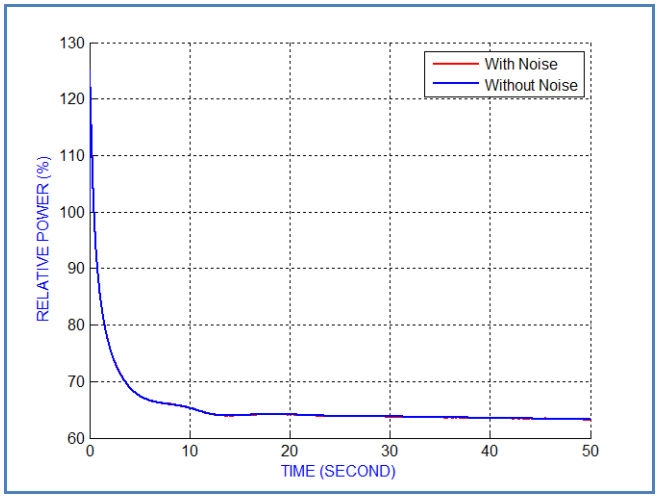

Figure 9-24 – Case *a* P3D/R5 and EKF Reactivity

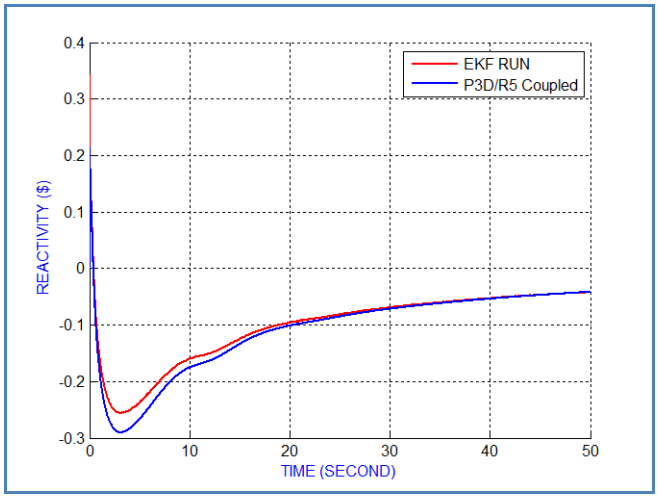

Figure 9-25 – Case *a* P3D/R5 and IPK Reactivity

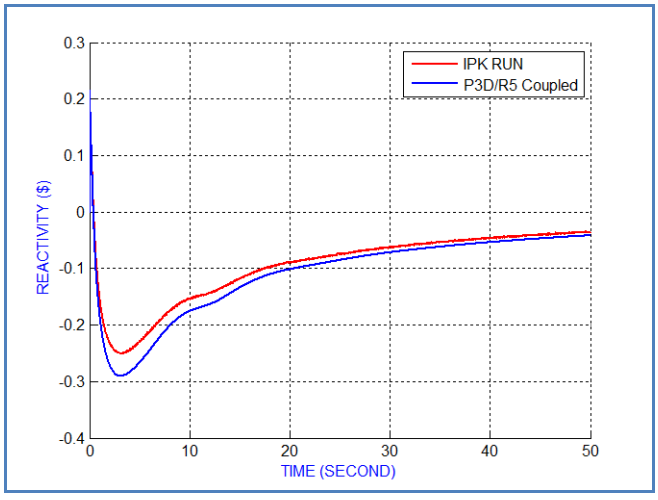

Figure 9-26 – Case *b* P3D/R5 Power Distribution With and Without Noise

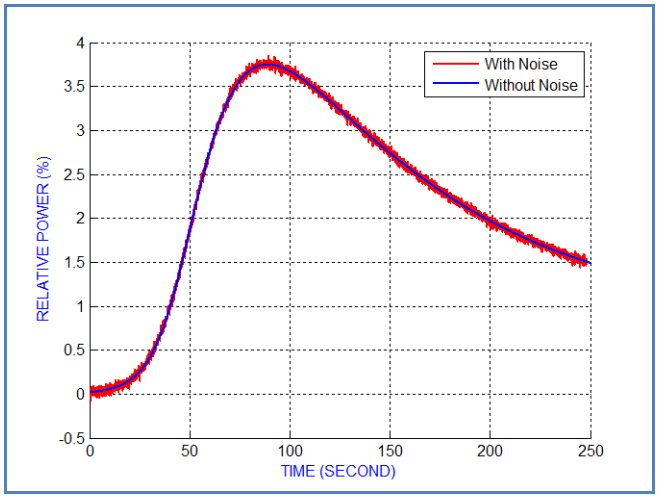

Figure 9-27 – Case *b* P3D/R5 and EKF Reactivity

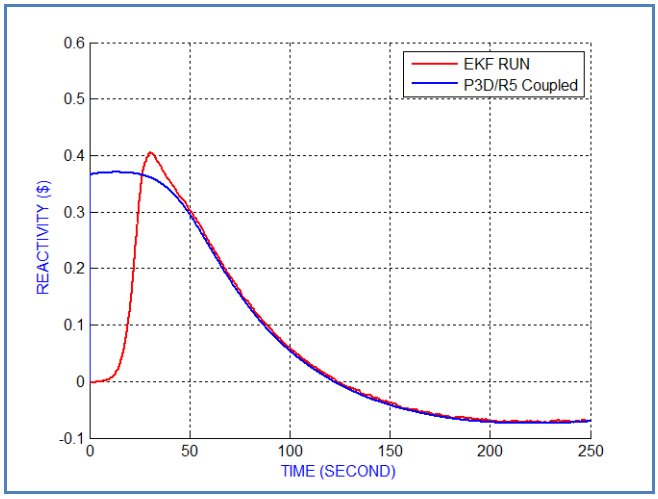

Figure 9-28 – Case *b* P3D/R5 and IPK Reactivity Zoom

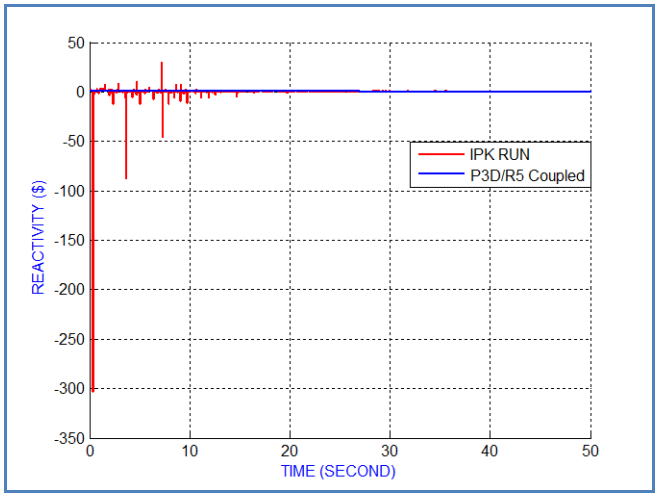

Figure 9-29 – Case *c* P3D/R5 Power Distribution With and Without Noise

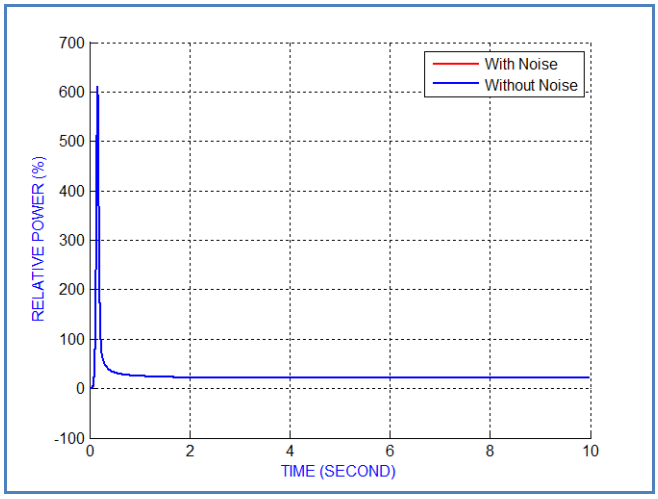

Figure 9-30 – Case *c* P3D/R5 EKF Reactivity

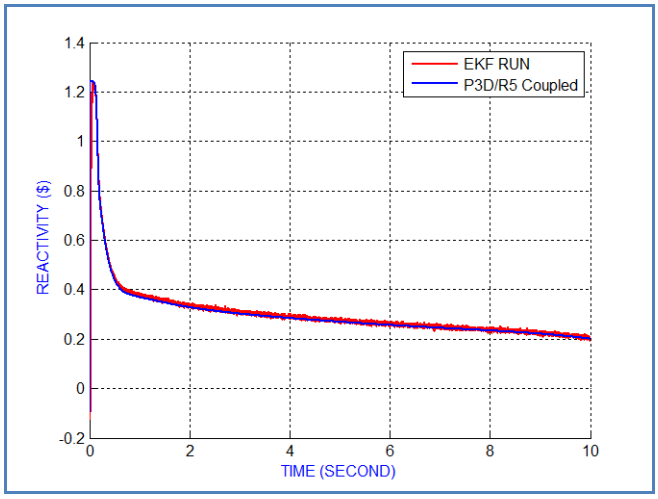

Figure 9-31 – Case *c* P3D/R5 and IPK Reactivity Zoom

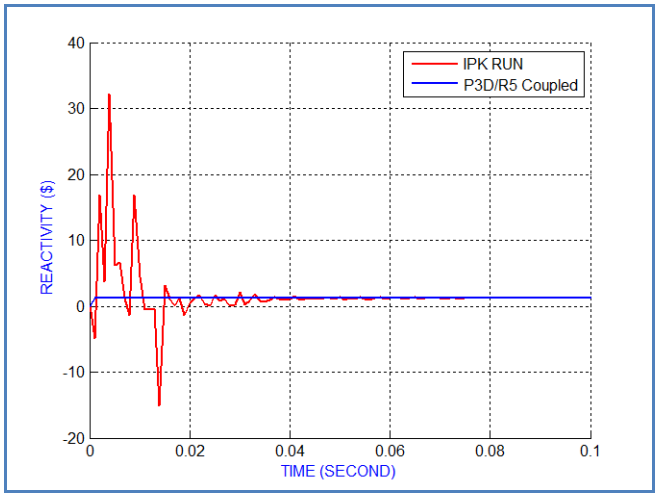

To benchmark results against the coupled code, the EKF SD is calculated over the difference between the EKF and the P3D/R5 reactivity, and the IPK SD is calculated over the difference between the IPK and the P3D/R5 reactivity. Therefore, the SD and mean are shown in Table 9-1.

Table 9-1 –EKF and IPK SD & Mean for 3% Noise

NPP #	Case	EKF SD		IPK SD		Ratio IPK/EKF SD
		SD ($)	Mean ($)	SD ($)	Mean ($)	
1	a	0.001	0.014	0.002	-0.011	1.50
	b	0.074	-0.005	0.449	0.001	6.10
	c	0.091	0.001	0.181	0.002	1.99
2	a	0.001	0.017	0.002	0.019	1.45
	b	0.067	-0.001	0.405	0.002	6.03
	c	0.099	-0.002	0.210	0.009	2.12
3	a	0.006	0.015	0.009	0.029	1.61
	b	0.089	-0.005	0.534	-0.008	6.02
	c	0.099	0.001	0.200	0.009	2.02

As a conclusion, the core size does not have any influence on the application of both IPK and EKF to estimate the reactivity upon RIA initiation based on the measurement of the reactor power profile, after the addition of random noise.

9.3. NPP1 Reactivity Assessment Sensitivity Analysis

9.3.1. Sensitivity Analysis for Different Noise Loads

Results from previous sections suggest that, under the core supercritical conditions, the use of EKF for reactivity estimation provides better results for the three cases under analysis, especially for a very slow power response to a small insertion of reactivity (case *b*). Furthermore, the results are independent of the core size. Therefore, a sensitivity analysis of five distinct carry-over effects of different random noise loads are presented in Figure 9-32 to Figure 9-43 (zoom scales near the reactivity peak). It can be seen that independent of the

noise load applied to the power profile, the relative method performance (between the IPK and EKF) is similar to the ones discussed in the previous section: the EKF presents superior results.

Figure 9-32 – Case *a* Sensitivity Analysis for EKF Reactivity

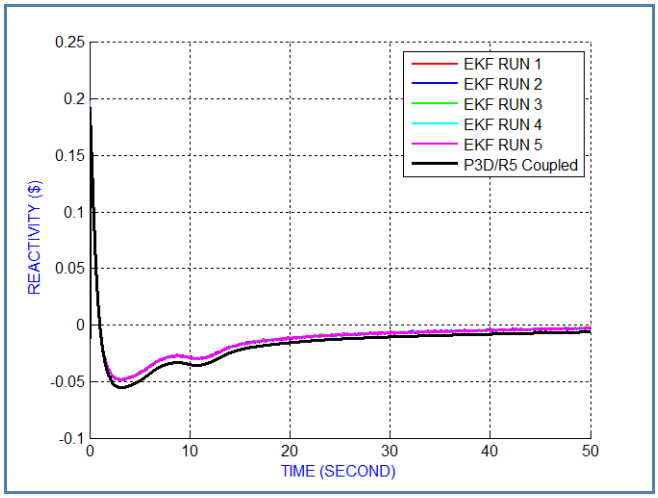

Figure 9-33 – Case *a* Sensitivity Analysis for EKF Reactivity Zoom

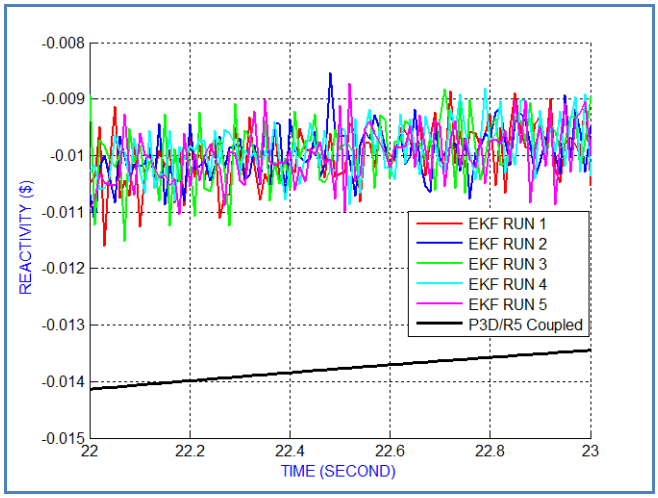

Figure 9-34 – Case *a* Sensitivity Analysis for IPK Reactivity

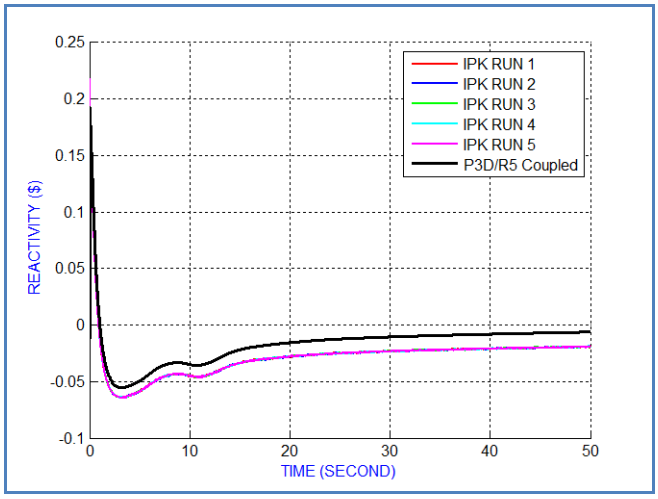

Figure 9-35 – Case *a* Sensitivity Analysis for IPK Reactivity Zoom

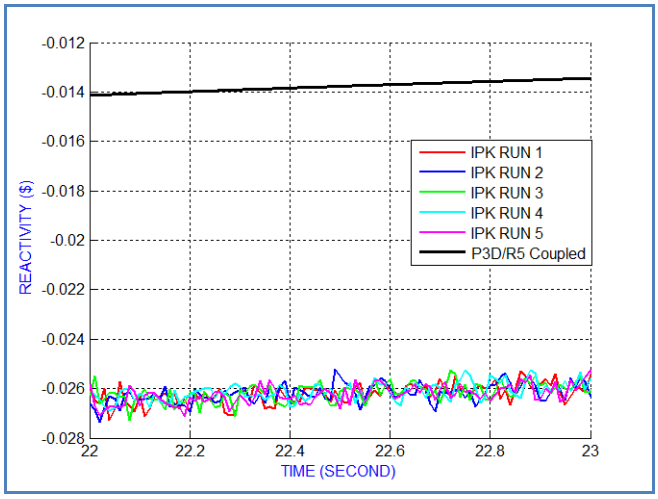

Figure 9-36 – Case *b* Sensitivity Analysis for EKF Reactivity

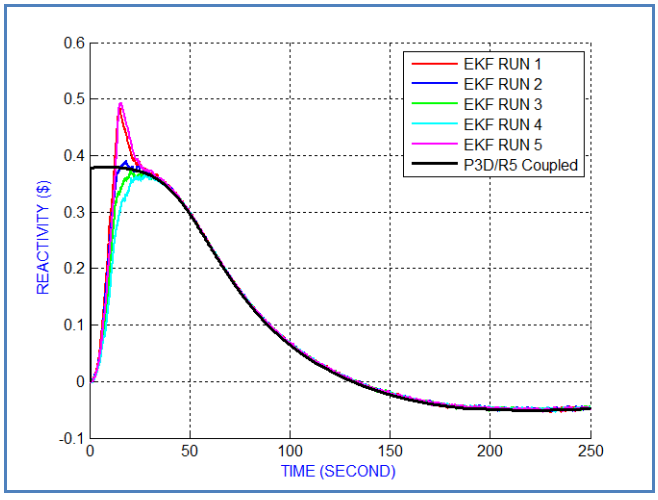

Figure 9-37 – Case *b* Sensitivity Analysis for EKF Reactivity Zoom

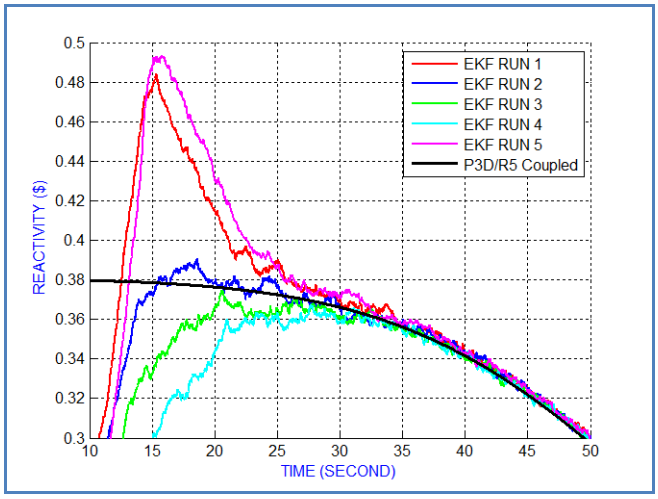

Figure 9-38 – Case *b* Sensitivity Analysis for IPK Reactivity

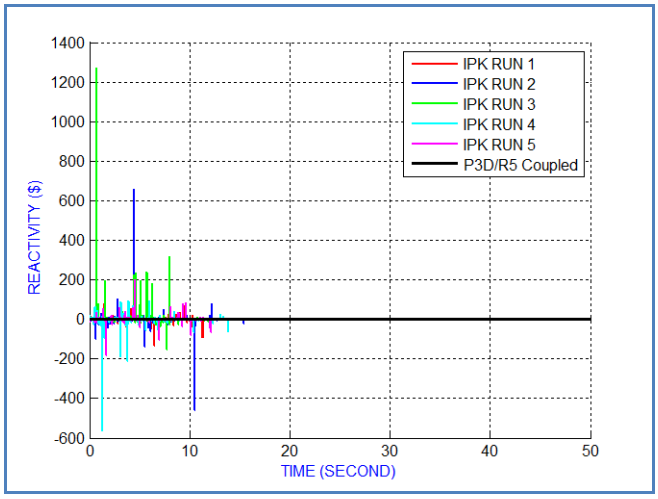

Figure 9-39 – Case *b* Sensitivity Analysis for IPK Calculated Reactivity Zoom

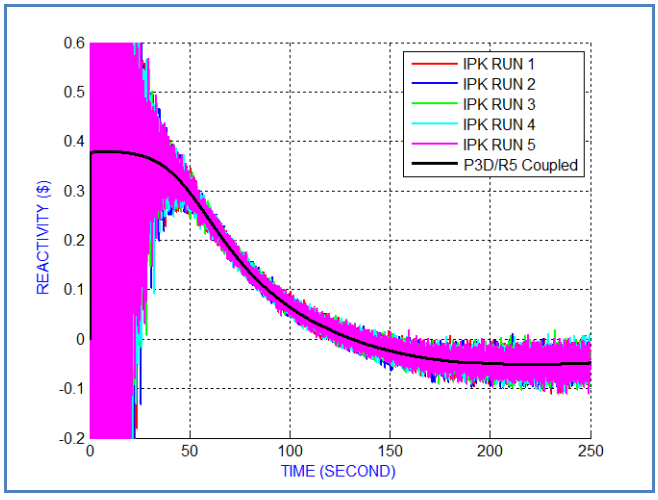

Figure 9-40 – Case *c* Sensitivity Analysis for EKF Reactivity

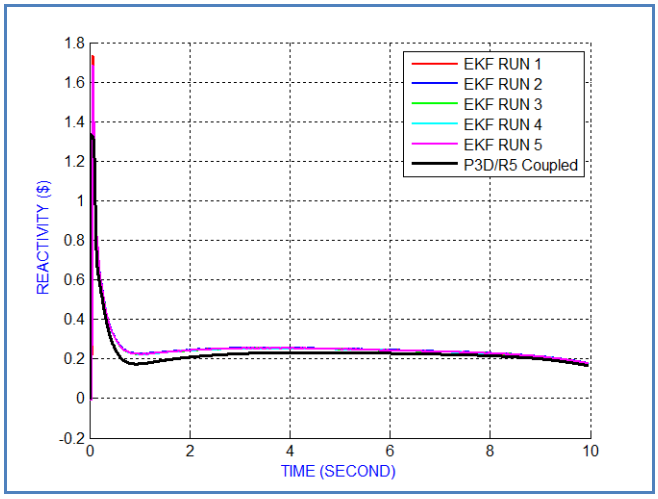

Figure 9-41 – Case *c* Sensitivity Analysis for EKF Reactivity Zoom

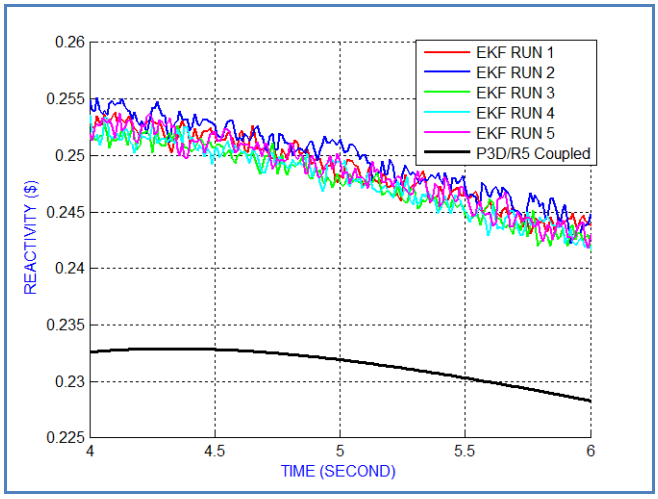

Figure 9-42 – Case *c* Sensitivity Analysis for IPK Reactivity

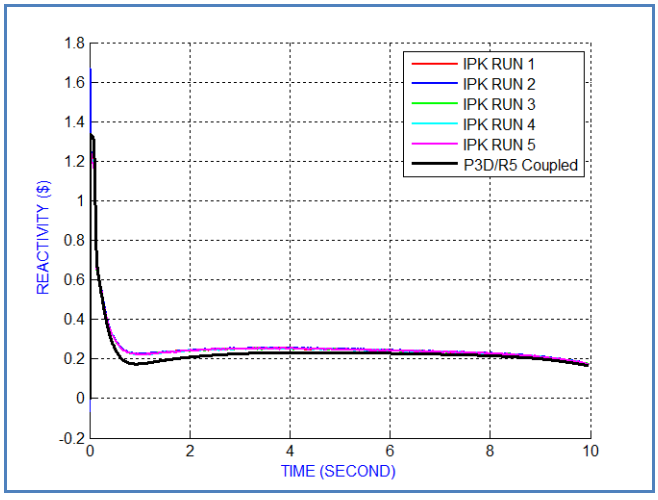

Figure 9-43 – Case *c* Sensitivity Analysis for IKF Reactivity Zoom

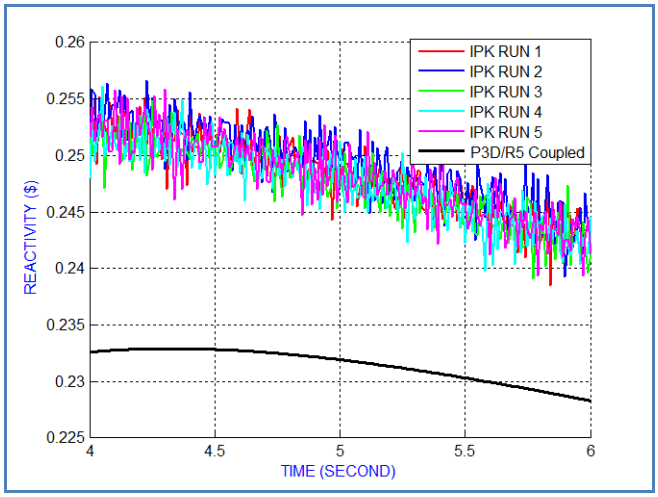

To be able to assess the impact that changes in the noise load will have on both the EKF and IPK methods for all cases under investigation, the five noise loads have the same 3% SD but different initial random seeds, which are automatically generated by MATLAB. As it can be seen in Table 9-2, the simulation results indicate that the EKF method is less sensitive to the differences of noise loads for all cases. Furthermore, it can be seen that for a sharp increase of reactor power (case *c*), the performance of the IPK regarding the noise content, i.e. the SD value, is about 2 times worse than the EKF (see the column "Ratio IPK/EKF SD" in Table 9-2), while for a HZP slow reactor power profile (case *b*), the IPK performance is about 6 times worse. The IPK method is more effective in the HFP case because the on-line neutron flux meters are less immune to noise content in the input signals under the HFP conditions.

Table 9-2 –NPP1 EKF and IPK Standard Deviation ($) Reactivity for Five Noise Loads

Case	Noise Load #	EKF SD ($)	IPK SD ($)	IPK/EKF SD
a	1	0.012	0.018	1.50
	2	0.012	0.016	1.33
	3	0.013	0.019	1.46
	4	0.013	0.017	1.31
	5	0.013	0.018	1.38
b	1	0.074	0.449	6.10
	2	0.065	0.404	6.20

Case	Noise Load #	EKF SD ($)	IPK SD ($)	IPK/EKF SD
	3	0.068	0.419	6.16
	4	0.083	0.511	6.18
	5	0.079	0.512	6.45
c	1	0.091	0.181	1.99
	2	0.021	0.044	2.09
	3	0.021	0.044	2.09
	4	0.023	0.044	1.91
	5	0.018	0.045	2.49

9.3.2. Sensitivity Analysis for Different Measurements Noise SD

In order to evaluate how effective the EKF is to the noise content in the measurement, the reactivity response to 1%, 2% and 3% noise SD is simulated. Figure 9-44 to Figure 9-55 present the estimated reactivity response against the P3D/R5 results. As expected, the EKF method predicts well the reactivity associated with the P3D/R5 simulation for the three distinct noise loads.

Figure 9-44 – Case *a* EKF Measurements Noise Sensitivity Analysis

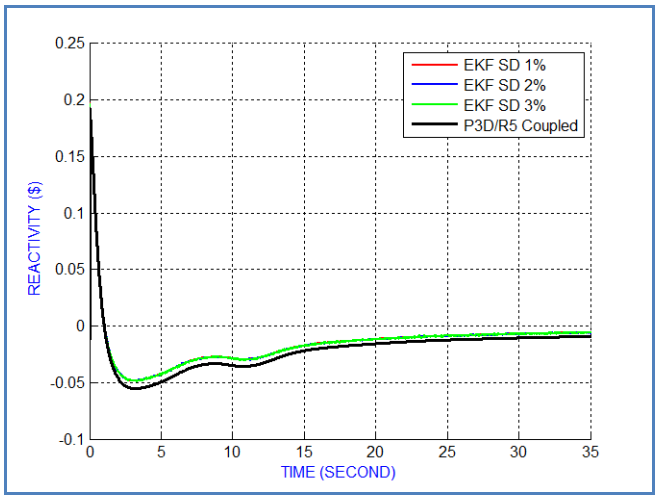

Figure 9-45 – Case *a* EKF Measurement Noise Sensitivity Analysis Zoom

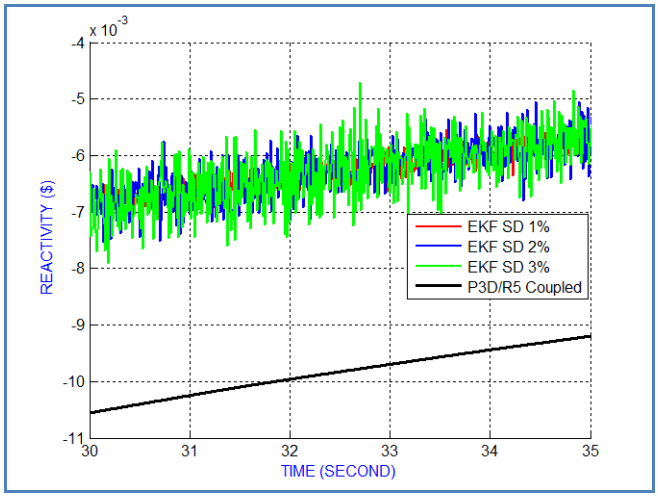

Figure 9-46 – Case *a* IPK Measurement Noise Sensitivity Analysis

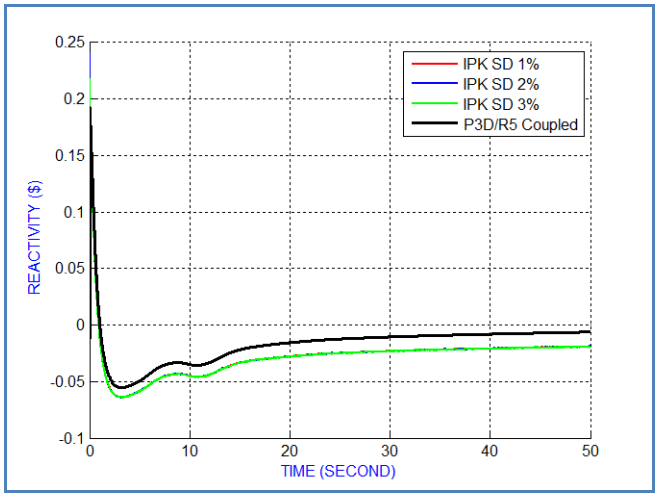

Figure 9-47 – Case *a* IPK Measurement Noise Sensitivity Analysis Zoom

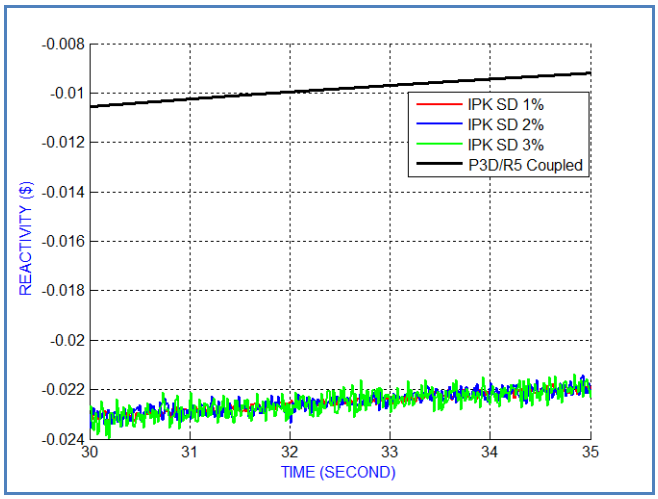

Figure 9-48 – Case *b* EKF Measurements Noise Sensitivity Analysis

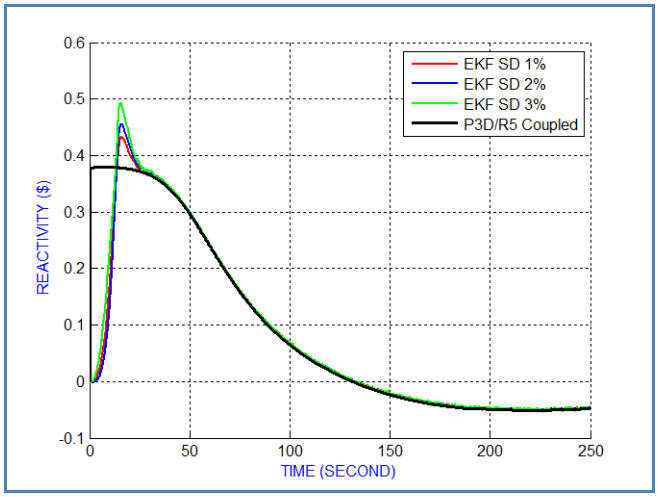

Figure 9-49 – Case *b* EKF Measurement Noise Sensitivity Analysis Zoom

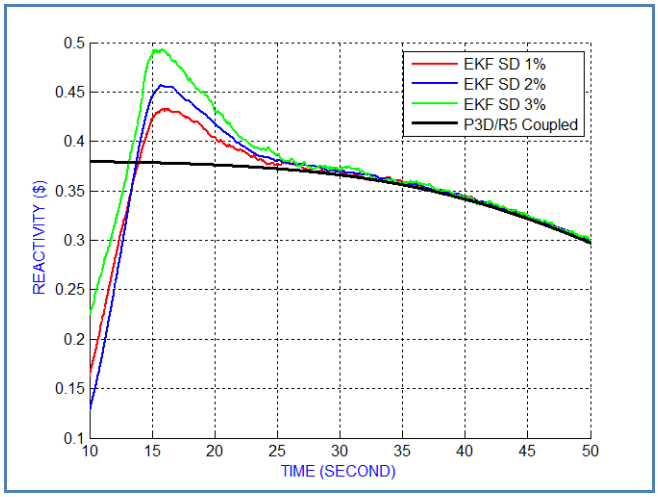

Figure 9-50 – Case *b* IPK Measurement Noise Sensitivity Analysis

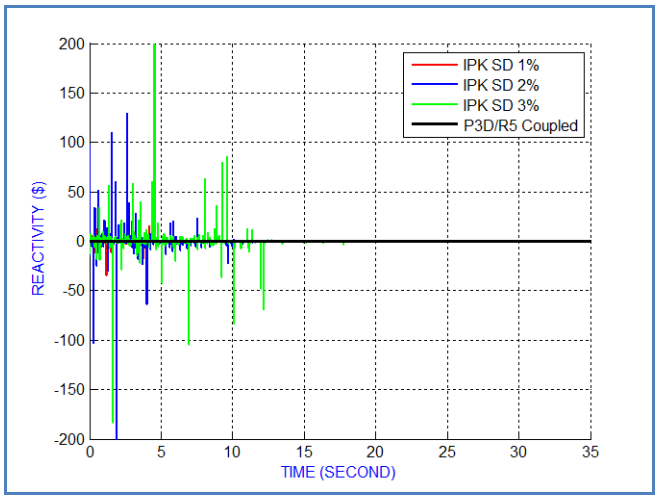

Figure 9-51 – Case *b* IPK Measurement Noise Sensitivity Analysis Zoom

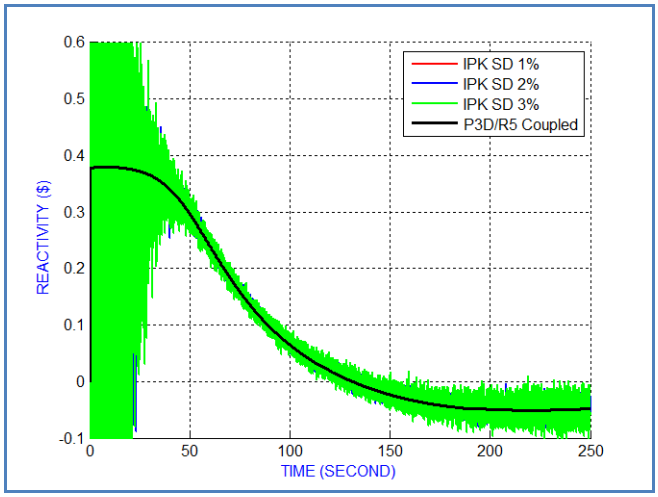

Figure 9-52 – Case *c* EKF Measurement Noise Sensitivity Analysis

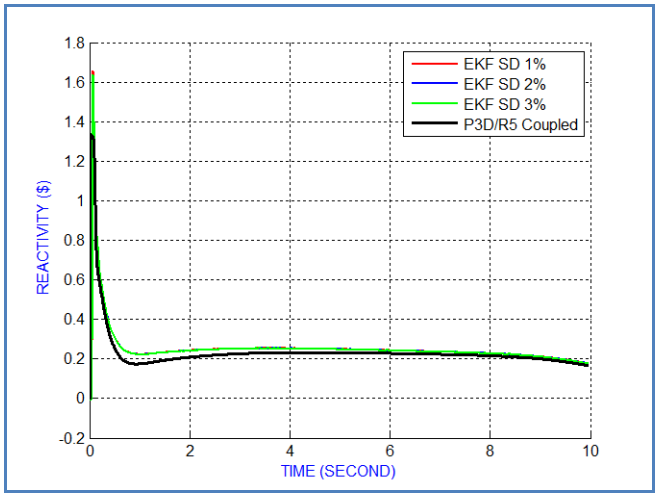

Figure 9-53 – Case *c* EKF Measurement Noise Sensitivity Analysis Zoom

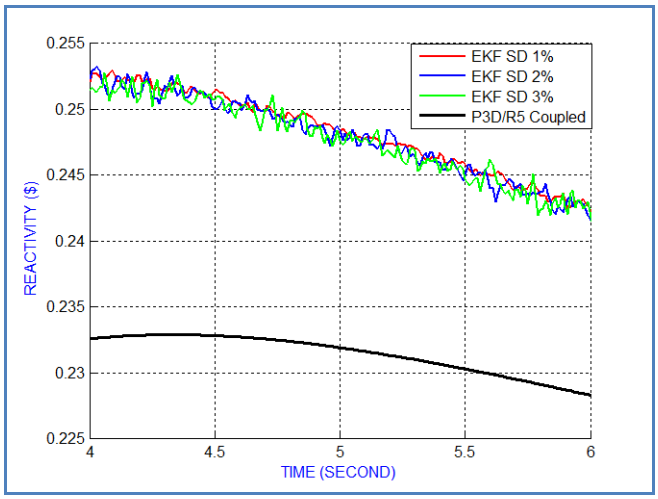

Figure 9-54 – Case *c* IPK Measurement Noise Sensitivity Analysis

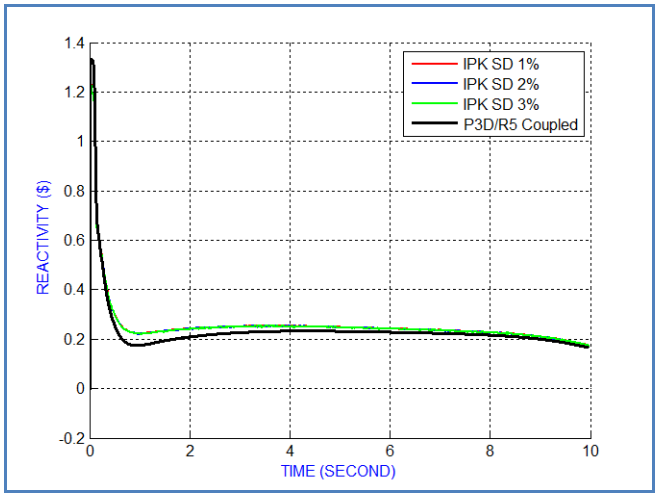

Figure 9-55 – Case *c* IPK Measurement Noise Sensitivity Analysis Zoom

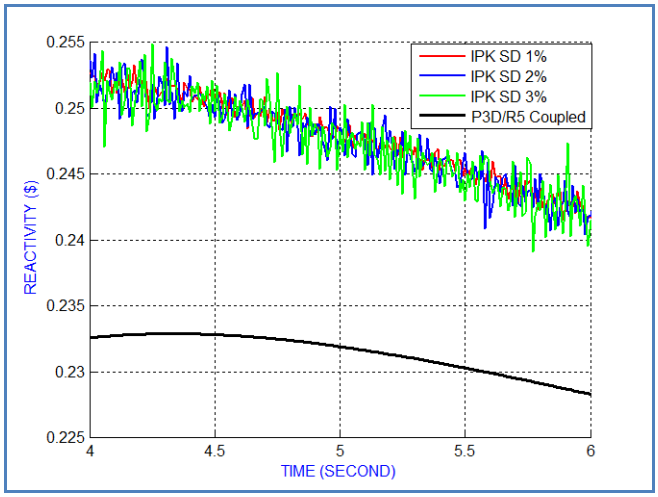

Table 9-3 presents the reactivity SD for all cases under investigation, assuming a 1%, 2% and 3% random noise power profile. It can be seen that EKF provides the best results compared to IPK, and the IPK SD increases, due to its deterministic calculation method, as the measurement noise contents is higher. The ratio IPK/EKF SD shows the improvements of the EKF compared to the IPK as the noise content increases. Also, it confirms the results from previous sections: the EKF exhibits better performance for a slow insertion of reactivity under HZP (case *b*).

Table 9-3 – NPP1 EKF and IPK Reactivity Different Noise SD ($) Sensitivity

Case	Noise Load	EKF SD ($)	IPK SD ($)	Ratio IPK/EKF SD
a	1%	0.012	0.014	1.17
	2%	0.013	0.017	1.31
	3%	0.012	0.018	1.50
b	1%	0.063	0.316	5.02
	2%	0.068	0.388	5.70
	3%	0.074	0.449	6.10
c	1%	0.019	0.015	0.77
	2%	0.021	0.024	1.18
	3%	0.091	0.181	1.99

9.4. NPP1 Computation Running Time

By the application of similar coding techniques and by running the simulations in the same computer, an assessment of the running times of each approach can be compared. The computation time is presented in Table 9-4. The running time depends on the dynamics of the case being simulated and on the length of the simulation (50 seconds for case *a*, 250 seconds for case *b* and only 10 seconds for case *c*). It can be seen, under the stated assumptions, that the computation time is not a constraint or a key decision point for choosing EKF or IPK techniques for reactivity estimation. Both techniques are very fast on today's computers. The simulations run on iMac OS X 2.7 GHz i7 Intel 16Gb. It is noted that the calculation of the *Delayed Neutron Kernel* is the time demanding module in the IPK code.

Table 9-4 –Running Time

Case	EKF Elapsed Time (seconds)	IPK Elapsed Time (seconds)	Ratio EKF/IPK Elapsed Time
a	3.41	3.19	1.07
b	12.66	11.54	1.10
c	1.02	0.95	1.08

The EKF and IPK algorithms' implementation depends on the appropriate use of MATLAB nested functions, such as "random", "load" and "ones"; in the application of well known basic mathematical techniques, such as "Taylor series" and "Euler method"; and on the use of systematic programming techniques. Thus, the same coding approach was used in both IPK and EKF MATLAB scripts. Furthermore, nowadays the instrumentation and control systems computer capacity at a nuclear plant will not be a major issue for both IPK and EKF implementation.

9.5. Chapter Summary

The performances of the EKF and IPK algorithms have been assessed by the proximity of their predictions to the coupled code P3D/R5 simulation and by the reactivity's SD. In the tests performed, it was found that the IPK reactivity had higher noise content compared to the EKF reactivity for all cases under investigation (see Table 5-1). Furthermore, the core size, as expected, does not have any influence in the application of both IPK and EKF to estimate the reactivity upon RIA initiation based on the measurement of the reactor power profile, after addition of random noise (see Table 9-1). Therefore, the EKF method presented more accurate results when compared to the IPK method.

Furthermore, under a RIA where small reactivity insertion and slower power response were simulated (case *b*), the IPK reactivity varied widely from positive to negative and at times by an order of magnitude different, which may add extra difficulty to the task of controlling a reactor that may go supercritical. These were also confirmed by a sensitivity analysis for five different noises loads and for three distinct SD noise measurements (see Table 9-2 and Table 9-3 for details). It is worth noting that although the P3D/R5 simulates the reactivity using a spatial nuclear kinetics method, the use of the PKRE to model the EKF to estimate the reactivity for a given power profile under noise environment gave accurate results.

The benefits of using a stochastic tool such as EKF should be weighed against the use of the well-known IPK method. The EKF requires special attention to the filter's tuning task while the application of the IPK method is quite straightforward. In addition, by applying the same coding approach for both algorithms, the computational time is not a constraint or a key decision point for choosing between IPK and EKF for reactivity estimation.

As a conclusion, this work indicates that, with the appropriate choice of the R and Q' matrices, based on the sensor error (R) and on the initial variation of some of the state variables (Q'), the EKF is a powerful method for accurate estimation of reactivity under various RIA conditions.

10. CONCLUSIONS AND RECOMMENDATIONS

10.1. Conclusions

The need to operate current NPPs close to their power safety limits, and the design of new advanced NPPs, have motivated the development of new nuclear modeling and simulation techniques, to ensure maximum power production with appropriate safety margins. The design and construction of nuclear power plant are feasible only through the combination of state-of-the-art knowledge in several technical areas, such as nuclear, mechanical, electrical, and chemical engineering, among others. A NPP is a very complex system, among the most sophisticated energy system ever designed [73], and its construction and operation demand high technological expertise and industrial capabilities. The NPP design, licensing and operation rely on a myriad of computer codes, which have been developed and used in the last 30 years.

Furthermore, the operation of NPPs demands that a large number of postulated accidents, during normal operation or off-normal conditions must be well characterized and with design features that mitigates their consequences. However, the nuclear power plant's size, the demanding capital cost and the radioactive nature of its fuel limit the number of severe accidents that could be evaluated by means of experimental programs. Therefore, computer reactor models have been developed to simulate the NPP behavior during transients and abnormal operation. This approach improves performance, leading to cost reduction and increased safety.

This work evaluated the predicted response of RIA by different methods. The response was measured through the reactivity behavior, the total power and the 3D core power distribution. In addition, the response to RIAs of three NPPs, with similar core designs but different levels of power were addressed. The methods used included the thermal-hydraulic RELAP (R5) code with simplified neutronic feedback; the neutronic PARCS (P3D) code with simplified thermal hydraulic feedback; and the coupled version P3D/R5. In addition, this study implemented a stochastic extended Kalman Filter (EKF) algorithm to estimate the nuclear reactor reactivity behavior under a RIA. To assess the reliability and consistency of EKF simulations, the IPK deterministic method was also implemented and the results of the

application of both algorithms (EKF and IPK) were compared to the P3D/R5 simulation. The EKF and the IPK algorithms were implemented using MATLAB.

The P3D/R5 RIA simulation strategy starts first with the construction of P3D and R5 nuclear power plant models. P3D simulates the core only, while R5 couples the core to the rest of the thermal hydraulic system. These models include the core nodalization in the radial and axial directions, their correlation using a mapping scheme, the secondary reactor system and the generation of the input files. Then, the HZP (core at start up) and HFP (reactor under normal operation) rods to be ejected, and the correspondent reactivity insertion ($), are identified. Next, the standalone and coupled codes are applied to simulate the rod ejection within 0.1 seconds, which is the worst possible scenario for addition of reactivity in LWRs. Moreover, the implementation of the stochastic EKF method uses the reactor power profile generated by the P3D/R5 coupled version as an input, after the addition of random noise by means of a MATLAB script. The cases under investigation are: at HFP conditions, control rod assembly (CRA) ejection with reactivity insertion of 0.2$ (case *a*); at HZP conditions, CRA ejection with reactivity insertion of 0.4$ (case *b*); and at HZP conditions, control rod bank ejection with reactivity insertion of 1.3$ (case *c*). Then, the reactivity estimated by the EKF, the IPK reactivity and the simulated P3D/R5 reactivity were benchmarked.

The major issues and lessons learned from this work can be summarized as follows:

Methodology**:**

1. The severity of a nuclear RIA depends on the reactor core design, on the control rod grouping and location, and on the rod reactivity worth. Therefore, the use of TH and NK codes, and their coupled version, to model RIA accidents should be carried out through a systematic approach (the six step approach), otherwise the results would not capture the true transient behavior of the core under analysis.
2. The use of NK/TH coupled codes implies not only the knowledge of the problem and of the model being simulated, but also the appropriate selection of the code parameters. To have the simulation results consistent among the NK and TH codes, and to apply them to the coupled version so it generates accurate results, the simulation of one code depends on the adequate configuration of parameters generated by the other code.

3. The P3D/R5 coupled code mapping determines where to set the NK node power into the TH channel and where to assign TH properties into the NK node. The correct determination of the mapping weight factors, thus the generation of the MAPTAB file, is among the most important tasks to obtain accurate coupled code solutions.
4. The power response and the reactivity behavior during the RIA are different among the three cases under investigation: case *a* has a fast increase in the reactivity, a power peak of about 25% due to the lack of reactivity control, and a slow power return to steady-state; case *b* has a very slow power dynamics; and on the other hand, case *c* has a sharp power peak. These different trends are explained by the reactivity worth and the core initial conditions for each case.

Total Power and Reactivity:

1. The simulation of a RIA considering the offline exchange of data between P3D and R5 standalone, using the six step approach and the appropriate code configuration, may give similar transient maximum reactivity compared to P3D/R5. Nevertheless, the coupled P3D/R5 simulation (NK and TH parameters exchanged at each time step) is not time demanding and provide more accurate answers than the standalone analysis.
2. The standalone codes (R5 and P3D) predicted more conservative magnitude of power increase compared to the coupled P3D/R5 simulation. This conservatism increased as the core size shrunk, implying that performing coupled simulation sounds more essential in licensing of smaller cores.
3. From the design point of view, the P3D transient simulation typically predicts lower peak reactivity (up to 30% depending on the NPP and case under analysis – see Table 7-4) than the steady-state simulation. The magnitude of such underestimation of reactivity relative to NPP size becomes larger as the core size shrinks.
4. The P3D steady-state simulation looks conservative and does not correspond to the expected peak in reactivity due to the ejection of CRA. Furthermore, during transients, all three codes have the maximum similar value of the reactivity (difference of less than 10% among them – see Table 7-4).

5. Since the reactivity coefficients (listed in Table 6-8) are similar among the three NPPs sizes (difference less than 6% - thus, the reactivity and power response due to different core is not due to differences in the Doppler and Moderator coefficients among the cases under investigation), the results indicate that the smaller cores yielded a lower peak power, and thus a safer response, for a given inserted reactivity, compared to larger cores.
6. The HFP simulation results (case *a*) indicate that the power transient peaks for the three NPPs have the same value, but the steady-state power following the ejection is lower for the small core (about 51%). On the other hand, the HZP simulation (case b and c) suggests that the transient power peak is lower for the small core (about 3% - case *b*, and 400%, case *c*), but the steady-state power following the ejection is at the same level of 20%.

3D Power Distribution:

1. The use of P3D coupled with R5 allows a 3D assessment of the power distribution during a RIA. At the beginning of the simulation, the core is at steady-state with the CRA/CRB#8 fully inserted and the power being generated uniformly within all the fuel assemblies. However, after the RIA, the 3D power distribution looks different among the various cases, but it does not depend on the size of the core (under the stated assumptions of similar core designs).
2. The simulation results indicate that the 3D power distribution depends on the reactivity worth due to the rod ejection, as expected, but also on the core initial condition. Although the core reduction has a small impact on the HFP 3D power distribution, the core power increasing happens in the area surrounding the rod/bank being ejected.
3. The simulation results indicate that the 3D peak assembly factor (power distribution) becomes lower, during and after transients, as the NPPs shrinks. This feature confirms that the smaller cores yielded to a power safer response for given inserted reactivity compared to larger cores.
4. The 3D analysis also indicates that the peak power under HFP (case *a*) core conditions is well-distributed after the transient, while under HZP conditions (case

b and case *c*) the area surrounding the CRA ejection stays hotter (from 15 to 90%, depending on the case under investigation – see Table 8-1) for all core sizes.

5. The 3D assessment indicates that for the HFP, although the total power increases rapidly, the peak assembly factor (3D power distribution) turns back quickly (just after the transient) closer to its original value (see Table 8-1). In addition, the insertion of reactivity increases the neutron population and, therefore, the fuel power level and temperature.

EKF Reactivity Estimation:

1. The system is modeled by continuous time nonlinear stochastic differential equations, while the power measurement happens at discrete times. The EKF code uses the time step directly from the power measured data and it applies to the system model for discretization and linearization at every time step.
2. The tuning of the filter (initial spectral density *Q'(i,i)*-entries) goes automatically up to the simulation first time step based on a representative change in the variables during the time step, i.e. by assuming that the state variable is likely to change by an amount Δy over the interval of interest Δt.
3. The covariance matrix of the state noise is updated at each time step. Moreover, the state variable representation of the reactivity uses the same initial conditions for all cases under evaluation. These sophisticate strategies (number 1, 2 and 3) make the algorithm robust and it gives accurate results.
4. The EKF and IPK capabilities are assessed by the convergence of the algorithm and by the reactivity's SD. The IPK reactivity has higher noise content, e.g. higher standard deviation, compared to the EKF reactivity for all cases under investigation. Therefore, the EKF method presents more robust results compared to the IPK method, as can be seen in Table 9-1.
5. Under a RIA starting with low power, due to small reactivity insertion and slower power response (case *b*), the IPK calculated reactivity varies widely from positive to negative values, which may add extra difficulty to the task of controlling a reactor that may go supercritical.
6. A sensitivity analysis for three distinct SD noise measurements suggests that the EKF method is superior to the IPK method, independent of the magnitude of noise

loads. On the other hand, the IPK simulation result for the same measurements indicates that as the noise content increases, the difference between the IPK and P3D/R5 reactivity also increases.

7. A sensitivity analysis for five distinct carry-over effects of different random noise loads indicates that the random addition of different noise loads to the reactor power does not change the overall performance of both IPK and EKF algorithms; and the EKF method is less sensitive to the different set of noise loads.
8. Although the P3D/R5 simulates the reactivity using a spatial kinetics method, the use of the PKRE to model the EKF to estimate the reactivity for a given power profile under a noisey environment provided accurate results.
9. Due to the appropriate choice of the R and Q' matrices, based on the sensor error (R) and on the initial variation of its entries (Q'), the EKF winds up with accurate reactivity estimation under RIA conditions.
10. The estimation of the reactivity by means of EKF stochastic tools may help to increase the performance by better controlling the operation. Moreover, the application of EKF may reduce the sensitivity to reactor parameters and noise in the input signals.
11. By applying the same coding approach for both algorithms, the computation time is found not to be a constraint, or a key decision point, for choosing between IPK and EKF for reactivity estimation. The use of the EKF may be computationally more demanding due to the online real time matrix computation and tuning needs, but nowadays instrumentation and control systems are well equipped for both EKF and IPK implementation.

To summarize, the accuracy of the coupled simulation results has strong dependence on the depth of systematic modeling and simulation strategy. That includes running the standalone codes with consistent configuration and tuning. While this work shows an inherent safe performance of smaller cores relative to RIAs, the severity of the transients is strongly dependent on individual core designs and control rod groupings. In view of these findings, new reactor designs may include comprehensive RIA assessment of different-size cores to ensure that performance and safety trade-offs are adequately understood and evaluated.

Furthermore, the measure of the reactivity is important on solving practical NPP issues related to accident analysis, reactivity control and safety. Thus, the benefits of using an estimation tool like EKF in real applications shall be weighed against the use of the well know IPK method because the use such estimation tool requires special attention to the filter's tuning task while the application of the IPK method is quite straightforward.

10.2. Recommendations

The main recommendations for further studies follow:

Methodology Improvements:

1. The EKF may be directly implemented within the P3D/R5 coupled package to exchange information at each time step;
2. Artificial intelligence tools such as artificial neural networks, genetic algorithm and Fuzzy logic, may be used for reactivity estimation and the results should be compared to this work;
3. An automated method for an offline Q tuning may be implemented to benchmark results; and
4. A statistical method to improve the EKF algorithm initial guess, during large RIA scenarios, via improvements in the initial slope of the reactivity model, may be implemented.

New Applications and Sensitivity Studies:

1. A commercial SMR may be used as a base model to perform comprehensive RIA assessment of different-size cores;
2. The simulation results using a set of cross sections with Boron dependence may be benchmarked against this work. Unlike a typical PWR cross section set, the provided NEA benchmark neutron cross section set does not have dependence on boron concentration. Therefore, the control rods are the only method by which the core reactivity is controlled;

3. The application of EKF with the noise loads being dependent on location of assemblies in the core should be analyzed (in a PWR, there is more uncertainty in prediction of power distribution for assemblies in the periphery); and
4. A commercial SMR may be used as a base model to assess RIA conditions via the EKF. The results should be compared to the IPK method.

11. REFERENCES

[1] International Atomic Energy Agency (AIEA). *Fukushima Nuclear Accident Update Log*. https://www.iaea.org/newscenter/news/fukushima-nuclear-accident-update-log-51/. Accessed in January 8th 2015.

[2] International Atomic Energy Agency (AIEA). *Power Reactor Information System*. http://www.iaea.org/pris/. Accessed in January 12th 2015.

[3] J. Duderstadt, L. Hamilton. *Nuclear Reactor Analysis*. John Wiley and Sons (1976).

[4] D.P. Griggs, M.S. Kazimi, A.F. Henry. *Advanced Methods Development for LWR Transient Analysis, Final Report*. Massachusetts Institute of Technology (1982).

[5] Organization for Economic Co-Operation and Development (OECD) , Nuclear Energy Agency (NEA). *Nuclear Fuel Behavior under Reactivity-Initiated Accident (RIA) Conditions - State of the Art Report*. ISBN 978-92-64-99113-2 (2010).

[6] T. Yoritsune, T. Ishida, S. Inayoshi. *In-vessel Type Control Rod Drive Mechanism using Magnetic Force Latching for a Very Small Reactor*. Journal of Nuclear Science and Technology. Vol. 39, n° 8, p. 913–922 (2002).

[7] Zhe D. *Robust Kalman Filter with Application to State Estimation of a Nuclear Reactor*. Institute of Nuclear and New Energy – Intech (2010).

[8] T.U. Bhatt et al. *Estimation of Sub-criticality using extended Kalman Filtering Technique*. Annals of Nuclear Energy. N° 60, p. 98-105 (2013).

[9] H. Finnemann, A. Galati. *NEA-L-335: 3-D LWR Core Transient Benchmark Final Specification*. Organization for Economic Co-Operation and Development (OECD), Nuclear Energy Agency (NEA) (1991).

[10] H. Finnemann et al. *Results of LWR Core Transient Benchamarks*. Organization for Economic Co-Operation and Development (OECD), Nuclear Energy Agency (NEA) (1993).

[11] M.H. Kim, T.A. Taiwo, H.S. Khalil. *Analysis of the NEACRP PWR Rod Ejection Benchmark Problems with DIF3D-K*. American Nuclear Society Topical Meeting on Advance in Reactor Physics, Knosville, Tennesse (1994).

[12] K.N. Ivanov et al. *Pressurized Water Reactor Main Steam Line Break (MSLB) Benchmark. Volume I: Final Specifications*. Organization for Economic Co-Operation and Development (OECD), Nuclear Energy Agency (NEA) (1999).

[13] V.H. Sanchez-Espinoza et al. *Analysis of the OECD/NEA PWR Main Steam Line Break (MSLB) Benchmark Exercise 3 with the Coupled Code System RELAP5/PANBOX*. Forschungszentrum Karlsruhe GmbH, Karlsrhe (2002).

[14] K. Invanov, N. Todorova, E. Sartori. *Using the OECD/NRC Pressurized Water Reactor Main Steam Line Break Benchamark to Study Corrent Numerical and Computational Issues of Coupled Calculations*. Nuclear Technology. Vol. 142, p. 95-115 (2003).

[15] T. Kozlowski, T. Downar. *OECD/NEA and US. NRC PWR MOX/UO2 Core Transient Benchmark. Final Specitications, Revision 2*. Organization for Economic Co-Operation and Development (OECD), Nuclear Energy Agency (NEA) (2003).

[16] T. Kozlowski, T. Downar. *Final Results: PWR MOX/UO2 Control Rod Eject Benchamark*. Purdue University (2006).

[17] R. M. Millwer, T. Downar. *Competion Report for the Coupled TRAC-M/PARCS Code*. Purdue University, U.S. (1999).

[18] U.S. Nuclear Regulatory Comission (NRC). *Computer Codes*. http://www.nrc.gov/about-nrc/regulatory/research/ safetycodes.html. Accessed on January, 21st 2014.

[19] O. Zerkak et al. *LWR Multi-physics Development and Applications within the Framework of the NURESIM European Project*. Joint International Topical Meeting on Mathematics & Computation and Supercomputing in Nuclear Application. Monterey, California (2007).

[20] W. Weaver III. *Programmers Manual For the PVM Coupling Interface in the RELAP5-3D Code.* Idaho National Laboratory, U.S. (2005).

[21] D.L. Aumiller et al. *A Coupled RELAP5-3D/CFD Methodoloy with a Proof-of-Principles Calculations*. 2000 International RELAP5 Users Seminar, Jackson Hole, Wyoming, US. (2000).

[22] D.J. Diamond et al. *Power Level Effect in a PWR Rod Ejection Accident. Energy Science and Technology Department*. Brookhaven National Laboratory (1998).

[23] C. Marciulescu, Y. Sung, C. Beard. *Three Dimensional Analysis of 3-Loop PWR RCCA Ejection Accident for High Burnup*. Proceedings of the International Conference on Nuclear Engineering. Miami, Florida, U.S. (2006).

[24] C. Jonsson et al. *Severe Reactivity Initiated Accidents with SIMULATE-3K and SIMULATE-3K/RELAP5 in FORSMARK-3 BWR*. Proceedings of the LWR Fuel Performance. Orlando, Florida, U.S. (2010).

[25] Z. Tabadar et all. *Simulation of a Control Rod Ejection Accident in a VVER-100/V446 using RELAP5/Mod3.2*. Annals of Nuclear Energy 45, 106-114 (2012).

[26] M. Fritz. *Control Rod Drop During Hot Zero Power RIA in BWR*. Uppsal Universitet (2013).

[27] R. Miro et al. *Implementation of New Simulation Capabilities in RELAP5/PARCS V2.7 Coupled Codes*. Nuclear Energy for New Europe (2010).

[28] P. Meloni, G. Bandini, M. Polidori. *Validation of the RELAP5/PARCS Coupled Thermalhydraulics-Neutronics Model of the CASACCIA TRIGA Reactor*. ADSS Experiments Workshop. College Station, TX, U.S. (2006).

[29] H. Kantee. *Application of RELAP5/MOD3.1. to ATWS Analysis of Control Rod Withdrawn from 1% Power Level*. International Agreement Report. U.S. Nuclear Regulatory Commission (2000).

[30] M. Hursin, T. Downar, B. Kochunas. *Analysis of the Core Power Response During a PWR Rod Ejection Transient using the PARCS Nodal Code and the DeCart MOC Code*. Nuclear Science and Engineering. N° 172, p. 151-167 (2012).

[31] O. M. Carvalho Junior. *Coupled 3D Neutron-Kinetic and Thermal-Hydraulic Codes Applied to Control Rod Ejection Accident in Pressurized Water Reactors*. University of Pisa. PhD Thesis (2005).

[32] C. Jonsson et al. *Severe Reactivity Initiated Accidents with Simulate-3K and Simulate-3K/RELAP5 in Frosmark-3 BWR*. Proceedings of 2010 LWR Fuel Performance TopFuel/WRFPM (2010).

[33] Organization for Economic Co-Operation and Development (OECD), Nuclear Energy Agency (NEA). *Neutronics Thermal Hydraulic Coupling in LWR*. Vol. 1 (2004).

[34] Organization for Economic Co-Operation and Development (OECD), Nuclear Energy Agency (NEA). *Nuclear Safety Criteria Technical Review*. N° 7072, second edition. (2012).

[35] k. Ivanov et al. *Validation of Coupled Thermal-Hydraulic and Neutronics Codes in International Co-operation*. Pennsylvania State University, U.S. (2005).

[36] D. Barber, T. Downar. *Software Requirements Specification for the General Interface in the Coupled Code*. Purdue University, U.S. (1998).

[37] D. Barber et al. *A Generalized Interface Module for the Coupling of Spatial Kinetics and Thermal-Hydraulics Codes*. Ninth International Topical Meeting on Nuclear Reactor Thermal Hydraulics NURETH-9 (1999).

[38] J. Peltonen. *Development of Effective Algorithm for Coupled Thermal-Hydraulics - Neutron Kinetics Analysis of Reactivity Transient*. Licentiate Degree Thesis. Department of Physics, Division of Nuclear Power Safety, Stockholm, Sweden (2009).

[39] I. Limaiem, F. Damian, X. Raepsaet. *VTHR Core Modeling: Coupling Between Neutronic and Thermal-Hydraulics.* Mathematics and Computation, Supercomputing, Reactor Physics and Nuclear and Biological Applications. (2005)

[40] S. Mittig et al. *Validation of Coupled Neutronic/Thermal-Hydraulic Codes for VVER Reactors – Final Report*. 5th Euratom Framework Programme (2002).

[41] J. Judd, G. Grandi. *Simulate-3K, a Coupled Code System*. Transactions of the American Nuclear Society and the European Nuclear Society. International Conference on Making the Reansaissance Real (2007).

[42] O. Zerkak et al. *Revisiting Temporal Accuracy in Neutronics/TH Code Coupling using the Nuresim LWR Simulation Plataform*. The 14th International Topical Meeting on Nuclear Reactor Thermalhydraulics, NURETH-14 (2011).

[43] J.N. Cardoni. *Nuclear Reactor Multi-Physics Simulations with Coupled MCNP5 and Star-CCM+*. Master Degree Thesis. University of Illinois, Urbana, U.S. (2011).

[44] J.E. Seifried. *Thermal Modeling and Feedback Requirements for LIFE Neutronic Simulations*. LLNL-TR-416167 (2009).

[45] F. Faghihi, H. Khalafi, M. Mirvakili. *A Literature Survey of Neutronics and Thermal-Hydraulics Codes for Investigating Reactor Core Parameters; Artificial Neural Networks as the VVEER-1000 Core Predictor*. InTech (2011).

[46] H. Kokame, Y. Hattoi. *Kalman Filter Applied to Estimation of Neutron Flux Distribution and Optimum Allocation of In-Core Detectors*. Journal of Nuclear Science and Technology. V. 14, p. 695-704 (1977).

[47] S.R. Valsalam. *Applications of Kalman Filtering in Industrial Control*. http://www.cdactvm.in/. Accessed in September 22th 2013.

[48] Y. Shimazu, W.F.G. van Rooijen. *Qualitative Performance Comparison of Reactivity Estimation between the Extended Kalman Filter Technique and the Inverse Point Kinetic Method*. Annals of Nuclear Energy. N° 66, p. 161-166 (2014).

[49] E. Hatamia, H. Salariehb. *Design of a Fault Tolerated Intelligent Control System for a Nuclear Reactor Power Control: Using Extended Kalman filter*. Journal of Process Control. Vol. 24 Issue 7, p. 1076-1084 (2014).

[50] J.C. Venerus, T.E. Bullock. *Estimation of the Dynamic Reactivity using Digital Kalman Filtering*. Nuclar Science and Engineering. N° 40, p. 199–205 (1970).

[51] Eletric Power Research Institute. www.epri.com. Accessed on January, 2nd 2014.

[52] World Nuclear Organization. ww.world-nuclear.org. Accessed on January, 2nd 2014.

[53] T. Downar, Y.Xu, V.Seker. PARCS v3.0. *U.S. NRC Core Neutronics Simulator Department of Nuclear Engineering and Radiological Sciences*. Rockville, MD, U.S. (2010).

[54] Idaho National Laboratory (INL). *RELAP5-3D Code Manual.* INEEL-EXT-98-00834, Revision 4.0 (2012).

[55] T. Downar et al. *PARCS: Purdue Advanced Reactor Core Simulator*. Physor 2002. Seoul, Korea (2002).

[56] Oak Ridge National Laboratory (ORNL). *Parallel Virtual* Machine (PVM). http://www.csm.ornl.gov/pvm. Accessed on January, 1st 2014.

[57] P. Boonsuwan. *RELAP 5 Fundamentals*. Nuclear Safety and Regulation (2010).

[58] Mathworks. *Accelerating the Pace of Engineering and Science*. http://www.mathworks.com. Accessed on January 2nd 2014.

[59] U.S. Nuclear Regulatory Commission (NRC). *Backgrounder on the Three Mile Island Accident*. http://www.nrc.gov/reading-rm/doc-collections/fact-sheets/3mile-isle.html. Accessed on January, 2nd 2014.

[60] Y. Xu. *Nuclear Power Plant Simulation with Coupled Neutronic/Thermal-Hydraulic Codes*. University of Michigan (2010).

[61] Nuclear Energy Insider. *Nuclear Energy Insider's SMR Report 2013* (2013).

[62] The Babcock & Wilcox Company. *Generation Mpower Snapshot*. http://www.generationmpower.com. Accessed in October 1st 2013.

[63] J. Buongiorno. *Small is Beautiful? A Review of the Small Modular Reactor (SMR) Designs*. Innovations on Nuclear Technology Workshop. University of Sao Paulo (2012).

[64] U.S. Department of Energy (DOE). *International Rector Innovative and Secure (IRIS) - Final Technical Progress Report*. Report Number STD-ES-03-40 (2003).

[65] T.U. Bhatt, SR. Shmmith and A.P. Tiwari. *Estimation of Shutdown Reactivity in Power Reactor: Comparative Study of Inverse Point Kinetics and Kalman Filtering*. BARC Newsletter. Issue 324. 2012.

[66] B.O. Anderson, J.B. Moore. *Optimal Filtering*. Prentice-Hall, Englewood Cliffs, U.S. (1979).

[67] A.H. Jazwinski. *Stochastic Processes and Filtering Theory*. Academic Press (1970).

[68] A. Gelb et all. *Applied Optimal Estimation*. The MIT Press (1974).

[69] J.J. Cruz. *Pilotagem Automática de Embarcações com Emprego de Controle Estocástico*. Master Degree Thesis (in Portuguese). University of São Paulo (1981).

[70] A.E. Aboanber, Y.M. Hamada. *PWS: an Efficient Code System for Solving Space Independent Nuclear Reactor Dynamics*. Annals of Nuclear Energy. N° 29, p. 2159-2172 (2002).

[71] B. Quintero-Leyva 2008. CORE: *A Numerical Algorithm to Solve the Point Kinetics Equations*. Annals of Nuclear Energy. N° 35, p. 2136-2138 (2008).

[72] T. Sathiyasheela. *Power Series Solution Method for Solving Point Kinetics Equations with Lumped Model Temperature and Feedback*. Annals of Nuclear Energy. N° 36, p. 246-250 (2009).

[73] J.V. Leeuwen. *Nuclear Power – The Energy Balance Report* (2008).